MEASUREMENT AND NUMERICAL MODELING OF MICROORGANISM INACTIVATION OF AN ANNULAR ULTRAVIOLET GERMICIDAL AIR REACTOR

By

QING SHENG KE

A thesis submitted to the Faculty of Graduate Studies and Research
in partial fulfilment of the requirements for the degree of

MASTER OF SCIENCE

in

ENVIRONMENTAL ENGINEERING

DEPARTMENT OF CIVIL AND ENVIRONMENTAL ENGINEERING
EDMONTON, ALBERTA

Spring, 2008

Library and Archives Canada

Published Heritage Branch

395 Wellington Street
Ottawa ON K1A 0N4
Canada

Bibliothèque et Archives Canada

Direction du Patrimoine de l'édition

395, rue Wellington
Ottawa ON K1A 0N4
Canada

Your file Votre référence
ISBN: 978-0-494-45829-7
Our file Notre référence
ISBN: 978-0-494-45829-7

NOTICE:
The author has granted a non-exclusive license allowing Library and Archives Canada to reproduce, publish, archive, preserve, conserve, communicate to the public by telecommunication or on the Internet, loan, distribute and sell theses worldwide, for commercial or non-commercial purposes, in microform, paper, electronic and/or any other formats.

The author retains copyright ownership and moral rights in this thesis. Neither the thesis nor substantial extracts from it may be printed or otherwise reproduced without the author's permission.

AVIS:
L'auteur a accordé une licence non exclusive permettant à la Bibliothèque et Archives Canada de reproduire, publier, archiver, sauvegarder, conserver, transmettre au public par télécommunication ou par l'Internet, prêter, distribuer et vendre des thèses partout dans le monde, à des fins commerciales ou autres, sur support microforme, papier, électronique et/ou autres formats.

L'auteur conserve la propriété du droit d'auteur et des droits moraux qui protège cette thèse. Ni la thèse ni des extraits substantiels de celle-ci ne doivent être imprimés ou autrement reproduits sans son autorisation.

In compliance with the Canadian Privacy Act some supporting forms may have been removed from this thesis.

While these forms may be included in the document page count, their removal does not represent any loss of content from the thesis.

Conformément à la loi canadienne sur la protection de la vie privée, quelques formulaires secondaires ont été enlevés de cette thèse.

Bien que ces formulaires aient inclus dans la pagination, il n'y aura aucun contenu manquant.

Canada

ABSTRACT

This is a preliminary study on the application of the CFD modeling technique for in-duct UVGI (Ultraviolet Germicidal Irradiance) air inactivation system design. A bench-scale UVGI air inactivation reactor was constructed and inactivation efficiencies under different flow rate and baffle conditions were measured by using aerosolized *B. subtilis* as the challenge microorganism. In order to supply reliable modeling data, a collimated beam batch reactor system was built and used to measure the UV inactivation constants of aerosolized *Bacillus subtilis* spores. Eulerian and Euler-Lagrangian CFD models were used to simulate the inactivation process and to predict the inactivation efficiencies of the UVGI reactor. Agreements between experimental results and CFD predictions showed that CFD can be a useful tool for design of in-duct UVGI air inactivation systems.

DEDICATION

To my wife, Jane Gu Zhuang for her love and her supports.

To my families and friends for their encouragements.

ACKNOWLEDGEMENTS

I would like to express my sincere appreciations to my supervisors, Dr. Stephen A. Craik, Dr. James R. Bolton, and Dr. Mohamed Gamal El-Din for their creative ideas, guidance, financial support, and patience in this research. Thank you all for turning this research project into a precious experience in my life.

I would like to thank Maria Demeter, Garry Solonynko, and Nick Chernuka for their technical support in the lab works.

I would like to thank the Natural Science and Engineering Research Council (NSERC) for funding this project.

Table of Contents

List of Tables

List of Figures

List of symbols used

List of abbreviations

1 Introduction 1

1.1 Definition and units 1

1.2 Background 5

1.3 Research Objectives 7

1.4 Organization 8

2 Literature Review 9

2.1 Bioaerosols and health concerns 9

2.2 UVGI air inactivation systems 10

2.3 Mechanisms of UVGI inactivation of aerosolized microorganisms 13

2.4 Factors affecting the UVGI air system's efficiency 18

2.5 UVGI Air disinfection system modeling 20

2.5.1 Components of a UVGI air disinfection system model 20

2.5.2 UVX program 24

2.5.3 Application of CFD in UVGI air disinfection system modeling 25

2.6 Research statement and the need for this research 28

3 Determination of the UV Inactivation Constants of Aerosolized *B. subtilis* Spores 31

3.1 Introduction 31

3.1.1 Research on UV susceptibility of aerosolized microorganisms 31

3.1.2 Aerosolized *B. subtilis* spores 34

3.2 Materials and Methods 36

3.2.1 Culture and enumeration of *B. subtilis* spores 36

3.2.2 Nebulizer and impingers 37

3.2.3 Collimated beam and the well mixed batch reactor 40

3.2.4 Fluence (UV dose) calculation in the well-mixed batch reactor 42

3.2.5 Inactivation tests 45

3.2.6 Model fitting 46
3.3 Results and discussion 47
3.3.1 Fluence (UV dose) calculation 47
3.3.2 Estimation of the inactivation model parameters 47
3.3.3 Discussion 50
4 Bioassay for an Annular In-duct UVGI Air Disinfection Reactor 53
4.1 Introduction 53
4.2 Material and methods 55
4.2.1 In-duct UVGI air disinfection reactor 55
4.2.2 Operating conditions for the annular UVGI reactor 57
4.2.3 UVC output measurement 61
4.3 Results and discussion 69
4.3.1 Measurement of the UVC output 69
4.3.2 Bioassay experimental results 70
4.3.3 Discussion 71
5 CFD modeling of the UVGI air inactivation reactor 75
5.1 Introduction 75
5.2 Development of the CFD model of the UVGI air reactor 79
5.2.1 Flow chart of the model building 79
5.2.2 Meshing and grid independency study 82
5.2.3 Air fluid modeling in the annular duct 86
5.2.4 Thermal effects of the lamp 88
5.2.5 UVC fluence rate field modeling 90
5.2.6 Euler method: Spore concentration as a scalar 93
5.2.7 Euler method: Source terms in the scalar transportation equations 94
5.2.8 Euler-Lagrange model and the fluence distribution curves 99
5.2.9 Boundary conditions of CFD models 100
5.3 Results and discussion 102
5.3.1 Results from the Euler models 103
5.3.2 Results from Euler-Lagrange models 106
5.3.3 Discussion 109

6 Conclusions 114
7 Recommendations 116
References 117
APPENDIXES 122
Appendix 1. Raw data from B. Subtilis Spores UV inactivation constants measurement experiments 122
Appendix 2. Raw data in Lamp UVC output measurement 125
Appendix 3. Raw data from bioassay on UVGI air inactivation reactor 126
Appendix 4. Data analysis of the bioassay data in appendix 3 128
Appendix 5 . Source code list of the UDFs used in Fluent modeling. 130

List of Tables

Table 1. A UV inactivation constant table 16

Table 2. Recent aerosolized microorganism UV susceptibility studies 32

Table 3. Flow rate and other experimental conditions in the UV inactivation constant measurement experiments 46

Table 4. Testing conditions for the in-duct UVGI reactor 57

Table 5. Summary of the Turbulences Model available in Fluent® CFD Software 77

Table 6. Comparison of measured temperature CFD predicted temperature 89

Table 7. Inactivation levels from the models and bioassay experiments 109

List of Figures

Figure 2. 1. Breakdown of currently installed UVGI air inactivation systems 11
Figure 2. 2. An in-duct UVGI system installed in an HVAC duct 12
Figure 2. 3. Factors affecting UVGI system efficiency 19
Figure 2. 4. Relative lamp UV light output of a low pressure lamp versus the ambient temperature 20
Figure 2. 5. Sub-models in UVGI air disinfection system design 21

Figure 3. 1. Impinger efficiencies under various sampling flow rates and collecting liquid volumes 39
Figure 3. 2. Photos of the 3-jet nebulizer (left) ; and a standard Midget impinger 40
Figure 3. 3. Schematic of the well-mixed collimated beam batch reactor 41
Figure 3. 4. Well mixed -collimated beam batch reactor system use for UV inactivation rate constant measurement 44
Figure 3. 5. Aerosolized *Bacillus subtilis* spore UV response curves 48
Figure 3. 6. JCR of the multi-target inactivation model parameter estimations at RH=50-60% 49
Figure 3. 7. JCR of the multi-target inactivation model parameter estimations at RH=70-83% 50

Figure 4. 1. Section of the annular induct UVGI air inactivation reactor 55
Figure 4. 2. Schematic diagram of the operation and sampling arrangement at 11 L/min flow rate 59
Figure 4. 3. Schematic diagram of the operation and sampling arrangement at 26.5 and 44 L/min flow rates 60
Figure 4. 4. Schematic used to derive the relationship between the I_0 and P 63
Figure 4. 5. Schematic for the UVC output measurement (Keitz method) 65
Figure 4. 6. Goniometric measurement schematic 67
Figure 4. 7. Schematic for reflection factor measurement 68

Figure 4. 8. Log inactivation levels under 3 flow rates conditions and 3 baffle arrangements 71

Figure 5. 1. Flow chart of the development of the CFD model 80
Figure 5. 2. UVGI air inactivation reactor 3D model with Cartesian coordination system 83
Figure 5. 3. Axial views of the three structured hexahedral grids with different density meshes 84
Figure 5. 4. Longitudinal y- velocity profiles computed at two z positions (z = 0.035 m and z = 0.045 m using) three different density meshes 85
Figure 5. 5. A concentric annulus and the location of the velocity profile line 87
Figure 5. 6. Comparison of the radial velocity profiles calculated by using analytical formulas and computed by using CFD 88
Figure 5. 7. Thermal effect on the velocity profiles 90
Figure 5. 8. Fluence rate profiles by UVCal2D and View factor models 92
Figure 5. 9. Contour map of the fluence rates field of the UVGI reactor section 93
Figure 5. 10. Linearization of the multi-target model 95
Figure 5. 11. CFD output of the validation model for the double scalar source terms 98
Figure 5. 12. UVGI air disinfection reactor log inactivation levels 103
Figure 5. 13. U_z profiles at z = 0.02 m at flow rate = 44 L/min along the UVGI reactor longitudinal axis with different baffle conditions 104
Figure 5. 14. Cumulative fluence profiles under three baffle arrangements 105
Figure 5. 15. Fluence distributions generated from the particle tracking CFD models .. 107

List of Symbols Used

div	operator, divergence
E	Irradiance, W
E'	fluence rate, W m^{-2} or mW cm^{-2}
grad	operator, gradient
F	fluence or accumulative fluence, J m^{-2} or mJ cm^{-2}
H	radiant exposure, J m^{-2}
I	radiant intensity, W sr^{-1}
k	inactivation rate constant in fluence-inactivation model
K	turbulent kinetic energy, m^2 s^{-1}
k_m	inactivation rate constant in multi-target model
L	length, m
N_{off}	number of viable spores without UV exposure
N_{on}	number of viable spores after UV exposure for time t
n_C	inactivation constant in multi-target model
p	pressure, Pa or kg m^{-1} s^{-2}
P	radiant power W
Q	flow rate m^3/s or Liter/minute (L/min)
R	radius, m
S	survival rate or survival fraction
S_φ	source term of φ
S_F	source term of F
t	time, s
u	velocity scalar, m/s

List of Symbols Used (Continued)

Γ	diffusion coefficient, $m^2\ s^{-1}$
φ	concentration of the viable spores, CFU m^{-3}
$\vec{U}$	velocity vector, m/s
U_x, U_y, U_z	velocity component along the *x, y, z* axis, m/s
V	volume, m^3

List of Abbreviations

3D	3 Dimensional
AGI	All Glass Impinger
ANOVA	Analysis of Variance
ASHRAE	American Society of Heating, Refrigerating and Air-conditioning Engineers
ATCC	American Type Culture Collection
CFD	Computational Fluid Dynamics
CFU	Colony Forming Unit
CI	Confidence Interval
DNA	Deoxyribonucleic Acid
HVAC	Heating, Ventilation, Air-conditioning and Cooling
JCR	Joint Confidence Region
PR	Photoreactivation
REF	Reduction Equivalent Fluence
RH	Relative Humidity
RNA	Ribonucleic Acid
SARS	Severe Acute Respiratory Syndrome
TB	Tuberculosis
UDF	User Defined Function
UDS	User Defined Scalar
UV	Ultraviolet
UVC	UV irradiance in the 200-280 nm wavelength region
UVGI	Ultraviolet Germicidal Irradiance
XDR TB	Extensive Drug Resistant Tuberculosis

1 Introduction

1.1 Terminologies and units

The terminologies used to discuss UV radiation were adopted mainly from Bolton (2001) and Bolton and Linden (2003).

Radiant power (symbol P; units W): the rate of radiant energy emitted by a radiant source. For a UVGI lamp, the radiant power of concern is the radiant emission in the 200-300 nm range. The radiant power in this range is mainly in the UVC range (200-280 nm); hence, the germicidal irradiation portion of the radiant power emitted by a low pressure UV lamp can be named the "UVC power".

Radiant intensity (symbol I; units W sr^{-1}): the total radiant power P emitted by a source in a given direction about an infinitesimal solid angle.

Radiance (symbol L; units W sr^{-1} m^{-2}) is the radiant intensity divided by the orthogonally projected area which subtends the solid angle $d\Omega$. According to Lambert's cosine law, the observed radiant intensity is proportional to the cosine of the angle between the observer and the normal direction of the radiant source's surface.

Irradiance (symbol E; units W m^{-2}): the total radiant power (P) incident from all upward directions on an infinitesimal element of surface of area dS containing the point under consideration divided by dS. UV sensors with a flat shape can measure the irradiance at a spatial point from a UV lamp.

Fluence rate (symbol E'; units W m^{-2}) : the total radiant power incident from all directions onto an infinitesimal sphere of cross-sectional area dA, divided by dA. Compared to "irradiance", "fluence rate" is the proper term for the inactivation of microorganisms suspended in air or water media because the particles receive radiant

energy from all directions in a UV field. Terms like "all-angle irradiance" (VanOsdell and Foarde 2002), "spherical irradiance" (Peccia et al. 2001) are also used. In a UV susceptibility study using a collimated beam system, the UV light is cast from the above directions. Under this situation, "fluence rate" and "irradiance" are interchangeable terms.

Radiant Exposure (symbol H; units J m^{-2}): the total radiant energy incident from all upward directions on an infinitesimal element of surface of area dS containing the point under consideration divided by dS. UV exposure is more suitable for the UV surface disinfection process than a UV reactor inactivation process.

Fluence (symbol F, units J m^{-2}): also known as "UV dose", is the total radiant energy passing from all directions through an infinitesimal sphere of cross-sectional area dA, divided by dA. "Fluence" refers to the UV energy incident on the microorganism particles regardless of whether or not it is absorbed by the microorganisms, whereas "UV dose" implies that the energy is absorbed by the particles. Since only the incident energy can be measured in the UV inactivation process, "fluence" is an appropriate term in UV inactivation process.

UV inactivation rate constants (symbols: k, k_m, n_C; units depend on model): parameters in relevant fluence-inactivation level models that describe the UV susceptibility of a species of microorganism.

View factor: the fraction of the total energy emitted by one surface directly incident on another surface. A model built by using the view factor method can describe the transfer of radiation energy between two surfaces. UV radiation can be treated as radiation energy and, hence, can be calculated by using the view factor model.

Disinfection: inactivation of pathogenic microorganisms by using a disinfectant or disinfectants.

Inactivation: the process of reducing microorganisms' reproductive ability and/or the ability to induce disease by applying chemical or physical stress (e.g., UV exposure).

Inactivation efficiency (units %): the percentage form of the removal rate, denoted as $(1\text{-}N/N_0) \times 100\%$, where N and N_0 are the concentrations of viable microorganisms before and after the inactivation process, respectively. "Inactivation efficiency" is used to describe the efficiency of a UV inactivation device or system.

Inactivation level (unitless): the logarithm form of the survival rate, denoted as $-\log (N/N_0)$. The "inactivation level" is also called the "log inactivation level" to emphasis the logarithm form in this thesis.

The terminologies used in CFD section were adapted mainly from Versteeg and Malalasekera (1995) and Fluent (2005).

Control volume: is also known as "cell", "finite volume" and is an element in a grid of the computational domain. A control volume is the smallest element in a domain over which the governing equations of fluid flow are integrated.

Domain: the computational domain, defining the geometry of the region of interest. In this thesis, the "domain" is the UVGI air inactivation reactor, including the inlet, outlet, UVGI sections.

Euler-Lagrange method: a method to solve the discrete phase dispersion in a fluid problem in CFD. With the Euler method, the fluid phase is treated as a continuum by solving the time-averaged governing equations. With the Lagrange method, the

discrete phase (the particles) is solved by a particle tracking method through the calculated flow field.

Finite volume method: also known as the "control volume method". The finite volume method is a popular numerical solutions technique in CFD modeling. Given a conservative flow property φ, the balance of various processes over a finite volume can be described as:

$$\begin{bmatrix} Rate\ of\ change\ of \\ \varphi\ in\ the\ control \\ volume\ with \\ respect\ to\ time \end{bmatrix} = \begin{bmatrix} Net\ flux\ of \\ \varphi\ due\ to \\ convection \\ into\ the \\ control\ volume \end{bmatrix} + \begin{bmatrix} Net\ flux\ of \\ \varphi\ due\ to \\ diffusion \\ into\ the \\ control\ voluem \end{bmatrix} + \begin{bmatrix} Net\ rate\ of \\ creation\ of \\ \varphi\ inside\ the \\ control\ volume \end{bmatrix}.$$

Grid: the geometry system built with the preprocessor of the CFD program. The computational domain is divided into sub-divisions, cells, or control volumes. The sub-divisions are smaller than the domain and do not overlap with each other. Grid is also called mesh. Hence, the process of building the grid system is called "meshing".

Governing equations: a serial set of equations that describe the mass, momentum, and energy conservation laws of the fluid flow.

Navier-Stokes equation: equations that describe the relations between the change of momentum for a finite volume and the forces acting on the volume.

1.2 Background

Recent incidents involving travelers with extensive drug-resistant tuberculosis (XDR TB) (CDC 2007) have raised public concerns about the spread of airborne contagious pathogens, such as tuberculosis (TB), in confined aircraft cabins and other public spaces. These concerns have led to an increasing need to develop effective air quality treatment units to eliminate the threats.

UltraViolet Germicidal Irradiation (UVGI) is regarded as an effective and safe method for indoor air-quality control. UVGI systems are widely installed in public places to prevent the spread of airborne pathogens and to protect vulnerable individuals from being infected by harmful microorganisms in air streams. According to the accepted theory, UVGI within a 200-300 nm wavelength range inhibits the multiplication of the irradiated microorganisms. UV photons within this wavelength range are readily absorbed by the microorganisms' DNA or RNA, resulting in the formation of lesions that inhibit DNA replication. Because no chemical addition is needed, UVGI is gaining more and more popularity in air quality control practice. According to different demands and installation requirements, UVGI systems can be categorized into room recirculation systems, microbial growth control systems, upper air disinfection systems and in-duct air disinfection systems. In-duct UVGI air inactivation systems offer a possible solution for controlling the spread of airborne contagious pathogens inside confined spaces. In these systems, UV radiation is contained inside the treatment unit, preventing the exposure of the occupants inside the confined space to dangerous UV radiation.

The characteristics of the factors affecting the in-duct UVGI system's inactivation efficiency make predicting the efficiency difficult. The microorganism inactivation efficiency of in-duct UVGI systems depends on the aerodynamic conditions inside the duct, the UVC output of the germicidal lamp, and the UV susceptibility of the target microorganisms. The aerodynamics determines the trajectories of the microorganism particles. The fluence (UV dose) received by microorganism particles is equal to the fluence rate times the exposure time, which of both are determined by the trajectories of the particles. The UV inactivation kinetics determines the inactivation level of a microorganism species exposed to a given fluence. For most microorganisms of interest, the UV inactivation kinetics can be described mathematically in an exponential or first-order rate form. The UVC output power of the lamp determines the fluence rate distribution inside the duct. The fluence rate distribution around a UV lamp is ruled by optical and radiation laws, which describe the non-linear, non-uniform distribution characteristics of the fluence rate in a three-dimension space. The complex aerodynamic conditions and the non-uniform fluence rate distribution along with the exponent kinetics of the UV inactivation process make it difficult to predict the microorganism inactivation efficiency of in-duct UV inactivation systems.

However, the accurate prediction of the inactivation efficiency is critical in a UVGI air inactivation system design. The difficulties in predicting the aerodynamic conditions, the fluence rate, and the fluence distribution in in-duct air inactivation systems are the main obstacles that must be overcome in order to rationally design these systems. The traditional design method and estimation of the volume average fluence rate and the average exposure time may lead to unreliable designs and performance

predictions. Similar difficulties exist in water and wastewater UV reactor design. To solve these difficulties, water-based UV reactor designers have introduced Computational Fluid Dynamics (CFD) modeling techniques to help improve the accuracy of the inactivation efficiency prediction. In water and wastewater UV reactor design, CFD can predict the fluid dynamics accurately. When integrated with the inactivation kinetics of the microorganism of interest, and a reliable fluence rate distribution model, a CFD model can simulate the physical conditions and biochemical reactions of a UV reactor in detail and can produce reliable predictions of inactivation efficiency. Compared to the traditional method, CFD simulation normally provides a more accurate prediction and gives the designer more details about and insight into the inactivation process. Due to the similarities between the air-based and water-based UV reactors, the CFD modeling technique may be a possible way to improve the inactivation efficiency prediction accuracy of the UVGI air inactivation systems.

1.3 Research Objectives

The main objectives of this research were to:

1. Develop a method for measuring the UV inactivation constants of a species of microorganism suspended in air to provide reliable UV inactivation rate constants for use in CFD simulations of an UVGI air reactor,
2. Construct an annular UVGI air disinfection reactor and measure its performance for inactivating airborne microorganisms under different flow rates and baffle conditions, and
3. Apply CFD modeling techniques to predict the inactivation efficiency of the UVGI air reactor and to compare the CFD predictions to measured performance.

1.4 Organization of the thesis

This thesis consists of 7 chapters. Chapter 1 provides the basic information on the application and design aspects of the in-duct UVGI air system and gives an outline of the research's scope. Chapter 2 reviews the factors affecting the in-duct UVGI air systems' performance and the design process, as well as the application of CFD modeling to UVGI indoor quality control systems. Chapter 3 details the methodology and experiments used to develop a well mixed batch reactor to measure the UV response of *Bacillus subtilis* spores suspended in air. Chapter 4 investigates the efficiency of the in-duct annular UVGI air reactor. Chapter 5 uses the UV inactivation rate constant measured in Chapter 3 and the bioassay results from Chapter 4 as inputs into the CFD model and validation data to verify the UV disinfection process simulation. Chapter 6 presents the conclusions for the work done in this research. Chapter 7 concludes the thesis by recommending possible research directions for future studies.

2 Literature Review

2.1 Bioaerosols and health concerns

Some microorganisms can form bioaerosols, and some species in the bioaerosol form pose threats to human health. Bioaerosols are ubiquitous in indoor and outdoor environments because they can be generated from various sources. Bioaerosols can originate from plants, water bodies containing microorganisms, and the respiration systems of animals and humans. Heating, Ventilation, Air-conditioning and Cooling (HVAC) systems and the building structures can be possible sources of bioaerosols when the environment is suitable for the growth of the microorganisms. Bacteria, fungi, virus, pollen and mammal allergens are the common aerosolized biological entities found in outdoor and indoor air (Burge 1995; Baron and Willeke 2001). In indoor environments, human activities, such as talking, coughing, and sneezing, can generate significant amounts of aerosols containing human pathogens (Baron and Willeke 2001).

The physical characteristics of a bioaerosol make it a possible disease transmission medium. Bioaerosol particles may be comprised of a single isolated microorganism cell, agglomerates of several microorganisms, fragments of the microorganism cells, or aggregates of microorganisms with other non-biological particles, such as dust particles. Bioaerosol particles often attach to water droplets. Because of evaporation, bioaerosols are comprised mainly of droplet nuclei which the water droplets reach a critical size and do not further decrease in size. Small nuclei with micrometer or sub-micrometer aerodynamic diameters can remain suspended for a very long time in air. Convection of the air causes the bioaerosols to spread inside a confined

space (Beggs 2003). The bioaerosols thus become a potential transmission vector in indoor environments if a pathogenic microorganism species is present within the bioaerosols.

Most aerosolized microorganisms are harmless to humans, but some can cause infection, fever, allergy, other diseases, and even pandemics. The transmission of potentially pathogenic microorganisms in bioaerosols is of great concern in an indoor environment with occupants with weak immunity systems, and with poor ventilation conditions. Even non-pathogenic microorganisms present in bioaerosol form, like *Bacillus* spp. spores, may cause severe infection in patients with large area burn wounds (Beggs 2003). Investigations have revealed that airborne transmission plays an important role in nosocomial (originating in a hospital) infections (Beggs 2003). Among the diseases carried and transmitted by bioaerosols, TB, smallpox, and influenza are of great interest because they are not only highly infectious, but may also be used as biological weapons by terrorists (Kowalski and Bahnfleth 2003).

2.2 UVGI air inactivation systems

The threat of outbreaks of highly transferable respiratory diseases such as avian flu, SARS, and TB has stimulated the invention and application of engineered indoor air treatment systems. Ultraviolet Germicidal Irradiation (UVGI) systems, air filtration purification systems, filtration and UVGI combination systems, electrostatic precipitation systems, and isolation systems are either commercially available or under development (Griffiths et al. 2005). UVGI air inactivation systems apply UV radiation with germicidal effects to inactivate microorganisms in the aerosol form. The key component of a UVGI

system is the lamp that emits the germicidal radiation. Low-pressure lamps and medium pressure lamps are used in UVGI systems. Based on their installation locations, applications, and configuration, UVGI air disinfection system can be further classified into various systems. Figure 2.1 shows the breakdown of the UVGI system types currently installed in buildings, basing on air UVGI manufacturers' data.

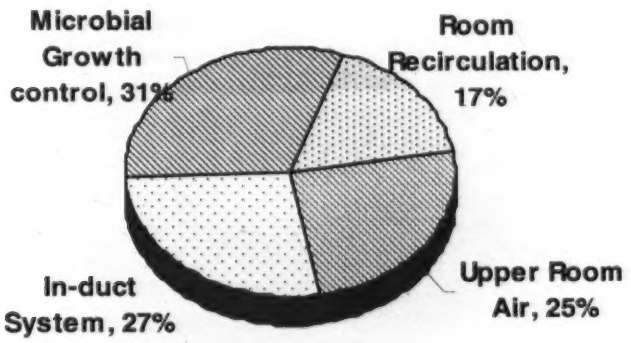

Figure 2. 1. Breakdown of currently installed UVGI air inactivation systems (Adapted from Kowalski 2001)

According to Kowalski (2001), in-duct UVGI air disinfection systems are one of the most popular UV disinfection systems installed in hospital wards and isolation rooms, HVAC ducts, and domestic homes. Figure 2.2 shows a typical induct UVGI air system installed in an air-handling unit. The two mayor types of in-duct UV air disinfection systems are the fixed type installed inside a HVAC system, and the portable type in which all the devices are built into a portable assembly.

Figure 2. 2 An in-duct UVGI system installed in an HVAC duct (Courtesy of Catalyx technologies)

Because of their configurations, in-duct UV inactivation systems are superior to other UVGI air disinfection systems in terms of system efficiency, occupant safety, and installation flexibility. An in-duct system can not only effectively inactive the pathogen microorganisms in the air, but also can prevent the growth of the molds and bacteria which can cause build-up problems in the HVAC system. In an in-duct UV air disinfection system, the UV lamps are enclosed in the duct, so that the UV light is retained inside the duct. No UV light is emitted that can harm the occupants close to the system. Compared to other UVGI disinfection systems, in-duct UV air disinfection systems are more compact and flexible. They can be installed in the upstream section of a HVAC system to treat the incoming air or be set up in the downstream section to disinfect the pathogen-laden air before it is released to the outdoor environment. Portable in-duct systems have even more flexibility. They can be placed close to a pathogen aerosol source to disinfect the air before releasing it into an ambient environment. These advantages lead to wide applications in various human occupied spaces, including hospital wards, hospital isolation rooms, office rooms, elevators, domestic homes and aircraft cabins. In a challenging experiment using MS2 coliphage, Griffiths et al. (2005)

verified that the inactivation efficiency of a commercial portable in-duct UV air inactivation system can reach 98.3% in the single-pass mode.

2.3 Mechanisms of UVGI inactivation of aerosolized microorganisms

The mechanisms involved in the inactivation process of airborne microorganisms with UVGI are similar to those involved in the water-based UV inactivation process. Ultraviolet germicidal irradiation (UVGI) in the 200 - 300 nm wavelength range can inactivate aerosolized microorganisms mainly by altering the structure of the deoxyribonucleic acid (DNA) and/or the ribonucleic acid (RNA) in the cell. After receiving sufficient UV exposure, the inactivated microorganisms may be alive, but they can no longer replicate. The ability to inhibit the reproduction of microorganisms at the DNA/RNA level is regarded as the main mechanism involved in the UV inactivation process, regardless of the medium (i.e., air or water).

The UV susceptibility of a species of microorganisms suspended in air is prone to change with the changes in the ambient environment. Relative Humidity (RH) and photoreactivation (PR) are the two main factors affecting the UV inactivation of airborne microorganism. Several studies investigating these two issues have been carried out (Ko et al. 2000; Peccia and Hernandez 2001; Peccia et al. 2001; Fletcher et al. 2003; Peccia and Hernandez 2004). Peccia et al. (2001) determined the UV inactivation constants of aerosolized vegetative *Serratia marcescens, Mycobaterium parafortuitum* and *B. subtilis* cells and *B. subtilis* spores in a flow-through UV reactor under different RH conditions. In the experiments of Peccia et al. (2001), spherical actinometry cells were placed evenly

throughout a 0.8 m^3 completely mixed UV reactor to measure the average fluence rate at those positions. The measured fluence rates from the spherical actinometry showed that, from 20%-95% RH, the changes of RH levels did not affect the fluence rate levels significantly. The inactivation rate constants from bioassay experiments showed that the UV inactivation constants of bacterial vegetative cells in an aerosolized state were a function of the RH in the ambient air. Although the inactivation rate constants for each species decreased as the RH level increased, the magnitude of the change differed from species to species. Six-stage Andersen impactors were used to collect the vegetative bacterial particles from the air stream under different RH levels to determine the aerodynamic diameters of the bacterial particles. The aerodynamic diameter data helped the authors understand the physiological changes due to the cellular sorption of water vapor. Based on the results from the physiological and bioassay experiments, the authors proposed the following hypotheses by to explain the phenomenon:

(1) the protein structure change during the RH fluctuation leads to a change in the performance of the DNA repair enzymes, and

(2) the hydration of nucleic acids and cell wall biopolymer also affects the susceptibility to UV.

Peccia and Hernandez (2004) later found that the UV inactivation constants of *B. subtilis* spores were not sensitive to the RH levels in the range of 20-95%. These researchers also found no significant difference between the UV inactivation rate constants of *B. subtilis* spores suspended in air and in water.

Photoreactivation (PR) is also a major factor affecting the UV susceptibility of aerosolized microorganisms. Visible light has the ability to stimulate the self-repair

mechanism of some aerosolized species. Fletcher et al. (2003) and Peccia and Heranandez (2001) exposed aerosolized *S. marcescens* and *M. parafortuitum* bacteria to visible light (using fluorescent lamps as light sources) during the UV inactivation process to study the role of photoreactivation. The experimental data from both studies showed that photoreactivation could significantly affect the UV susceptibility of the two bacteria species. The experimental data also showed that the photoreactivation rates were fluence and RH dependent.

The quantification of Cyclobutane Thymine Dimers (CTDs) in the bacterial cells helped the authors understand the mechanisms behind the RH effects and photoreactivation phenomena. CTD is a type of lesion in DNA caused by UV light which is known to undergo repair in cells. The authors proposed that the RH level in the ambient environment determines the hydration level of the aerosolized cells' DNA and its conformational changes. The type and number of DNA lesions induced by UV irradiation depend on the hydration level and the associated conformational changes. At lower RH, the dominant lesions in UV irradiated vegetative cells were found to be a spore photoproduct (SP). At a higher RH level (>75% for *M. parafortuitum* and *S. marcescens*), the major lesions are CTDs. CTDs and other types of photoproducts are known to have different repairing abilities; hence, the UV inactivation efficiency of aerosolized vegetative cells depends heavily on the number and types of lesions on the DNA.

However, Peccia and Hernadez (2001) pointed out that photoreactivation ability had not been observed in *B. subtilis*, in neither its vegetative nor its endospore forms. The aerosolized *B. subtilis* spore's insensitivities to UV irradiation, RH level, and photoreactivation will be discussed in more detail in Chapter 3 of this thesis.

Many tabulated first-order UV inactivation constant, k, (Kowalski 2000; Fletcher 2003; IUVA 2005a) of various species microorganisms include the RH values at which the constant is measured. See Table 1 as an example. Notice that an increase in RH is associated with either an increase or a decrease in the microorganism's sensitivity to UV, depending on the species.

Table 1. A UV inactivation constant table (IUVA 2005a)

Microbe	Medium	RH (%)	k (cm^2/mJ)	Source
Bacillus subtilis (vegetative)	Air	-	1.68	Nakamura 1987
Bacillus subtilis s(vegetative)	Water	-	0.919	Lojo 1985
Bacillus subtilis spores	Water	-	0.256	Homeck 1985
Bacillus subtilis spores	Water	-	0.134	Qualls 1983
Bacillus subtilis spores	Air	50	0.27	Peccia 2001
Bacillus subtilis spores	Air	55-85	0.2	van Osdell 2002
Bacillus subtilis spores	Air	95	0.25	Peccia et al. 2001
Mycobacterium parafortuitum	Water	-	0.08	Peccia et al. 2001
Mycobacterium parafortuitum	Air	50	1.7	Peccia et al. 2001
Mycobacterium parafortuitum	Air	95	1.0	Peccia et al. 2001
Serratia marcescens	Air	25-57	2.86	Kowalski 2001
Serratia marcescens	Air	-	7.49	van Osdell 2002
Serratia marcescens	Air	50	4.5	Peccia et al. 2001
Serratia marcescens	Air	95	0.65	Peccia et al. 2001

In most UV susceptibility studies of air-borne microorganisms, the single stage exponential model is often used to fit the UV response curve. The single stage exponential model is given as

$$S = e^{-kE't}, \tag{2.1}$$

where S is the surviving fraction of the microorganism population, k is the UV inactivation constant (cm^2/mJ), E' is the fluence rate (mW/cm^2), and t is the microorganism's exposure time (s) to the UV light.

As alternatives, the multi-target model and series-event models have been also used to model the microorganisms' response to UV radiance because of these models' ability to describe the shoulder characteristics that are often observed in the fluence-log inactivation level curve (Harm 1980) for some species. Severin et al. (1983) gave the mathematical form of the multi-target model as

$$S = 1 - (1 - e^{-k_m E't})^{n_c}, \tag{2.2}$$

where k_m is the UV inactivation constant (cm^2/mJ), and n_C is the number of the critical sites in the microorganism particles. According to the multi-target model hypothesis, each of the critical sites has to absorb sufficient UV light in order to inactivate a microorganism or a microorganism clump. In the single-hit multi-target assumption, n_C is then the number of these critical sites (Harm 1980). The possibility of a particle receiving sufficient hits by the photons increases as the fluence increases. After the fluence reaches a certain value, the log inactivation rate becomes first-order in respect to the fluence. Hence, the fluence-log inactivation level curve consists of a shoulder section at low

fluence, where there is little inactivation, followed by section where the log inactivation increases linearly with fluence.

2.4 Factors affecting the efficiency of UVGI air system

To design an in-duct UV air disinfection system, one has to consider the factors affecting its efficiency. These factors, identified in Figure 2.3, are the aerodynamic conditions that determine the mixing and velocity in the system, the lamps' germicidal radiant output, the fluence rate distribution in the duct, the UV inactivation kinetics of the target microorganism and the working condition of the ventilation system served by the in-duct system. The arrows in the radial diagram, Figure 2.3, indicate that some factors may affect other factors. Although Relative Humidity (RH) inside the UV duct does not affect the fluence-rate's spatial distribution, it can change the UV susceptibility of the target microorganism. The UV lamp's output may be affected by the air temperature, resulting in what is called the 'cooling/heating effect'. For mercury lamps, this cooling/heating effect affects the mercury plasma's pressure inside the lamp, hence changing the UVC output. The cooling/heating effect does not always decrease the lamp's output. In fact, it sometimes boosts the output (Kowalski and Bahnfleth 2000; IUVA 2005a). Figure 2.4. shows how the output of a typical low-pressure mercury UV lamp fluctuates with temperature changes. The output of the lamp in Figure 2.4 reaches a peak value at 40°C, denoted as 1.0. The output under other temperatures is a value relative to the peak value.

The values of the factors are determined by the HVAC system in which the UVGI air system is installed. Air velocity, RH and temperature values can be obtained from the HVAC system's design specifications. A UV lamp's germicidal output should be

measured under the working temperature. The fluence rate distribution in an UVGI system is often calculated by using appropriate models (Kowalski and Bahnfleth 2000) or is measured in a mock-up of the UVGI system (VanOsdell and Foarde 2002). UV reflecting materials can alter the fluence rate distribution if they are used to construct the UVGI system. The target microorganisms' inactivation constants should be measured under the RH level at the location where UVGI system is installed. An in-duct UVGI air inactivation system designer needs these values to size the system and predict the inactivation efficiency.

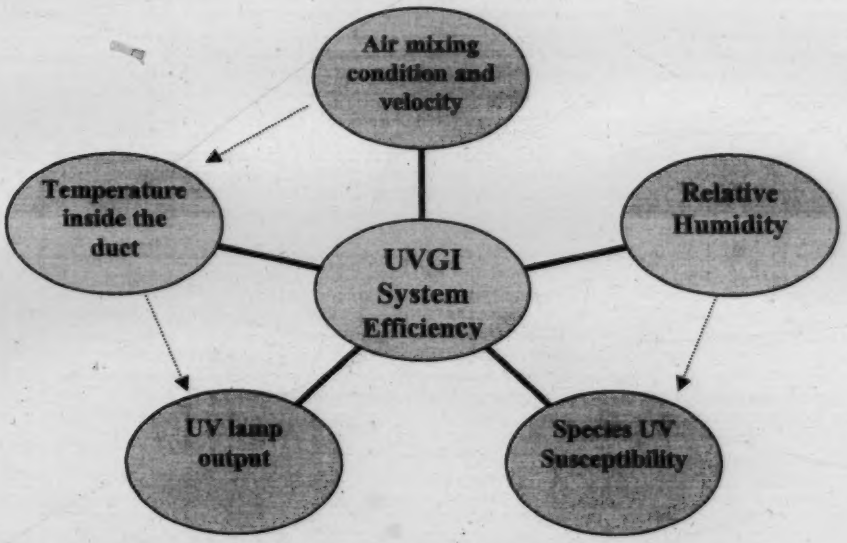

Figure 2. 3 Factors affecting UVGI system efficiency

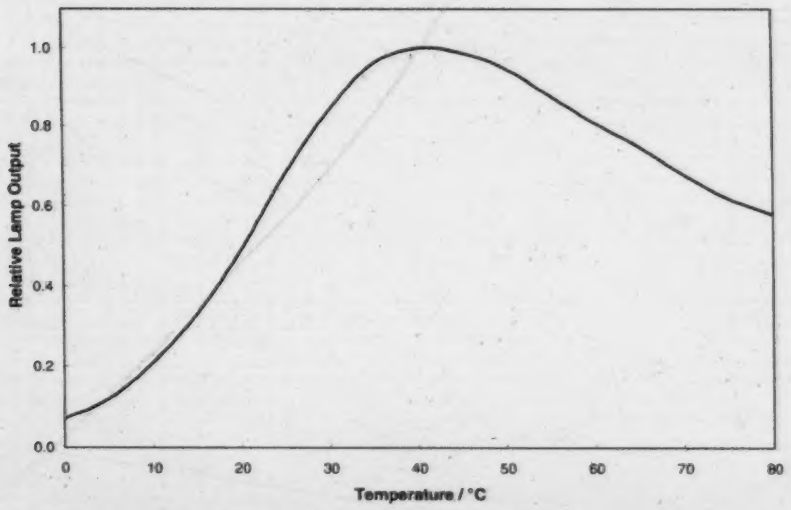

Figure 2. 4. Relative lamp UV light output of a low pressure lamp versus the ambient temperature. (Courtesy of Philips Lighting)

2.5 UVGI air system modeling

2.5.1 Components of a UVGI air disinfection system model

Once the factors affecting the performance of the UVGI system (described in Figure 2.3) are known, the inactivation efficiency can be predicted by inputting the values of these factors into an appropriate model. The mathematical models used to predict inactivation consist of several sub-models including a fluid dynamic model describing air flow through the duct, a fluence rate field model describing fluence rate spatial distribution, a model describing movement of microorganism particles in the UV field, and a UV inactivation model describing how a target microorganism reacts to fluence. Only the fluid dynamic model and fluence rate field model are independent of each other. The other models use the results from these two models as inputs or preconditions, as seen in Figure 2.5. The air fluid dynamic model determines the velocity profiles of the air passing through and the trajectory taken by the microorganism particles

inside the UV field. If the fluence rate spatial distribution within the duct is known, the fluence for each microorganism particle can be calculated by integrating the fluence along the trajectory of the microorganism. The efficiency of the inactivation then can be calculated by substituting the fluence into the UV inactivation kinetic model.

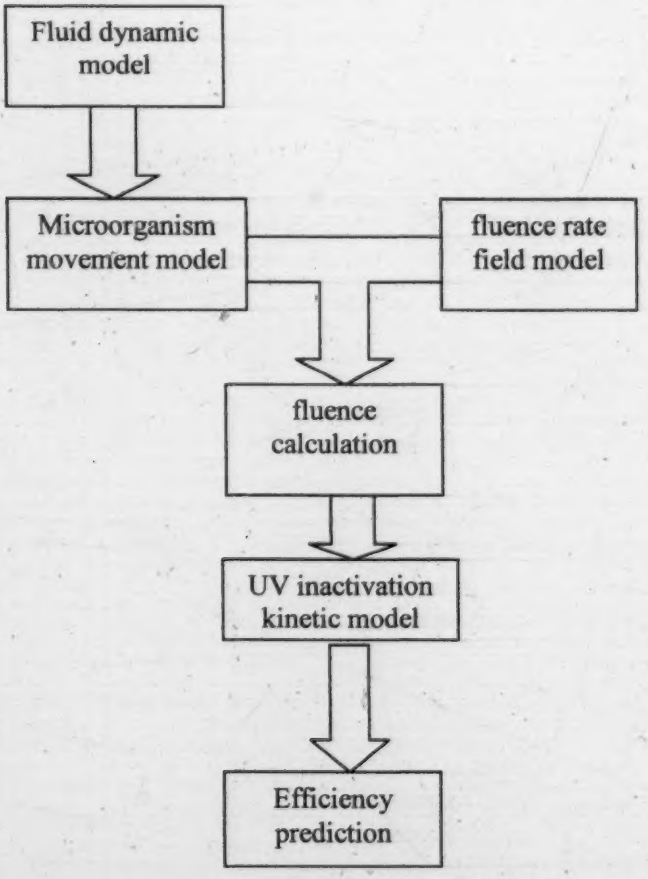

Figure 2.5. Sub-models in UVGI air disinfection system design and their relationships

When the fluence rate field is known, the fluid dynamic model is the key model for predicting the efficiency accurately. The more accurate the predictions of fluid flow and the velocity field in the UVGI system, the more reliable is the inactivation efficiency prediction. However, in design practice, the air mixing condition is unknown before the reactor is built, especially for complicated geometries. In UVGI air system design, completely mixed, multi-zone and CFD models have been used to model the flow conditions.

Designers often assume that the air inside the design geometry is completely mixed at the working air velocity. fluence is then the product of the volume average fluence rate and the average air retention time (Kowalski and Bahnfleth 2000). However, a completely mixed model for the air dynamics is an only rough approximation of the physical phenomena inside the UVGI system, especially when the geometry of the UVGI system is a complicated one with a gradient of microorganism concentration. This complete air mixing assumption does not account for the real air fluid regime inside the duct; therefore, the fluence received by microorganisms may be overestimated. This simplifying assumption ignores the possibility of flow short-circuiting and/or flow dead zones inside a UVGI system with complex geometry. The weakness in this simplified design approach does not give the designers enough confidence in the inactivation efficiency of their proposed in-duct UVGI air disinfection system.

Multi-zone models have also been used to evaluate the efficiency of upper-room UVGI systems (Nicas and Miller 1999; Xu et al. 2003; Peccia and Hernandez 2004; Noakes et al. 2004a). In a multi-zone model, the UVGI room is divided into 2 or 3 zones. The concentration of microorganism is assumed to be homogenous in each zone.

Microorganisms can travel from one zone to another at a certain velocity. The outcomes of the multi-zone model are average concentrations of the target microorganism for each zone. The division of the mixing zones inside a UVGI system is often arbitrary. Air velocities at the zone interfaces have to be measured or estimated before the UVGI room is built. A multi-zone model is superior to a single completely-mixed zone model in terms of the ability to account for the concentration gradient in a large room. However, the multi-zone model still cannot predict the dead zone or short circuiting that may occur in a real UVGI room. Neither the completely-mixed model nor the multi-zone model can give UVGI system designers more information to improve their design.

More complex models such as those built with Computational Fluid Dynamics (CFD) approaches (Alani et al. 2001; Noakes et al. 2004a; Noakes et al. 2004b; Noakes et al. 2006), attempt to describe the flow condition within the UVGI vicinity more accurately. CFD techniques have been used to produce a more rigorous description of the air-flow in a variety of physical systems. In CFD modeling, the fundamental mass, momentum, and energy balance equations of the fluid are solved numerically. These are coupled with a turbulence model in order to predict the velocity and kinetic energy fields and other transport properties of the fluid. With the development of low- computational-cost algorithms and high-speed computers, CFD applications are becoming more and more popular for solving chemical reaction and mass transport problems that involve the flow of fluids.

2.5.2 UVX program

Kowalski (2001) developed a sophisticated computer program, called UVX, based on mathematical models to predict the performance of an in-duct UVGI air disinfection system and to aid and optimize UVGI in-duct air disinfection system design. In his unprecedented work, not only the efficiency of the in-duct UVGI air inactivation system was modeled, but economical aspects of the UVGI system were also implanted into the UVX code. A fluence rate distribution model, called the view factor model, was chosen to calculate the fluence rate distribution field inside the UVGI air inactivation duct. However, because the aerodynamic equations were not included in the UVX code, the program was not able to model the flow regime accurately. Instead, the fluence was calculated for two flow condition extremes: one for the ideal plug flow and the other for the fully stratified flow. All particles that pass through an ideal plug flow reactor receive an identical fluence. Thus, the survival rate from an ideal plug flow should reach the upper limit of the inactivation efficiency. Meanwhile stratified flow represents the worst scenario case: no axial mixing but complete longitudinal mixing occurs in the duct, and the flow streamlines are assumed to be parallel. In the Kowalski (2001) study, the worst scenario case resulted in the lower limit of the predicted inactivation efficiency. The actual inactivation efficiency of the UVGI system was somewhere between the upper and lower efficiency predicted by these two extreme conditions.

For simple geometries, the UVX model can predict inactivation well. However, Kowalski and Bahnfleth (2000) pointed out, as the system geometry becomes more complicated, accuracy of the predictions decreases. When the lamps are shorter than the entire duct's width and length, the difference between the upper and lower limits

becomes particularly large. The large gap between the two efficiency limits (e.g., 30%-80%) makes the prediction of inactivation meaningless. Hence, Kowalski (2001) recommends the CFD method as a solution for UVGI air disinfection simulations.

2.5.3 Application of CFD in UVGI air disinfection system modeling

Application of CFD techniques in water-based UV disinfection process design has been extensively studied, but CFD application to UVGI air disinfection simulation has rarely been examined. Several recently published papers (Alani et al. 2001; Noakes et al. 2004a; Noakes et al. 2004b; Noakes et al. 2006) focus mainly on upper room UV disinfection systems, which are widely installed in hospital isolation rooms to prevent the spread of highly contagious pathogens such as TB. A review of the applications of CFD techniques in these UV disinfection systems can help to explain the relevant issues in UVGI air inactivation CFD modeling.

CFD modelers have tried different methods to predict the fates of the aerosolized microorganism particles exposed to UV light. Alani et al. (2001) treated the pathogens extracted by patients' coughs in an isolation room as individual particles. After being released from a cough, the particles were tracked along the air streamline predicted by CFD technique with a Monte Carlo method to account for the random turbulent variation. The cumulative fluence received by a particle was determined by integrating the fluence along the particle path. The UV intensity field was modeled by using a data set supplied by the UV lamp manufacturer, but the authors did not clearly explain how the data were generated. The UVGI decay model used by Alani et al. (2001) differs from the common ones presented in formulas (2.1) and (2.2) in this thesis. Instead, a fluence level is set as the maximum tolerance fluence for the microorganism particles. Once the tolerance

fluence (in this case, the value is 500 $\mu J/cm^2$) is reached, the particles are considered to be killed. Two-thousand and seven hundred particles were released into the reactor in the CFD simulation. Particle tracking was conducted under different ventilation rates, various inlet and exhaust arrangements, and fluence rate levels to evaluate the UVGI effects in the ventilated room. After each particle was released for 300 seconds, the particles were classified into 3 bins according to their fates: killed, ventilated (escaped the room through the ventilation system) and alive. By comparing the numbers of the particles killed or ventilated, the best UVGI ventilated room design can be chosen.

Noakes et al. (2004a) used a passive scalar method to model the air-suspended microorganisms in their upper room UVGI system CFD simulations. Because of their small sizes (aerodynamics diameter of several micrometers or less), aerosolized microorganism particles can remained suspended in the air for hours (Baron and Willeke 2001; Beggs 2003). In the experiment of Noakes et al. (2004a), the movements of the suspended particles were driven by the air flow and the particle concentration gradient. The distribution of the microorganism particles in air, therefore, was treated as a passive scalar. The model remained as a single-phase problem with a scalar representing the viable microorganism concentration. For a finite control volume in a CFD model domain, let φ denote the scalar representing the concentration of viable microorganisms in CFU/m^3, assume that the UVGI inactivation obeys first-order reaction kinetics as described in Equation (2.1), and also assume that the air at low velocity and low ambient pressure is an incompressible fluid; then the viable microorganism concentration scalar transport equation is given as:

$$\frac{\partial \varphi}{\partial t} + div(\vec{U}\varphi) - div[\Gamma grad(\varphi)] - kE'\varphi = 0, \qquad \textbf{(2.3)}$$

where:

φ is the concentration of the viable microorganism (CFU/m^3),

$\vec{U}$ is the velocity vector of the air control volume, (m/s),

Γ is the kinematic diffusion coefficient (m^2/s),

k is the first-order UV inactivation constant (m^2/J),

E' is the fluence rate at the centroid of the control volume cell.

Equation (2.3) was solved with the other governing momentum, turbulence and energy equations based on finite volume methods in the CFD code. By introducing the passive scalar to represent the concentration of microorganisms in air stream, with the visualization tools in CFD code, a designer can see the interaction between the UVGI and the microorganisms. The contour map of the microorganism concentration can actually help the designer visualize the viable microorganism distribution inside a UVGI room. The designer could move the location of the UV lamps, rearrange the inlet or exhaust configuration, change the air-exchange rate, and even adjust the furniture layout in the room to increase the inactivation level and avoid blind zones (i.e., zones where the fluence rate is low). Compared to the traditional multiple mixing zones method in which the UVGI room is divided into two or three complete mixed zones, the CFD simulation not only predicts the overall inactivation level by UVGI device and ventilation system more accurately, but also provides the designer with more details on the expected air flow pattern in the UVGI-ventilation system.

Noakes et al. (2004b) continued to use the same concentration scalar method to simulate the UVGI inactivation efficiency in a flow-through apparatus. Although the

aerodynamic model was not validated against any experiment measurement or analytical solutions (Noakes et al. 2004b), the CFD predictions of the microorganism inactivation levels were very close to the results of bioassay experimental data.

Noakes et al. (2006) later used an alternative CFD method to assess upper room UVGI inactivation efficiency. A scalar was introduced to present the accumulative fluence F received by the bulk air flow through the UVGI room. For a control volume, given the fluence rate E', the rate of change of the fluence F is $\frac{dF}{dt} = E'$. The transportation equation governing the accumulative fluence is given as

$$\frac{\partial F}{\partial t} + div(\vec{U}H) - E' = 0, \qquad \textbf{(2.4)}$$

where F is the cumulative fluence of the bulk air received in the UVGI field in J/m^2. The other symbols have the same meanings as in (2.3). The difference between equation (2.3) and (2.4) is that (2.4) has no diffusion term because cumulative F is not a physical property that moves along a gradient. As a benefit from introducing a cumulative fluence scalar, the fluence distribution inside the UVGI field can be predicted independently of the inactivation level of a specific microorganism species.

2.6 Research statement and the need for this research

The UV inactivation constants of microorganisms suspended in air are critical parameters for sizing UV air disinfection systems and for use in CFD modeling. However, the measurements of the UV inactivation constants reported in the literature have been carried out by using different methods and apparatuses (Miller and Janet 2000;

Peccia and Hernandez 2001; Fletcher et al. 2003; Xu et al. 2003). This practice makes it difficult to compare and reproduce experimental results. In this present research, the method and apparatus which have been widely accepted and used in developing fluence-inactivation level curves of microorganisms suspended in water were adapted to measure the UV inactivation constants of a species of microorganism (*Bacillus subtilis* spores in this case) suspended in air. Similar to the batch reactors in the water-based UV inactivation studies, a batch reactor was constructed. A collimated beam system, which is normally used in water or wastewater UV inactivation studies, was used as the source of UV light in this study. By using this apparatus and methodology, the UV inactivation constants could be readily measured.

In current in-duct UVGI air disinfection system design, the flow regime inside the system is treated as a plug flow with complete radial mixing across the fluence rate gradients. The volume-averaged fluence is calculated, and the fluence (UV dose) is determined by multiplying the average fluence rate by the theoretical retention time. A UV inactivation kinetics model is then used to predict the system's overall efficiency. However, the plug flow assumption is not accurate for all cases. When the UVGI in-duct system has a complicated geometry such as a curvature feature or baffles, flow short circuiting, dead zones or UV blind zones can occur. This problem in the completely-mixed model hinders the accuracy of the efficiency prediction in UVGI design.

In order to improve the in-duct UVGI air disinfection design, a CFD technique was used to simulate the inactivation process in a prototype UVGI air disinfection system. Compared to the current techniques (Kowalski and Bahnfleth 2000) used in UVGI air disinfection system design, the CFD technique can simulate the flow regime at

a very detailed level. The local flow conditions in the UVGI air disinfection reactor can be predicted by the CFD simulation. A 3D UV lamp fluence rate distribution model can predict the fluence rate inside the UVGI system accurately. The UV inactivation kinetics model can then be used to predict the efficiency of the UVGI inactivation effect by using the local fluence rate as an input. Visualization tools like contour map drawings can show the flow regime and the inactivation effects at every point in the UVGI in-duct system. This study is the first attempt to model the in-duct UVGI air inactivation system by using the CFD technique.

The validation of the CFD simulation results is as important as the results themselves. In order to simulate the physical biochemical phenomena numerically, one has to make many assumptions and approximations. From assumptions about inlet boundary profile initiation to the turbulence model, many assumptions are made. The discretisation and iteration solutions of the fluid dynamic equations also can make the simulation results uncertain. The discrepancy between the simulation results and the physical and biochemical reality should be studied. Validation by using parallel experimental data or analytical solutions should be used to gain confidence in CFD modeling. In this research, a bench-scale annular in-duct UVGI air inactivation reactor was built, and its efficiency for microorganism inactivation was measured experimentally. The results of the CFD modeling of the UVGI reactor were compared to data from microorganism challenge experiments that were conducted at different air flow rates and baffle conditions.

3 Determination of the UV Inactivation Constants of Aerosolized *Bacillus subtilis* Spores

3.1 Introduction

3.1.1 Studies on UV susceptibility of aerosolized microorganisms

Due to its ability to inactivate aerosolized microorganisms, Ultraviolet Germicidal Irradiation (UVGI) at 254 nm is widely accepted as an effective inactivation technique in indoor air quality control. The study of the UVGI inactivation kinetics is important and has been carried out in various ways. The parameters in mathematical UV inactivation kinetics models that describe how a species of microorganism responds to the fluence are called UV inactivation constants. In UVGI air inactivation system design, the target species' UV inactivation constants are critical parameters in sizing the system, and the sizing determines the power of the UV lamps under certain flow and other running conditions. Without a standard testing protocol, aerosolized microorganism UVGI inactivation kinetics studies for the determination of UV inactivation constants have been carried out by using various methods and apparatus. Recent work (Miller and Janet 2000; Peccia and Hernandez 2001; VanOsdell and Foarde 2002; Fletcher et al. 2003; Xu et al. 2003) showed the diversity of methods and apparatus in the aerosolized microorganism UV inactivation studies. Table 2 summarizes the recent studies in terms of the apparatus and the fluence rate measurement methods used.

Table 2. Recent aerosolized microorganism UV susceptibility studies

Source	Flow apparatus and flow regime	Fluence measurement
Miller and Janet (2000)	Completely mixed 2-zone room (36 m^3) with ventilation	12 point radiometer readings to estimate the average fluence
Peccia et al. (2001)	Pilot scale completely mixed flow cubic chamber (0.8 m^3)	25 KI/KIO_3 actinometry spherical quartz cells to measure the average fluence
VanOsdell and Foarde (2002)	ASHRAE full-scale test rig (95L)	Radiometer reading in a test rig mock-up
Fletcher et al. (2003)	Pilot scale flow through chamber (4L)	Radiometer reading through an access port to estimate the fluence
Xu et al.(2003)	Complete mixed room (87 m^3) with ventilation	20 spherical actinometry cells and radiometer readings to measure the average fluence

The researchers in these studies had to face challenges in terms of UV inactivation efficiency measurements, fluence calculations, and flow condition controls. These experiments covered not only the microorganism losses due to UVGI inactivation, but also the ventilation losses and deposition losses. To obtain the 'pure' UV inactivation constants, experiments were carried out in such a way that losses, other than those from UV inactivation, could be measured and deducted from the overall inactivation level. Measuring the volume average fluence rates in these UV apparatuses is very challenging. For the UV light source, UV lamps were installed in these apparatuses and resulted in spatially non-uniform fluence rates inside the apparatuses. The fluence rate measurements were often conducted by measuring a number of points in the UV irradiation field, from which the volume average fluence rates in the UV field were calculated. Radiometry and spherical quartz actinometry were the two common methods

used for fluence measurements. Since several factors in the radiometer reading method affect the reading accuracy (Severin and Roessler 1998), conversion of the irradiance rate from radiometer reading to the fluence rate at a spatial point was very difficult. The published papers do not show clearly if and how the radiometer readings were corrected. In order to calculate the fluence received by the aerosolized microorganisms, assumptions were made in these studies that the air in the irradiation zone was completely-mixed. Circulation fans were even installed in the apparatus to provide completely mixed conditions. In a completely mixed UVGI chamber, the fluence received by the air suspended microorganisms is the product of the volume averaged fluence rate and the theoretical retention time. How the mixing assumption affecting the measurement accuracy is unknown.

Some researchers have tried to set up a standardized protocol for UVGI air inactivation constant measurement. This protocol differs from that used in water-based studies. In the 'Standard for Laboratory testing of UVGI Air and Surface Rate Constants' proposed by the UV Air Treatment Topical Group of the International Ultraviolet Association (IUVA 2005a,b), a laboratory apparatus is recommended to match or scale down the full-scale air-handling units to simulate the environment of the working condition of the full-scale unit. By doing so, a susceptibility study can account for the effects of the UV inactivation and other physical and self-decay losses. This proposed standard differs from the standard protocol used in waterborne microorganism UV inactivation kinetic studies. In these water-based studies, a standardized protocol (Bolton and Linden 2003) has been widely being used, in which a Petri dish is used as a completely mixed batch reactor to hold the microorganism suspension in the collimated

UV radiation field. The fluence rate can be easily measured, and the fluence can be readily calculated. Moreover, a UV inactivation kinetic study is independent of the geometry and fluid regime of any UV reactor. This reactor independency is of great value in UV reactor design, especially when the Computational Fluid Dynamics (CFD) simulation technique is used to model the reactor.

In this study, the standardized protocol from water susceptibility studies was adapted to use a similar method and apparatus to determine the UV inactivation constants for *Bacillus subtilis* spores suspended in air. A well mixed batch reactor was built, and a collimated beam was used as the UV light source.

3.1.2 Aerosolized *Bacillus subtilis* spores

As an important surrogate organism in UV disinfection bioassay investigations, *B. subtilis* spores have been used extensively because of their relatively high resistance to UV exposure and biological stability in harsh environments. In order to survive harsh environments, in which critical nutrients are often absent, *Bacillus subtilis* vegetative cells produce endospores. A spore cell consists of several layers that protect the inner core of the spore cell from the outer environmental stress. The low water content (27-57 %) in the inner core plays an important role in reducing enzyme activities in spore cells (Setlow 2006). As a result of the multi-layer structure and the other dormant mechanisms, spores in a dormant state have a consistent metabolic behavior and consistent responses to disinfectants regardless of the ambient environmental change. In fact, aerosolized *B. subtilis* spores are so biologically stable that they have been widely used as a physical tracer or a stable biological reference to account for physical losses in aerobiological studies (Miller et al. 1961; Ehrlich et al. 1970a, 1970b; Marthi et al. 1990).

The survival of the UV irradiated aerosolized *B.subtilis* spores is not sensitive to the ambient relative humidity (RH) level and the presence of visible light. This feature of *B. subtilis* spores is supported by experimental data (Peccia and Hernandez 2001; Peccia et al. 2001; VanOsdell and Foarde 2002) and can be explained by theories proposed by Peccia and Hernandez (2001) and Setlow (2006) involving DNA lesions and their effect on the repairing mechanisms. It has been proposed that the types of lesions in the UV irradiated DNA and the repairing mechanisms are the major reasons that make *B. subtilis* spores differ from vegetative cells in terms of UV inactivation. Three main lesions generated in UV irradiated spores are cyclobutane dimmers (CPDs), 6-4-photonproducts (64PPs), and so-called "spore photoproducts" (SPs) which dominate in the wild *B. subtilis* spore cells after UV exposure (Setlow 2006). SPs were also found to be dominant in UV irradiated vegetative cells at lower RH levels (Peccia and Hernandez 2001). However, the unique SP repair mechanism by the SP lyase (Spl) enzyme exists only in spore cells. This unique repair mechanism mainly contributes to the spore's high resistance to UV exposure in spite of the RH level changes.

Because of its unique UV susceptibility, sporulated *B. subtilis* was selected as the challenge microorganism in this UV air inactivation study. The use of *B. subtilis* spores can simplify later studies on annular UV air treatment system bioassays and modeling. It was assumed that inactivation constants measured in a specific RH condition can be extrapolated into other RH ranges. However, in this research, although the inactivation constants are less likely to be affected by the RH level, two sets of experiments at two different RH ranges were conducted to demonstrate that the well mixed batch reactor can be used to study other microorganisms' UV susceptibility under different RH conditions.

3.2 Materials and Methods

3.2.1 Culture and enumeration of *Bacillus subtilis* spores

Bacillus subtilis spore culture

Bacillus subtilis spores (ATCC 6633) were cultured by using the Modified Schaeffer (MS) method. Frozen dry *B. subtilis* was pre-cultured in a 100 mL nutrient solution. The components of the nutrient broth solution are 8.00 g/L, $MgSO_4 \cdot 7H_2O$; 0.25 g/L, KCl; and 1.00 g/L Peptone (Fisher Sci. Canada) The flask was put into a shaker incubator (Innova, New Brunswick Sci) to re-hydrate the frozen dry *B. subtilis* spores for 24 h at 37.5°C at 180 rpm. In the biohazard fume hood, 1 mL of pre-cultured *B. subtilis* suspension was then inoculated into Modified Schaeffer (MS) nutrient media with the nutrients constituting $FeSO_4$ (1 μM), $MnCl_2$ (10 μM) and $CaCl_2$ (1 μM). The baffled flasks were put into the shaker incubator to culture the spores for 24 h at 37.5°C and 180 rpm; the culture was allowed to grow for 15 days.

Spore stain was used to verify the domination of the spores in the nutrient media. 5% Malachite green and 1% Safranin red stain solutions were used to stain the samples on a slide for 1 min and 30 s, respectively. The slide was then observed with a microscope to determine the domination of the spores. Spores are green and vegetative cells are red. Once the spores dominated the culture MS media, a centrifuge (Sorvall Refrigerated Superspeed Centrifuge, Mandel Sci.) was used to harvest the spores (centrifugation time 20 min at 7500 rpm). An 80°C water bath was used to kill the vegetative cells. The *B. subtilis* spores were stored in 50% ethanol in a 1L autoclaved bottle.

***Bacillus subtilis* spore enumeration**

A pour plate method was used to enumerate the concentration of spores in the collecting liquids in the impingers. In order to avoid any photoreactivation of the damaged spores, the impingers were wrapped with aluminum foil to keep the spore suspension in the dark. 9 mL of 0.1% autoclaved Peptone (Fisher Sci. Canada) solution was transferred into each glass tube. A serial of 1/10 dilutions of the sample were made by transferring 1 mL of the sample into the 9 mL of the peptone solution. 15 mL of Nutrient agar (8 g nutrient broth powder, 16 g agar, 1 L MilliQ® water) was transferred to each glass tube. The tubes filled with autoclaved agar were kept in a water bath at 50°C. 1 mL of the desired dilution sample was transferred into a 100 mm culture dish (Fisher Sci.). A methane flame was used to sterilize the top of the agar tubes. The agar was poured into the dish which was tilted until the agar-sample mixture was evenly distributed in the plate. The agar took 3 to 5 min to solidify.

Culture dishes with caps on were put into the incubator (Forma Series II, Thermo, USA) upside down to incubate for 36 hrs. The solidified agar maintained the spores in their positions. The colony forming units (CFU) in the culture dishes were counted. The valid range of the CFU counting was 30 to 300. For high log reduction rates, a CFU count below 30 was also treated as a valid count.

3.2.2 Nebulizer and impingers

Nebulizer

A Nebulizer (Collison 3-jet; BGI Inc., Waltham, Mass.) was used to generate the aerosolized microorganisms in this study. Nebulizers are commonly used in biological

aerosol studies to aerosolize the microorganisms. Jets inside a nebulizer work like micro-scale Venturi pumps. The microorganism suspension is sucked into the jets from the suspension reservoir due to the sudden pressure drop. Water droplets and microorganism aggregates are released from the jets at very high speed. Large droplets are deposited back on the suspension reservoir while the fine droplets escape from the outlet of the nebulizer (May 1973). More than 95% of the particles emerging from the nebulizer have an aerodynamic diameter of 0.9 μm (May 1973), which is the average aerodynamic size of *B. subtilis* spores (Baron and Willeke 2001).

Impingers

Several bioaerosol particle samplers are available in the market. The all glass impinger (AGI) and the Andersen sampler are recommended as the best two bioaerosol particle samplers because of their high biological efficiency in sampling (Baron and Willeke 2001). For this study, the impinger was chosen as the sampler for its low-collection-flow rate and simplicity in enumeration. Midget impingers (Standard Midget, Supelco Inc.) with 25 mL reservoir capacity were used because of the low spore concentration in the air trapped in the well mixed batch reactor.

The flow rate at which an impinger collects the bioaerosol particle is a critical parameter. Particles are removed from the air stream by inertial impaction into the liquid in the impinger reservoir. The flow rate determines the particle velocity released from the impinger nozzle. The high velocities of particles cause the particle trajectories to divert away from the air streamline and allow the particles to enter into the collecting liquid. For an AGI-4 type impinger (in which the nozzle tip to the bottom of the reservoir is 4 mm), the nominal sampling flow rate is 12 L/min. However, in biological particle sampling,

such a high flow rate may affect the culturability of the microorganisms. A high air-flow rate can also cause the former collected particles in the reservoir to re-aerosolize. To balance the collection efficiency and biological recovery rate, the impingers can be run at flow rates lower than the nominal critical flow rates. Figure 3.1 shows how the flow rate and collecting liquid volume in the impinger reservoir affect the impinger's sampling efficiency (ACGIH 1999). In this UV susceptibility study the collecting flow rate for the Midget impinger was controlled at 8 L/min, and the liquid in the reservoir was 5 mL. Figure 3.2 shows the photos of the nebulizer and impinger used in this research.

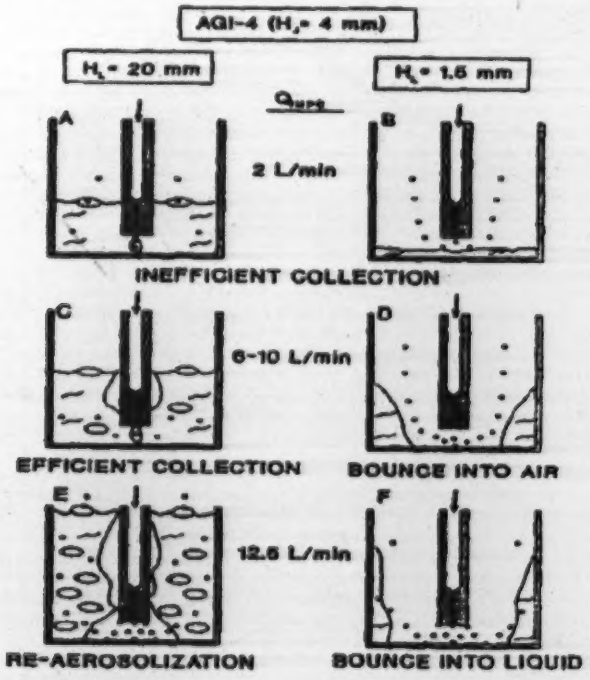

Figure 3. 1. Impinger efficiencies under various sampling flow rates and collecting liquid volumes (ACGIH 1999)

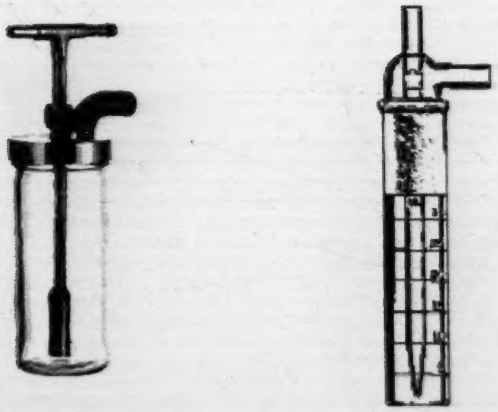

Figure 3. 2. Photos of the 3-jet nebulizer(left) ; and a standard Midget impinge

3.2.3 Collimated beam and the well mixed batch reactor

Construction of the well mixed batch reactor

A bath reactor was built from a 20 cm long PCV duct with an internal diameter of 100 mm. The bottom of the duct was sealed with a PVC plate as the reactor base. A small fan (12 VDC, Brushless, Taiwan) was installed on the bottom plate to mix the aerosol inside the duct. The top of the duct was sealed with a quartz plate (11 cm × 11 cm). Various ports were drilled into the duct, including the aerosol inlet port, the dry air inlet port, the sampling/waste outlet port, the flushing air inlet port, and the Relative Humidity (RH) probe port. Swage-lok® fitting and PVC valves (Edmonton Valves and Fittings Inc., Edmonton AB, Canada) were installed onto these ports and connected with Teflon tubing to the air supply's sources and impingers. Two types of impingers were used in the system. A Midget impinger (Standard Midget, Supelco Inc.) with 5 mL D.I. water was used as the sampling impinger to collect the spores from the air. A bubbling impinger (500 mL Pyrex®, Fisher Sci.) was used as the waste vessel to collect the spores in the effluent air. The nebulizer was driven by a compressed air cylinder (Extra-dry, Praxair,

Edmonton, AB, Canada) with a 2-stage regulator (Fisher Sci. Canada) to generate the spore aerosol. A barometer (Winters®, Cole Palmer Inc.) and a flow meter (Cole Palmer Inc.) were installed in the Teflon™ tubing to monitor the pressure condition of the nebulizer and the flow rate. Dry air was supplied by another compressed air cylinder (Extra-dry, Praxair, Edmonton, AB, Canada) and controlled with a 2-stage regulator, to dilute the water-saturated air from the nebulizer to the designated relative humidity level. A flow meter (Watchman II, Cole Palmer) was also used to monitor the dry air-flow rate.

The well mixed batch reactor was placed in the UV-beam position of a collimated beam system (Rayox®, Calgon Carbon Corporation, USA), in which a low-pressure mercury arc lamp (G12T6L, Atlantic Ultraviolet, USA) was used as the UV source. The construction schematic of the well mixed batch reactor is shown in Figure 3.3.

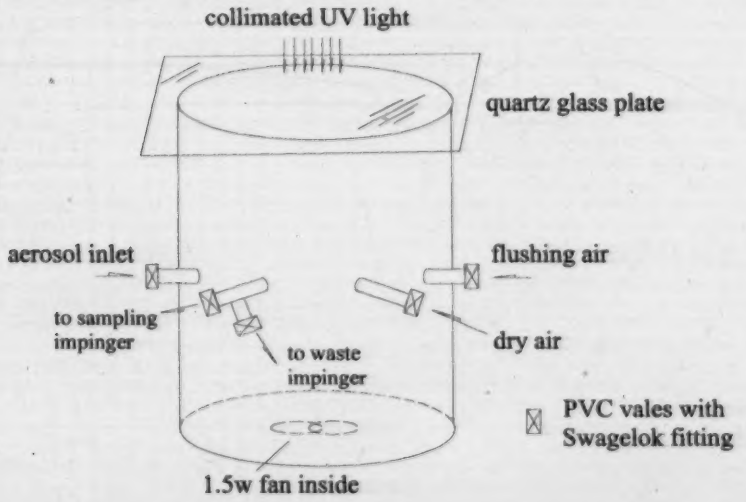

Figure 3. 3. Schematic of the well-mixed collimated beam batch reactor

3.2.4 Fluence (UV dose) calculation in the well-mixed batch reactor

Following the protocol of Bolton and Linden (2003), four critical factors are involved in the calculation of the average fluence rate inside the well-mixed batch reactor: the Petri dish factor, the divergence factor, the reflection factor and the media factor.

Petri dish factor F_{petri}

The Petri dish factor is a concept used in collimated beam testing in waterborne microorganism inactivation studies. It describes the non-uniformity of the UV irradiance rate at the Petri dish surface. In this case, the Petri dish factor is defined as the ratio of the average fluence rate passing through the quartz plate of the well mixed batch reactor to the fluence rate at the central point of the top quartz plate. The Petri dish factor was determined by using the grid-reading method (Bolton and Linden 2003) with a radiometer (Model P-9710 with detector UV3718, Gigahertz-Optik, Germany). A 0.5 × 0.5 cm orthogonal grid was drawn, and the centre of the grid was placed at the centre of the collimated beam. The two orthogonal lines passing through the central point (origin point) were denoted as the 'x' and 'y' axes. The radiometer probe was used to read the incident irradiance at each of the grid nodes. Irradiance readings were carried out from -4.5 cm to +4.5 cm on both the 'x' and 'y' axes. All the reading values were normalized to the value at the central node. The Petri dish factor F_{petri} is given by

$$F_{petri} = \frac{\sum \text{Readings at Grid nodes}}{\text{Reading at centre} \times \text{number of nodes}} . \qquad (3.1)$$

Divergence factor F_d

The divergence factor was determined by applying the inverse square law along the collimated beam path (Bolton and Linden 2003). According to this law, the ratio between the irradiance at $L + x$ distance from the lamp to the irradiance at L distance from the lamp is $\frac{L^2}{(L+x)^2}$. If L (in cm) is the distance from the lamp to the cap of the reactor, and dx represents the distance increment along the reactor height, the divergence factor $F_d = \int_0^H \frac{L^2}{(L+dx)^2} dx$. For a reactor height of D cm, the divergence factor can be integrated as

$$F_d = \frac{L}{L+D}. \tag{3.2}$$

Reflection factor F_r

The reflection factor was measured by conducting KI/KIO_3 actinometry tests. Dishes with a diameter of 91 mm and 8 mm depth were used to hold the actinometry solution mixed by a Teflon coated 3 mm × 12 mm magnetic stirring bar. The solution was exposed to UV radiation with and without the batch reactor cap covering above the Ø91 mm dishes for the same exposure time. The ratio of the irradiance values from the actinometry tests under the two cover conditions is the reflection factor of the quartz cap.

$$F_r = \frac{\text{irradiance without quartz cap}}{\text{irradiance with quartz cap on}}. \tag{3.3}$$

A medium factor is not applicable in this case because the absorbance in air within the testing relative humidity range for UV irradiance at 254 nm is negligible. The average fluence rate in the well mixed batch reactor is given by

$$E'_{avg} = E'_0 \times F_{Petri} \times F_r \times F_d . \quad (3.4)$$

where E'_0 is the incident fluence rate, as read by the radiometer with the detector placed at the center of the quartz plate (mW/mJ); F_{Petri} is the Petri factor; F_r is the reflection factor, and F_d is the divergence factor. Figure 3.4 shows the well mixed batch reactor-collimated beam system used in this study and the principles in determining the three factors. The average fluence (mJ/cm^2) delivered inside the batch reactor is then the product of E'_{avg} and the exposure time (s).

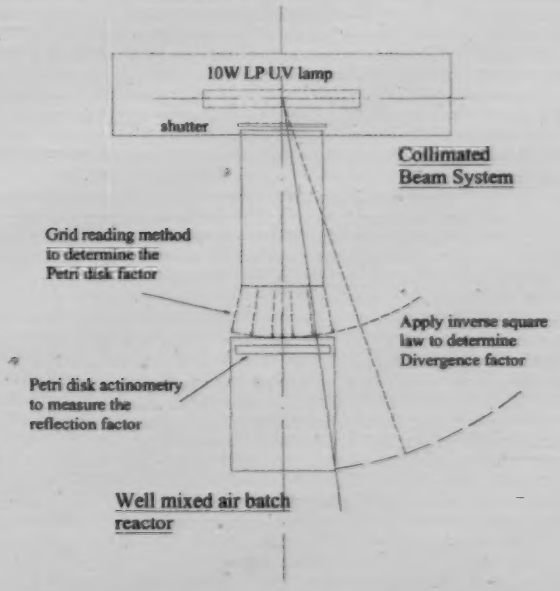

Figure 3. 4. Well mixed -collimated beam batch reactor system use for UV inactivation rate constant measurement

3.2.5 Inactivation tests

Inactivation tests of the aerosolized spores were performed under two relative humidity ranges: 50 to 60% and 70 to 83%. The well-mixed air batch reactor was run in a batch mode to measure the UV inactivation constants of the *B. subtilis* spores. Spore-laden air was trapped in the well mixed batch reactor for a designated time with or without UV radiation. Spore-free dry air from the flushing port was then injected to direct the spores toward the sampling impinger for collection. The inactivation levels were determined by enumerating the number of spores collected in the sampling impingers. If N_{off} is the number of viable spores in the 1 mL impinger liquid when UV radiation is off, and N_{on} is the corresponding number when the UV radiation is on for a desired time length t, the log inactivation level is $\log S = \log (N_{on}/N_{off})$. For every fluence level, N_{on} and N_{off} were measured with the same batch of spore suspension in the nebulizer. Triplicate samples were taken to determine N_{on} and N_{off}.

The inactivation experiments were run for two RH ranges: 50-60% (±3%), which is the typical relative humidity in living rooms (IUVA 2005b). The other RH range was set to be 70-83% (±3%) to determine how the RH level affected the UV inactivation to the spores. For each RH level, the entrapped spores were exposed to a different fluence by controlling the UV exposure time. The flow rates and the running conditions of the well mixed batch reactor are recorded in Table 3. The RH conditions were controlled by adjusting the ratios of the dry air to the saturated air from the nebulizer. The Relative Humidity meter probe (RH411 Thermohygrometer, Omega Inc.) was plugged into the batch reactor to measure the RH in the batch reactor. The experiments were carried out

in a well ventilated BioSafe Level 2 room with the room temperature ranging from 20 to 22°C.

Cross contamination is a major concern in these inactivation tests. In order to prevent residual spores from being trapped in the batch reactor and in the valves and tubing, UV light was used to disinfect the residual spores in the well mixed batch reactor for 10 min between the samplings, and high velocity (15 L/min) spore-free dry air was used to flush the well mixed batch reactor, valves and tubing.

Table 3 Flow rate and other experimental conditions in the UV inactivation constant measurement experiments

Condition	Dry air flow rate (L/min)	Nebulizer flow rate (L/min)	Relative humidity (%)	Sampling flow rate (L/min)
1	3.5	2.5	50-60%	8
2	1.2	2.75	70-83%	8

3.2.6 Model fitting

As discussed in the literature review section, the first-order kinetic model and a multi-target model [equations (2.1) and (2.2)] are the two most popular models used to describe a microorganism's response to UV light. Uvbiama (2005) used the multi-target model to describe the UV inactivation kinetics of the aggregated *Bacillus subtilis* spores in water. Since the spores used in this study and the ones used in the Uvbiama (2005) study were cultured from the same mother stock by using the same method, the multi-target model was chosen to model the UV inactivation kinetics for comparison. The

parameters k_m and n_C in the multi-target were estimated by applying a non-linear regression to meet the least square criteria on the logarithmic form of the equation (2.2).

3.3 Results and discussion

3.3.1 Fluence (UV dose) calculation

The Petri dish factor, divergence factor and reflection factor were measured or calculated as per Section 3.2.4. When L = 28.7 cm and D = 20 cm, the values of the three factors can be listed as in the following table:

Factors	F_{Petri}	F_d	F_r
value	0.825	0.589	0.933

The average fluence rates were calculated by using equation (2.7). The fluence that the suspended spores received inside the batch reactor was the product of the average fluence rate by the exposure time.

3.3.2 Estimation of the inactivation model parameters

The raw data from the UV susceptibility studies are presented in Appendix 1. The inactivation data were used to fit to the multi-target model. The resulting curves are plotted as Figure 3.5:

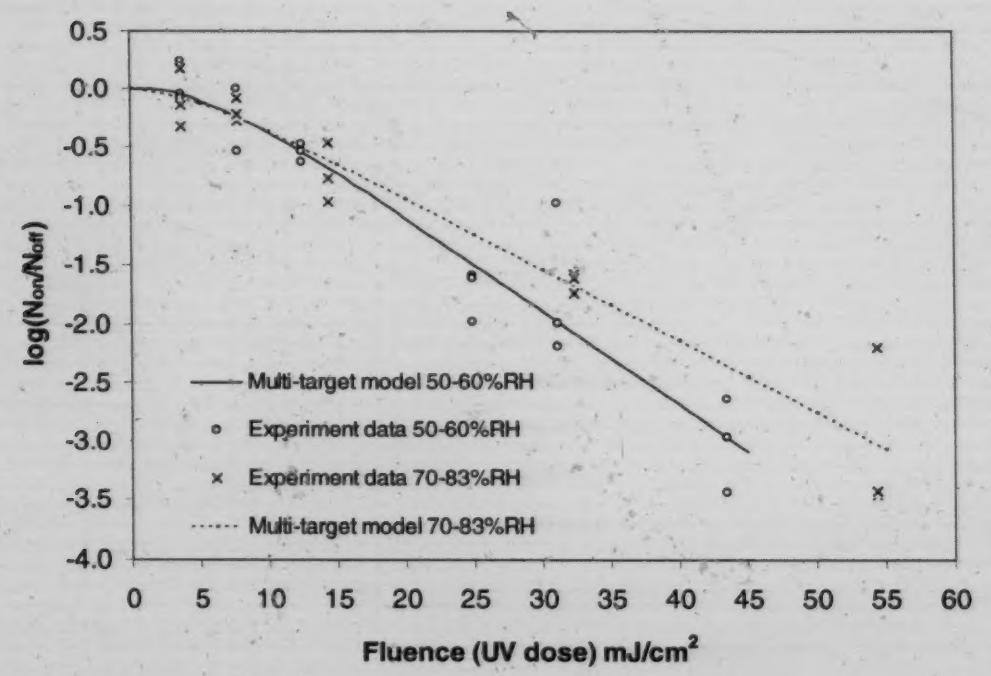

Figure 3. 5. Aerosolized *Bacillus subtilis* spore UV response curves

k_m and n_C were estimated by non-linear least squares regression to be 0.18 cm^2/mJ and 3 at RH = 50 to 60% (±3%), and 0.14 cm^2/mJ and 2 at RH = 70 to 83% (±3%). The k_m values in both RH ranges here are close to the average value 0.153 cm^2/mJ reported by Kowalski (2005). The inactivation curves at RH = 70 to 83% and RH = 50 to 60% indicate that the susceptibility of *B. subtilis* spores in aerosol form is not sensitive to the relative humidity in these two RH ranges. Unlike vegetative microorganisms suspended in air, the viable cells of the suspended spores are protected by the proteinaceous spore coats. During UV exposure, these spore coats prevent the moisture in the ambient environment from entering the cells; one can hypothesize that spores maintain their metabolic activities and the ability to repair UV damage at the same level regardless of the outside RH conditions.

The k_m values at the two RH levels are also close to the k_m = 0.18 cm^2/mJ reported by Uvbiama (2005) using the same batch of *B. subtilis spores*, which were inactivated by UV in water. This agreement of the results shows that the UV susceptibility of *B. subtilis spores* is not affected by the either an air or water medium. Note that at an inactivation level of 3 log reduction, the CFU number in this study was very low, with 1 CFU per dish in 6 dishes out of the 9 Petri dishes. These data are not very reliable because the CFU values per Petri dish are below 10 and are not considered as reliable colony counts.

The Joint Confidence Regions (JCRs) (see Figures 3.6 and 3.7) of the estimation of the parameters at the 95% confidence level show that n_C ranges from 1 to 15 in this study. Typical n_C values for *B.subtilis spores* suspended in water were reported as 8 to 9 (Uvbiama 2005). There was, therefore, no statistical difference between the n_C values determined in air in this study and the n_C values determined in water by Uvbiama (2005).

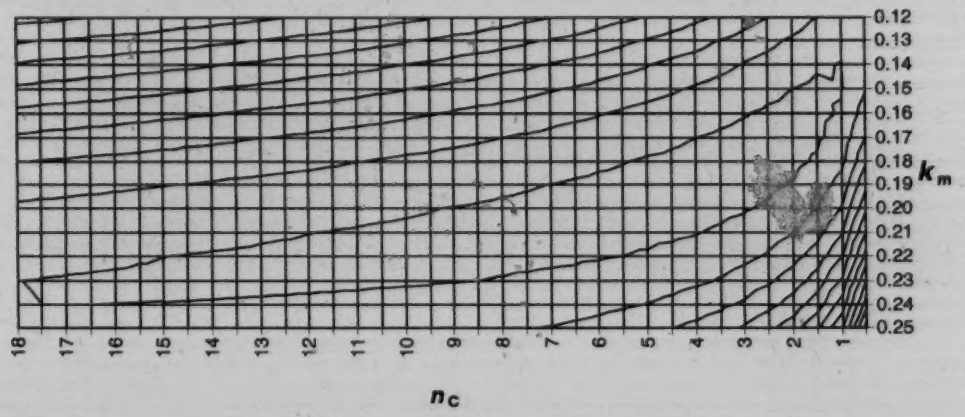

Figure 3. 6. JCR of the multi-target inactivation model parameter estimations at RH=50-60% (The least square value is 2.78 for the close contour line)

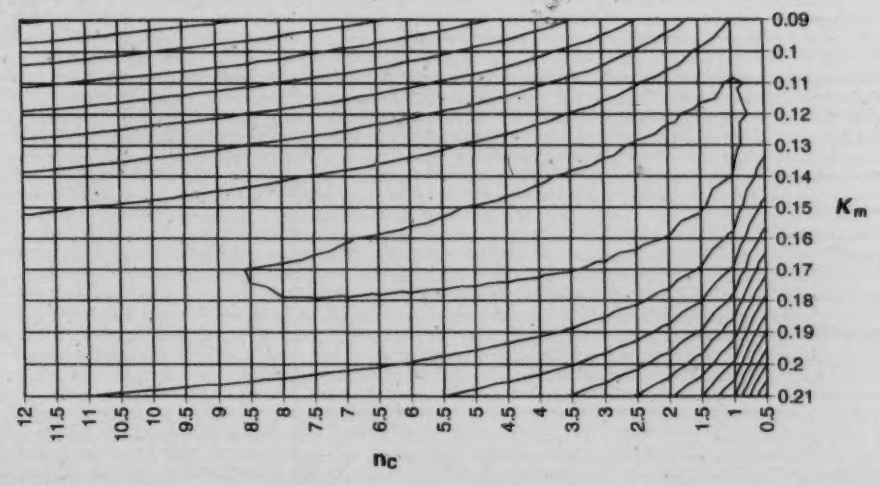

Figure 3. 7. JCR of the multi-target inactivation model parameter estimations at RH=70-83% (The least square value is 2.19 for the close contour line)

3.3.3 Discussion

The well-mixed batch reactor used in this study has the following advantages for determining the UV inactivation kinetics of airborne microorganisms, compared to the approaches used by other researchers.

1. Because of the simple geometry of the well-mixed batch reactor and uniformity of the collimated beam, the average fluence rate can be determined easily and accurately by using the standardized protocol established for collimated beam systems (Bolton and Linden 2003). The factors affecting the distribution of the fluence rate inside the well mixed batch reactor can be determined precisely by applying the protocol to the reactor. In contrast, the geometries used by other researchers (Miller 2000; Peccia et al. 2001; Fletcher et al. 2003) are more complex, and the fluence rates were measured either by carrying out actinometry at certain spatial points (Peccia et al. 2001), or by using a series of radiometer readings within the UV reactor (Miller and Janet 2000). When these approaches

are carried out, many measurements must be made. It is hard to determine the appropriate number of points and the locations of the points where measurements should be made in order to calculate the average fluence rate of the reactor accurately.

2. The well-mixed batch reactor was operated in a batch mode. The fan installed on the bottom of the reactor ensured the complete mixing of the spores suspended in the air. The re-circulation of the microorganisms ensured that each of suspended microorganisms received an identical fluence. The inactivation rate constants determined in the well mixed batch reactor are independent of the reactor geometry. The inactivation constants are, therefore, suitable for application in CFD modeling, in which the stereotype of a UV reactor is virtually divided into numerous finite volume cells, so that the local flow regime in each finite volume cell is regarded as completely mixed. In contrast, other researchers have used continuous-flow apparatuses in which a uneven fluence distribution exists. In these systems, the measured inactivation is a function of both the inactivation kinetics of the particular microorganism and the flow regime in the reactor.

3. The volume of the well-mixed batch reactor apparatus is relatively small (1.5 L) compared to that of the apparatuses used by other researchers (Miller and Janet 2000; Peccia et al. 2001; Fletcher et al. 2003). A small reactor is preferred in bioassay testing, especially when pathogenic microorganisms are the study objects. With a small reactor, controlling possible leakage of the microorganisms into the environment is much easier than doing so with a large one.

However, the apparatus used here also has its own limitations as compared to those of the apparatuses used by other researchers. Since the volume of the quartz cell was small, and the spore concentration was limited by the capacity of the nebulizer, the spore concentration in the trapped air was low. Thus, the colony counts at a 3 log reduction level were so low that the results were not regarded as reliable. Increasing the spores concentration in the nebulizer reservoir and using a 6-jet nebulizer may compensate for this limitation. As suggested by (IUVA 2005a), a scaled-down or a full-scale physical model should be built if the purpose of a susceptibility study of a UVGI air inactivation system is to account for the UVGI inactivation effect and microorganism losses due to physical factors like deposition losses.

4 Bioassay for an Annular In-duct UVGI Air Disinfection Reactor

4.1 Introduction

An annular UVGI air reactor was constructed. The goals of building the UVGI reactor were: (1) to carry out bioassay experiments to measure the efficiency of the UVGI reactor in continuous steady state operation, and (2) to supply the data required to validate the CFD modeling of the UVGI reactor (Chapter 6).

To construct the UVGI reactor to achieve the above goals, the factors that could have affected the performance of the UVGI reactor were controlled. As shown in Figure 2.3, the air flow dynamics, temperature, RH, and UV output can affect microorganism inactivation in a UV reactor. In previous studies (Kowalski 2001; VanOsdell and Foarde 2002; Noakes et al. 2004b), much effort was applied to control and measure the levels of these important factors. VanOsdell and Foarde (2002) used a standard full-scale American Society of Heating, Refrigerating and Air-Conditioning Engineer (ASHRAE) test rig to carry out the bioassay experiments. The factors measured and controlled included the lamp UVC output measurements at different in-duct temperatures induced by different air velocities, the fluence rates at different relative humidity levels, the fluence rates reflected by the duct walls, the UV inactivation constants of microorganisms at different humidity levels, contaminants including VOC, and ozone measurements. Building such a sophisticated ASHRAE full-scale test rig is a very expensive and time-consuming process, as are taking the measurements and carrying out the factor level controls.

For this present study, a small scale UVGI air inactivation reactor and simplifications in terms of factor control and measurements were considered in order to meet the study's limited financial and time budget. As discussed in the Chapter 3, the use of the *B. subtilis* spores as the challenge microorganism can simplify the bioassay study of the UVGI reactor. Because the UV inactivation kinetics were found to be insensitive to RH, the RH of the UVGI reactor did not need to be controlled to the level at which the UV inactivation constants were measured. The effect of temperature on the UV lamp power output was ignored because the lamp was enclosed in a quartz sleeve. The quartz sleeve isolated the lamp surface from the air flow passing through the UVGI reactor; hence, heat convection between the lamp and the air was mitigated. Another benefit from using the quartz sleeve was to block any UV radiation at 185 nm. UV radiation at 185 nm can lead to the generation of trace amounts of ozone.

The sampling strategies used should serve the goals of an experiment. In the bioassays carried out in previous studies, simultaneous upstream and downstream sampling was commonly applied. In the efficiency investigation of a commercial in-duct inactivation system (Griffiths et al. 2005), samples were taken from an upstream point and a downstream point with the inactivation system located at the middle of the two sampling points. The overall efficiency of the purification system could be measured because this sampling strategy could account for the primary filtration effect as well as the UVGI effect. VanOsdell and Foarde (2002), in their study of microorganism inactivation by UV lamps installed in recirculating air ducts, also used the upstream and downstream sampling strategy. However, in order to obtain the 'pure' UVGI efficiency, the upstream and downstream samples were taken both when the lamps were turned on

and turned off. The 'pure' UVGI effect on the challenging microorganism inactivation was calculated by subtracting the microorganism reduction when the lamps were off from the reduction when the lamps were turned on.

4.2 Material and methods

4.2.1 In-duct UVGI air inactivation reactor

The in-duct UV air inactivation reactor was constructed as shown in Figure 4.1.

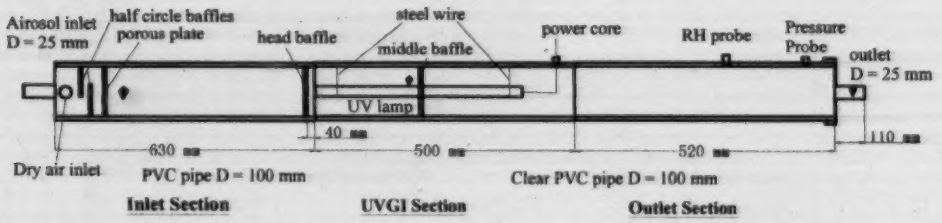

Figure 4. 1. Section of the annular induct UVGI air inactivation reactor (Closed diamond shape marks are the locations of the thermal probes)

The aerosol was released from a nebulizer (Collison 3-jet; BGI Inc., Waltham, MA), which was driven by a compressed air cylinder (Extra-dry, Praxair, Edmonton, AB, Canada) with a 2-stage regulator (Fisher Sci., Canada), with a rubber hose connected to the aerosol inlet attached to the reactor. Because the air from the nebulizer could not reach a high flow rate, another air stream (dry air) was introduced into the dry air inlet of reactor. The air stream was supplied by a compressor. The air flow rate was controlled by a ball valve and was monitored with air flow meters: Watchman II (ColeParmer Inc., Canada) for the low flow rate (less than 10 L/min) and a Polycarbonate Flowmeter (10-100 L/min, Cole-Parmer Inc., Canada) for the high flow rate. Prior to the experiment, this

stream of air was sampled to verify that it was free of *B. subtilis* spores. By increasing the dry-air flow rate, the air flow passing through the reactor could reach as high as 50 L/min.

Two half-circle-shaped baffles were installed at the inlet of the reactor to mix the spore-laden air with the dry air stream. A porous PVC circle plate was installed after the two half-circle baffles in order to straighten the streamlines. Well mixed air traveled through the inlet section and then entered the UVGI section, where a low pressure (LP) UV lamp in a quartz sleeve (M1-G1-15, Wyckomar Inc. Guelph, ON) was hung with stainless steel wires concentrically in the clear PVC pipe (Harvel Clear®, Harvel Plastics Inc., Easton, PA). The total length of the LP UV lamp with the sleeve was 46 cm including the electrical bin ends; the arc length of the lamp was 36.5 cm; the diameter of the sleeve enclosing the lamp was 2.5 cm. Stainless steel wires and the power cables have negligible volumes, so the effect of these components on the air flow was ignored in reactor modeling.

A ring baffle with an inner diameter of 4 cm and outer diameter of 10 cm and thickness of 6 mm was placed at one of two designated positions to test effect of baffle on inactivation performance. The three baffle arrangements tested were 'no baffle', which means that no baffles were installed, 'head baffle', which means that the baffle was placed at the inlet to the radiation zone 4 cm upstream of the lamp, and 'mid baffle', which means that the baffle was placed at the mid-point of the radiation zone. After the UVGI section, the air entered the outlet section. In order to collect representative samples, all the air was forced to pass through a smaller diameter (25 mm) outlet pipe. As discussed in Chapter 3, the protective and repairing mechanisms in *B. subtilis* spores and

experimental data support the assumption that the ambient air RH levels inside the UVGI reactor do not significantly affect the UV inactivation of the spores. The use of the *B. subtilis* spores UV inactivation constants outside the test RH level 50-60% in Chapter 3 was assumed to be valid. Therefore, no efforts were carried out to control the RH levels inside the UVGI reactor. Nevertheless, a RH probe port, through which the RH probe could be put into the reactor, was constructed for RH measurements. A pressure gauge (RK-68110, Cole-Parmer Inc.) was installed in a port constructed close to the outlet in order to monitor the pressure.

4.2.2 Operating conditions for the annular UVGI reactor

Experiments were run under three running flow-rate conditions, see Table 4.

Table 4 Testing conditions for the in-duct UVGI reactor

Condition	Flow rate from the Nebulizer (L/min)	Flow rate of compressed air (L/min)	Total flow rate (L/min)	RH in the UVGI reactor	Reynolds number in the outlet pipe
1	4	7	11	50-60%	632
2	4	22.5	26.5	21-24%	1521
3	4	40	44	9-11%	2526

All three flow rate conditions were run with 'no baffle', 'head baffle' and 'middle baffle' configurations. A total of 9 conditions were tested. The Reynolds number in the outlet pipe ranged from 632 to 2526, covering flow regimes ranging from laminar ($Re < 2000$) to the turbulent ($Re > 2000$). The flow rate from the nebulizer was monitored with a flow meter (Model C-32461-54, Cole Palmer. Inc.), and a barometer was used to monitor the pressure applied to the nebulizer. A flow meter (Watchman II, Cole Palmer)

was used to measure the flow rate of compressed air when the flow rate was low (7 L/min); another flow meter (Model 32900-54, Cole Parmer Canada Inc) was used to monitor the flow rate when the flow rate was higher (> 7 L/min).

Sampling strategies

Midget impingers (Standard Midget, Supelco Inc.) with 5 mL MilliQ® water in the reservoir were used to collect a portion of the air at the outlet, that is, samples from the downstream air. Unlike the upstream and downstream sampling arrangements used in other studies (Griffiths et al. 2005; IUVA 2005a; VanOsdell and Foarde 2002), the downstream arrangement used in the present study did not require the use of additional experiments to account for losses other than those from UV inactivation. The ratio between the UV lamp on and UV lamp off samples was sufficient to account for the UVGI effect.

When the total flow rate (11 L/min) was within the impinger optimum collecting flow-rate range (8-12 L/min), all the air was forced to flow through the impinger. For this condition, the sampling impinger could have caused back pressure inside the reactor. In order to create similar running conditions when air was not passing through the sampling impinger, another impinger (the waste impinger) was installed and connected with a three-way valve. The air was forced to pass to the waste impinger when it was not passing through the sampling impinger. Figure 4.2 shows the operation and sampling arrangement at 11 L/min flow rate. The air volume passing through the impinger was measured by a mass-flow meter (K-32648-19 Mass Flowmeter, Cole Parmer Canada Inc.). The sampling time was set to be 1 min.

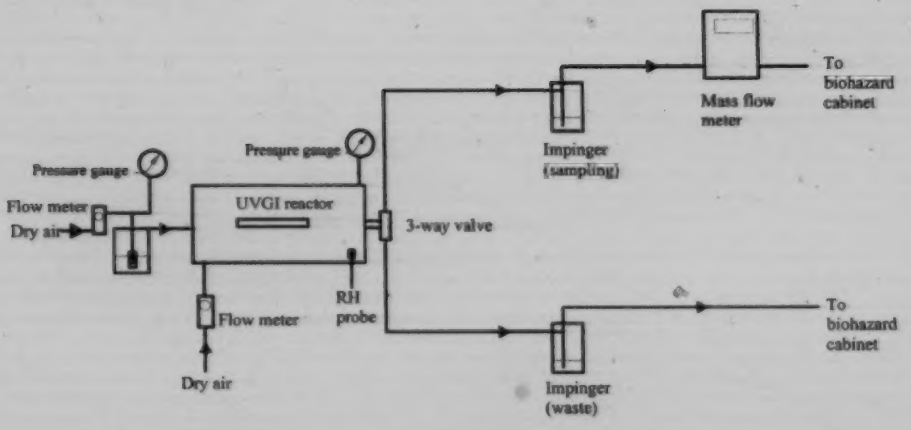

Figure 4. 2. Schematic diagram of the operation and sampling arrangement at 11 L/min flow rate

The flow rates of 26 and 44 L/min were high relative to the collecting capacity of the impingers. Passing all the air flow through the sampling impinger was impractical. Instead, a vacuum pump (Model 420-1901, Air Cadet, Barnant inc. Barrington, IL. USA) was used to sample air from the end of the outlet pipe. A 9.5 mm I.D. hose was used as the suction inlet linking the vacuum pump with the impinger. A needle valve (Edmonton Valves and Fittings, Edmonton) was installed between the hose inlet and the impinger inlet to adjust the average air-flow rate to 8 L/min. The air passing through the impingers was monitored by using a mass-flow meter (K-32648-19 Mass Flowmeter, Cole Parmer Canada Inc.) The sampling time was controlled to be 1 min; hence, 8 L of spore-laden air passed through the impinger collecting liquid (MilliQ water). Figure 4.3. shows the schematic of the operation and sampling arrangements at the 26.5 L/min and 44 L/min flow rates.

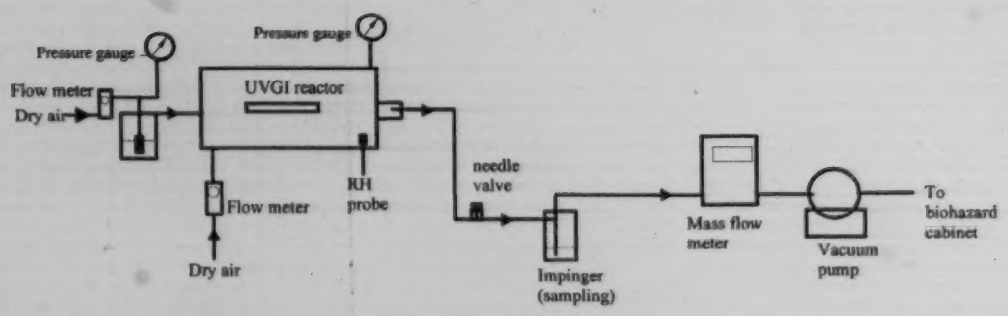

Figure 4. 3. Schematic diagram of the operation and sampling arrangement at 26.5 and 44 L/min flow rates

The UV lamp was turned on for 30 min, and the nebulizer was run for 15 min before samples were taken. Triplicate samples were taken from the outlet of the reactor for each of the 9 conditions (3 flow rates by 3 baffle arrangements) with and without turning the UV lamp on. The use of the Midget impingers and the enumeration of the *B. subtilis* spores are described in the inactivation constants measurement section (Chapter 3).

Data analysis

The number of viable spores collected in the impingers was enumerated using the techniques described in Chapter 3. For each of the 9 experimental conditions, let N^i_{off} be the number of viable spores collected when the UV lamp was turned off, and N^j_{on} be the number of viable spores collected when the UV lamp was turned on. The superscripts i and j represent the i^{th} or j^{th} sample of the three samples taken ($i = 1$ to 3; $j = 1$ to 3).

The concentrations of the aerosolized spores in the air were calculated by dividing the number of viable spores collected in the impinger by the volume of air that passed

through the impinger, which was constant volume for each test. A possible inactivation level, -log S_n was calculated as

$$-\log S_n = -\log\left(\frac{N^i_{on}/V}{N^j_{off}/V}\right) = -\log\left(\frac{N^i_{on}}{N^j_{off}}\right). \quad (4.1)$$

Because of the three N_{on} values and three N_{off} values, each experiment had nine possible -log S_n values, that is, n = 1 to 9.

The mean inactivation level for each experiment condition was calculated as

$$-\log S = \frac{\sum_{n=1}^{9} \log S_n}{9} = -\log \frac{\sqrt[3]{N^1_{on} N^2_{on} N^3_{on}}}{\sqrt[3]{N^1_{off} N^2_{off} N^3_{off}}}. \quad (4.2)$$

The above formula shows that the arithmetic mean of all the possible 9 $-\log S_n$ is in fact the logarithm of the ratio of the three samples' geometric means under the lamp on and off conditions. The benefit of calculating the 9 possible inactivation levels is to supply enough data points for the statistical analysis that was applied to the nine possible $-\log S_n$ values.

4.2.3 UVC output measurement

Since measuring the UVC output from the lamp in the UVGI reactor for the various running conditions is difficult due to the small size of the UVGI reactor, indirect measurement of the UVC was carried out in this study. The UVC output power was measured by removing the lamp and quartz sleeve from the UVGI reactor. With the presence of the quartz sleeve, an indirect measurement of the UVC output outside the UVGI reactor was possible. The UV lamp was placed in the quartz sleeve during the

experimental runs and when the UVC output was measured. The enclosing quartz sleeve prevented the cooling effect from heat convection. In order to prove the absence of the cooling effect, a thermocouple meter (Dual J-T-E-K®, Barnant, Barrington, IL USA) with a wire-shape probe was used to monitor the UV lamp surface temperature in both situations (i.e., inside the reactor and external to the reactor). If this temperature was the same in both situations, the UVC output should also be the same.

Also, temperatures inside the UVGI reactor were measured with thermocouple probes at the following locations: at a point 5 cm down-stream from the porous plate for measurement of inlet air temperature, at the surface of the quartz sleeve, and at a point near the reactor outlet. The temperature measurements at these points provided the thermal data needed in the later CFD modeling. The locations of the thermal probes are demonstrated in Figure 4.1 with closed diamond shape marks.

The accurate measurement of the total UVC output from a LP UV lamp in ambient air is critical in the fluence rate calculation. This task is a challenging task due to UVC detector measurement errors, the reflection of UVC from surrounding walls, ambient temperature variations, and the ballast performance (Sasges and Robinson 2005; Severin and Roessler 1998). In order to measure the LP UV lamp UVC output accurately, two methods were employed under the same measurement conditions and over the same period of time.

The Keitz method

The Keitz method is derived from a formula used to calculate the illumination rate at a spatial point in a light field (Keitz 1971). Because the formula was originally derived for use in illumination engineering, the terminology and units are quite different from

those used in UV disinfection engineering. In order to adapt this formula into UVGI disinfection engineering, the equation was re-derived as in following paragraphs.

A UV lamp can be regarded as a uniform diffuser; thus the radiant intensity at any point perpendicular to the UV lamp axis has the same value, I_0 (W sr^{-1}). For a sphere surrounding a line-shaped light source, the radiant power passing through an infinitesimal solid angle $d\Omega$ should be dP, and

$$dP = I_\alpha \cdot d\Omega, \tag{4.3}$$

where I_α is the radiant intensity in the direction that has an angle α with the lamp axis as shown in Figure 4.4. The lamp axis is placed such that the ends of the lamp are at 0° and 180°.

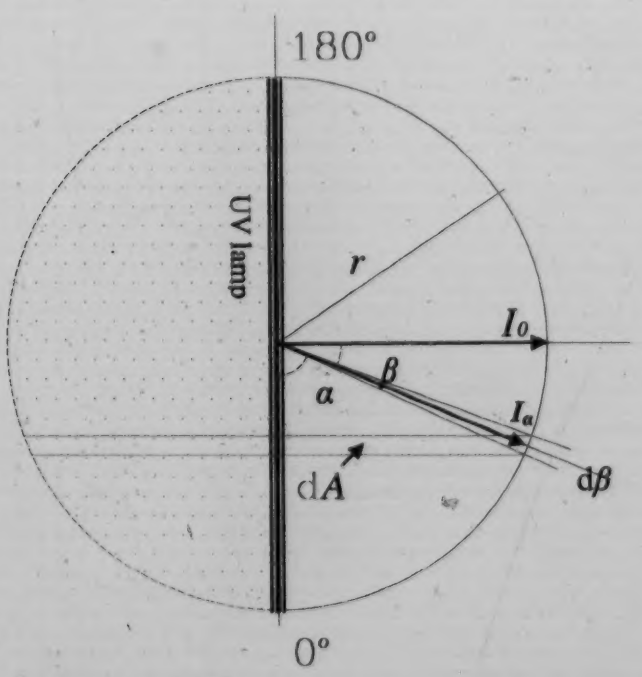

Figure 4. 4. Schematic used to derive the relationship between the I_0 and P

I_0 is the radiant intensity in the direction perpendicular to the lamp axis; that is, $\alpha = 90°$.

Consider an infinitesimal belt around the sphere with an area

$$dA = r\, d\alpha \cdot 2\pi r \sin\alpha = 2\pi r^2 \sin\alpha\, d\alpha . \tag{4.4}$$

The infinitesimal solid angle is

$$d\Omega = dA/r^2 = 2\pi \sin\alpha\, d\alpha . \tag{4.5}$$

Let $\alpha + \beta = 90°$. According to Lambert's law, $I_\beta = I_0 \cos\beta$.

Hence,

$$dP = I_\alpha\, d\Omega = I_\alpha\, 2\pi \sin\alpha\, d\alpha = I_0 \cos\beta\, 2\pi \sin\alpha\, d\alpha = 2\pi I_0 \cos^2\beta\, d\beta.$$

By integrating over the sphere from $\beta_1 = -\pi/2$ to $\beta_2 = +\pi/2$,

$$P = \int_{-\pi/2}^{\pi/2} dP = \int_{-\pi/2}^{\pi/2} 2\pi I_0 \cos^2\beta d\beta = \pi I_0 (\beta + \frac{1}{2}\sin 2\beta)\,\Big|_{-\pi/2}^{\pi/2} = \pi^2 I_0 . \tag{4.6}$$

Rearranging the above equation gives the normal radiant intensity from the lamp:

$$I_0 = \frac{P}{\pi^2} \tag{4.7}$$

For a lamp with a total arc length of L and a UVC output of P, the radiant intensity per unit length should be:

$$I_l = \frac{I_0}{L} = \frac{P}{\pi^2 L} \tag{4.8}$$

At the point A as shown in Figure 4.5, the fluence rate at that point equals the summation of the fluence rate from every finite dl section. Let r be the distance from point A to a finite section dl of the lamp, so that, as in Figure 4.5, dE_α represents the radiance incident from dl. By applying the inverse square law,

$$dE_\alpha = dI_\alpha / r^2 = I_l \cos\alpha / r^2\, dl .$$

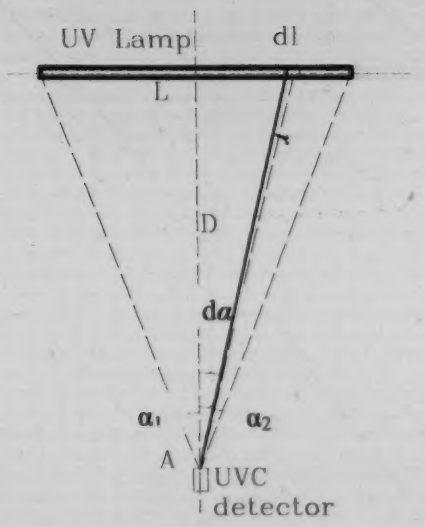

Figure 4.5. Schematic for the UVC output measurement (Keitz method)

Notice that when some UV lamp fluence rate distribution models for UV lamps were derived, I_l instead of $I_l \cos \alpha$ was used. This practice leads to the introduction of a $4/\pi$ factor to correct the calculated fluence rates (Sasges and Robinson 2005). This mistake is common when Lambert's law is ignored. Note that

$$\mathrm{d}l = r\,\mathrm{d}\alpha .$$

Let D be the perpendicular distance from point A to the lamp axis. Then

$$\mathrm{d}E_\alpha = I_l \cos^2 \alpha / D\,\mathrm{d}\alpha$$

The irradiance at point A is

$$E = \int_{-\alpha_1}^{\alpha_1} dE_\alpha = \frac{1}{D}\int_{-\alpha_1}^{\alpha_1} I_l \cos^2 \alpha d\alpha = \frac{1}{D} I_l (\alpha_1 + \frac{1}{2}\sin 2\alpha_1)$$

$$= \frac{P}{DL\pi^2}(\alpha_1 + \frac{1}{2}\sin 2\alpha_1) .$$

Rearranging gives:

$$P = \frac{2\pi^2 EDL}{2\alpha_1 + \sin 2\alpha_1} \tag{4.9}$$

By measuring the fluence rate at point A, the total UVC output P can be calculated according to the formula. Common UVC detectors measure the irradiance; that is, they can collect the radiant energy from one side only. The UVC detector probe has a limited 'view angle' within which it can respond to the UVC. Thus, the solid angle that the probe can cover is limited. In order to collect as much radiant energy as possible, D should be long enough. In practice, several distances should be tried out until the calculated UVC power is stable.

The goniometric method

The goniometric method is well documented in Sasages and Robinson (2005). A goniometric half circle is constructed by using the lamp's central point as the original point **O**, and the axis of the lamp is the diameter axis of the goniometric half circle, as shown in Figure 4.6. Starting from the lamp's normal direction (0°) at a far enough distance, finite irradiance readings were conducted at the same distance by using a UVC detector around the UV lamp (from –90° to +90°). Each reading can be regarded as the average irradiance of a circular finite section dA of a sphere subtending the whole lamp. The area of a dA is given by

$$dA = 2\pi r^2 \cos\theta d\theta \tag{4.10}$$

where r (in meters) is the distance measured from the original point of the half circle (in this case, r = 2.99 m), and θ (in radians) is the angle measured from the normal direction

of the lamp to the radial at which a finite irradiance reading was taken. $d\theta$ is then the angle (in radians) in even increments subtending a half circle (from -90° to +90°) . If $d\theta$ is set to be 0.174 rad (10°), then the number of readings is 19 (= 1 + π/0.174). Let E_θ be the irradiance reading at the θ direction; then the overall UVC output can be obtained from

$$P = \int_{-\pi/2}^{\pi/2} E_\theta dA = \sum_{i=1}^{19} E_i \Delta A = \sum_{i=1}^{19} 2\pi r^2 E_i \cos\theta \Delta\theta \,. \tag{4.11}$$

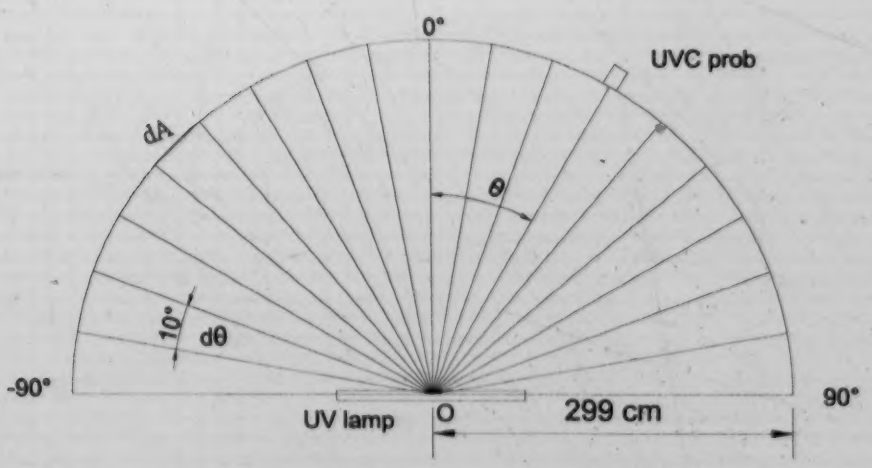

Figure 4.6. Goniometric measurement schematic

Both the Keitz and goniometric methods require that the UVC probe has a good cosine response and that the irradiance reading is taken at a distance at least two times that of the lamp length (Keitz 1971; Sasges and Robinson 2005). In both methods, a calibrated radiometer (Model P-9710 with detector UV3718, Gigahertz-Optik, Germany) was used to read the irradiance at the designated locations. Also, in order to avoid any

UVC reflections by the surrounding surface, the UV lamp was fixed in a position at least 85 cm away from any surface.

Reflection of the PVC pipe wall

In the UVGI reactor constructed for this research, the PVC pipe wall is very close to the lamp. If the walls reflect UVC significantly, the reflected UVC should be taken into account when fluence rates are calculated. In order to evaluate the reflection level, the reflection factor (reflectivity) of the PVC wall was measured by using the method proposed by Blatchley (1997), as shown in Figure 4.7. A radiometer (Model P-9710 with detector UV3718, Gigahertz-Optik, Germany) was used to measure the reflected irradiance (Point A) and the direct incident irradiance from the collimated beam (Point B). The reflecting material was placed at 45° to the collimated beam when the radiometer was placed a point A, and the reflecting material was removed from the collimated beam path when the radiometer was placed at point B. The distance OA equals the distance OB in Figure 4.7. The ratio of the reading at point A to the reading at point B is the reflection factor of the material.

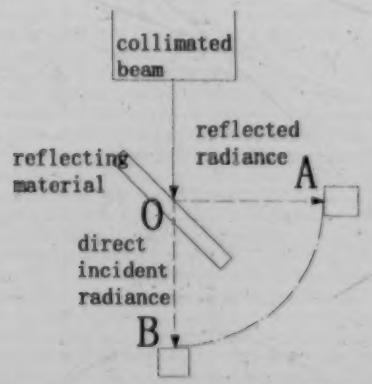

Figure 4. 7. Schematic for reflection factor measurement (Blatchley 1997)

4.3 Results and discussion

4.3.1 Measurement of the UVC output

UVC output of the lamp

The UVC output power of the LP UV lamp (G1-M1-15) with the sleeve on was measured to be 1.31 (±0.06) W using the Keitz method and 1.37 W using goniometric method. The average of these two values is 1.34 W. The average value was taken as the UVC output of the LP lamp for later calculations and modeling.

The average fluence rate inside the reactor was calculated with the Fluent® code by using the 'volume average' report function. The reactor was divided into numerous finite control volumes. The volume of each control volume is so small compared to the whole reactor that the average fluence rate inside a control volume can be approximated by the fluence rate at the centroid point of the control volume. The calculation of the fluence rates at the centroid points will be discussed in detail in the CFD fluence rate modeling section. Given that the fluence rate at each control volume is known, the average fluence rate inside the reactor can be reported by the formula

$$E'_{average} = \frac{1}{V}\sum_{i=1}^{n} E_i V_i \qquad (4.12)$$

where V is the total volume of the UVGI reactor; V_i is the i^{th} volume of the finite control volume; E'_i is the fluence rate at the centroid of the i^{th} control volume; n is the total number of the control volume in the reactor. When the lamp UVC output was 1.34 W, the

volume average fluence rate inside the reactor was calculated by the Fluent® code and found to be 0.40 mW/cm^2.

Reflection factors

The reflection factor of the Clear PVC used in the UVGI reactor was measured to be 3.4%. This value is so low that the reflected UVC inside the reactor can be ignored. The reflection factors of other materials were also measured: opaque PVC baffle (6.2%), aluminum foil (31.8%), wood (<1%). The fluence rate reflected by the opaque PVC baffle was ignored since the area of the baffle is small compared to the whole reactor. Materials with high reflection factors, such as aluminum sheets and ePTFE, are popular in UVGI air disinfection unit construction (Kowalski 2001). The high reflecting materials can boost the fluence rate inside the UVGI reactor without increasing the UV lamp power.

4.3.2 Bioassay experimental results

The inactivation levels are presented in Figure 4.8 for the three flow-rate conditions and the three baffle arrangements. The mean log inactivation levels are shown as numbers above the bars in Figure 4.8., and the 95% Confidence Intervals (CIs) are presented as error bars. Statistics were calculated based on the nine possible inactivation levels which were calculated according to equation (4.2). The statistics and the 95% CIs can be found in Appendix 4.

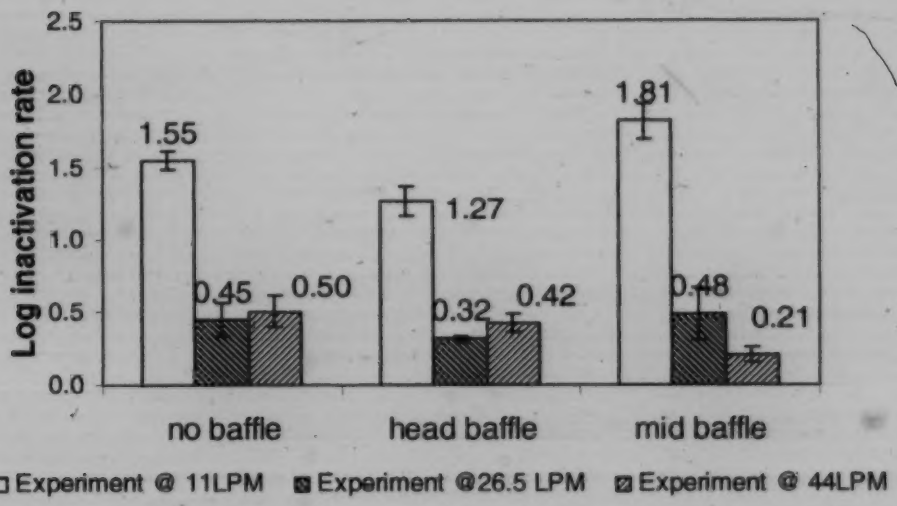

Figure 4.8. Log inactivation levels under 3 flow rates conditions and 3 baffle arrangements for the in-duct UVGI reactor

4.3.3 Discussion

Figure 4.8 shows that the flow rate of the air passing through the apparatus is the most critical factor in determining the microorganism inactivation levels. When the lamp UVC output is constant, the fluence (UV dose) of the spore particles received in the UVGI field is determined by the retention time and the particle trajectories due to the non-uniform fluence rate and the velocity field. Roughly, the inactivation level at a low flow rate of 11 L/min was three times higher that those at 26.5 and 44 L/min. However, the inactivation levels did not vary too much when the flow rate increased from 26.5 L/min to 44 L/min; that is, the difference between the two conditions without a baffle installed is not statistically significant (*P* value 44% > 5%).

The predictions based on the ideal plug-flow with complete radial mixing assumption and the multi-target kinetic model were compared against the experimental results obtained when baffles were not installed. The volume average fluence rate inside

the UVGI reactor was calculated to be 0.40 mW/cm^2. The retention times t at 11, 26.5 and the 44 L/min flow rates were calculated by using formula $t = V/Q$. The reactor volume V was calculated to be 12.5 L. The three retention times were 68, 28 and 17 s. The fluence values under the three flow conditions were calculated as F = 27.1, 11.3 and 6.8 mJ/cm^2, respectively. On substitution of the F values into the multi-target model $S = 1-(1-e^{-0.18F})^3$, the corresponding inactivation levels for these three fluence value were 1.65, 0.47 and 0.19. When there was no baffle installed in the UVGI reactor, the inactivation level predicted using the ideal-plug flow model was greater than the measured inactivation level at 11 L/min, was close to the measured inactivation at 26.5 L/min, and was lower than the measured inactivation at 44 L/min.

A predicted inactivation level (1.65) that was greater than the experimentally measured inactivation level (1.48-1.62) at a flow of 11 L/min was reasonable because the Reynolds number (625) implies that the flow was in the laminar flow regime rather than plug flow with mixing across fluence rate gradients. In the laminar flow regime the flow tends to be stratified. Radial mixing across fluence rate gradients is poor. As the Reynolds number increases, the flow regime moves closer to ideal plug flow. Hence, at 26.5 L/min, the ideal plug flow model can generate a value (0.47) close to the experimental result (0.37-0.57). However, it is hard to explain why the experimental result (0.39-0.61) is higher than the ideal plug flow prediction (0.19) at the 44 L/min flow rate and why no significant difference was found between the 26.5 L/min and 44 L/min experimental results.

The introduction of the baffles complicated the relations between the flow rates and the inactivation levels. For the low flow rate (11 L/min) case, installation of the head

baffle decreased the inactivation level (from 1.55 to 1.27), while installation of the middle baffle increased the inactivation level (from 1.55 to 1.81). At the 26.5 L/min flow rate, an ANOVA analysis found no statistically significant difference between the three baffle treatments (P value =8.8% >5%). However, at 44 L/min, ANOVA analysis found a significant difference among the three baffle conditions (P value = 0.0007% <5%).

The installation of baffles in the UVGI reactor did not always result in increased inactivation level. On the contrary, the experimental data showed that the baffles actually depressed the inactivation levels at the 44 L/min flow rate. Because the baffle volumes are negligible, the UVGI reactor's theoretical retention time ($t = V/Q$) should be the same under the three flow rate conditions, but some factors other than the theoretical retention time may affect the inactivation levels of the aerosolized *B. subtilis* spores. The retention time is determined by the flow rate, while the trajectories of the particles are affected by the streamlines of the air fluid, as well as turbulence mixing caused by the baffles. The ideal plug flow assumption for the multi-target model cannot explain the observed fluctuations in the inactivation levels when the baffles were installed. Baffles can cause extra turbulence and increased mixing in the reactor, but the effect of mixing caused by the baffles on the reactor efficiency are difficult to estimate because mixing effects can be beneficial or detrimental to inactivation efficiency.

Severin et al. (1984) found through their experimental data and mathematical modeling of a water-based UV disinfection process that radial mixing can boost the disinfection efficiency in a continuous-flow UV reactor while axial (or longitudinal) mixing can depress the efficiency. How the baffles in the UVGI reactor change the radial mixing or the axial mixing is not clear. How the mixing affects the UV inactivation levels

is even more difficult to demonstrate by experimental methods. Experimental approaches, such as tracer studies, did not reveal how the mixing affects the fluence distribution. In order to better understand the mixing inside the reactor, a tracer experiment using colored smoke was attempted in this study. Unfortunately, the smoke caused a chemical attack on clear PVC wall. To avoid greater damage, the smoke study was abandoned

The use of *B. subtilis* spores as the challenge microorganism simplified the experiments in terms of two major control factors: photoreactivation and relative humidity control. Most of the UVGI air reactor was made of clear PVC. Since photoreactivation is known to be absent in *B. subtilis* spores (Peccia and Hernandez 2001), there was no need to cover the clear section to block the visible light. If the challenge microorganism has significant photoreactivation capacity, it would be necessary to block visible light. Since the UV susceptibility of the *B. subtilis* spores was not sensitive to the RH, no effort was made to control the RH inside the UVGI reactor. However, when vegetative cell or other microorganism, of which UV susceptibility is sensitive to the RH levels, is used as challenge microorganisms in bioassays, the RH level should be strictly controlled. A humidifier can be used to increase the RH to a designated level.

5 CFD modeling of the UVGI air inactivation reactor

5.1 Introduction

Computational Fluid Dynamics (CFD) modeling has been used in industry to model fluid dynamics for decades and has about a 30-year history in environmental engineering. The emergence of commercially available CFD programs, the dramatic decrease in price, and the increased computational capacity of personal computers has made the application of the CFD technique more accessible to the practicing engineers and researchers than it was previously.

Most of the commercially available CFD solver codes such as Fluent® (R6.2.16 Fluent Inc, Lebanon, NH, USA) are based on the finite volume method (Fluent 2005). In finite volume based CFD codes, the computational domain is divided into numerous control volumes using a pre-processor program. For each control volume, the mass, momentum and internal energy conservation Partial Differential Equations (PDEs) in the Cartesian coordinate system are given by

$$\frac{\partial \rho}{\partial t} + div(\rho \vec{U}) = 0 \tag{5.1}$$

$$\frac{\partial (\rho U_i)}{\partial t} + div(\rho U_i \vec{U}) = -\frac{\partial p}{\partial x_i} + div[\mu \ grad(U_i)] + S_{Mi} \tag{5.2}$$

$$\frac{\partial (\rho E^*)}{\partial t} + div(\rho E^* \vec{U}) = -p div(\vec{U}) + div(k \ grad \ T) + \Phi + S_{E^* i} \ , \tag{5.3}$$

where ρ is the density of the fluid (assumed to be constant at low flow velocity and ambient temperature for air); p is the static pressure of the control volume; $\vec{U}$ is the velocity vector of the control volume; *div* is the divergence operator; *grad* is the gradient

operator; the subscript i represents the x, y, z directions in a the x-y-z Cartesian co-ordinate system; S_{Mi} is the source term of the momentum in the i direction; E^* is the internal energy; k is the thermal conductivity ; Φ is the energy dissipation function; S_{E^*i} is the energy source term in the i direction. When the Reynolds number for a fluid is small (<2000), the flow is in the laminar regime. The solutions of the above PDEs along with equations of state are sufficient to predict the flow behavior. In a turbulence regime with higher Reynolds number (>2000), fluid behavior will be chaotic and random (Versteeg and Malalasekera 1995). A Direct Numerical Solution (DNS) for turbulence flow will require a large number of control volumes and a very high resolution grid. DNS requires computers with very high capacity even for simple turbulence flow problems. In order to make a numerical solution for the turbulence problem possible at low computational cost, several turbulence models have been developed and have been embedded into CFD codes. However, there is no universal turbulence model that is suitable for all cases and types of turbulence. Each turbulence model has its advantages and limitations. Table 5 presents a summary of the most popular turbulence models used in CFD. All of these models are available in the commercial CFD code Fluent®. Table 5 is derived from Versteeg and Malalasekera (1995).

Table 5 Summary of the Turbulences Model available in Fluent® CFD Software (Versteeg and Malalasekera 1995)

Name of the model	Computational cost	Flows that can be predicted well	Number of PDEs	Flows that cannot be predicted well
Mixing length model	low	Jets, mixing layers, wakes, thin shear layers	1	Flows with separation and recirculation
k-ε model	low	Confined flows, many engineering flows	2	Unconfined flows, large extra strains, rotating flows, non-circular ducts
Reynolds stress equation model (RSM)	high	The most general of all classical turbulence models, wall jets, asymetric channel and non-circular duct flows	7	Axisymmetric jets and unconfined recirculating flows
Algebraic stress equation models (ASM)	fair	As RSM	2 + a system of algebraic equations	

Table 5 shows that the k-ε turbulence model is suitable for confined flow and has a relatively low computational cost. Hence, the k-ε model was chosen as the turbulence model for this study. The selection of appropriate boundary conditions and its initial values are critical to CFD modeling. The closer the boundary conditions are to the actual conditions in the real physical domain, the more accurate the CFD prediction will be.

Building a reliable model itself is a challenge to a modeler; validation of the model is another challenge the modeler has to face. The availability of commercial CFD solver codes has made the widespread use of CFD for engineering applications possible.

Modelers do not need to develop the solver routines by themselves but can focus on the nature of their fluid problems. To build a CFD model, modelers have to make many assumptions for the boundary and initial conditions according to the nature of their problems. Assumptions bring uncertainties into modeling. Choosing the turbulence model and the linearization and discretisation schemes also creates uncertainty. On the other hand, these commercial codes are like 'black box' tools to the modelers who are not involved in the development of the solver codes. Without knowing what algorithms are used in the code, the modelers are unaware of the software's reliability. Furthermore, commercial CFD programs like Fluent® are very reluctant to release their source codes. Coding errors occur even though the commercial codes are developed under very high-standard software engineering protocols. These limitations prevent the modelers from discovering mistakes in the commercial solver codes and in the specific model they have built. In order to gain confidence in CFD modeling with commercial solver codes, validation of the modeling results against experiment data or available analytical solutions is necessary.

Validation of the CFD model has to be designed carefully. Validation is 'the process of determining the degree to which a model is an accurate representation of the real world from the perspective of the intended uses of the model. (Oberkampf and Trucano 2002). A good way to validate a CFD model is to carry out parallel validation experiments on a full-scale model or prototype of the system under consideration. Researchers often assume during the validation process that the experimental outcomes are more accurate than the computational results. However, experimental results are subject to error and uncertainties, so parallel validation experiments alone cannot be used

as the only way to determine the accuracy of a CFD simulation. In a complex system, in which the experimental factors are hard to control, or when a full-scale experiment is either uneconomical or difficult to build, the validation process can be broken down to many sub-model validation processes (Oberkampf and Trucano 2002). The complex system can be divided into several sub-models, and validations for the sub-models are conducted. In this study, the validation process was designed in such a way that the sub-models and the whole model could be validated against the available experiment data or against analytical solutions.

5.2 Development of the CFD model of the UVGI air reactor

5.2.1 Flow chart of the model building

The development of the CFD model was based on the framework presented in Chapter 2, Figure 2.5. The processes of model building and validation are presented in Figure 5.1.

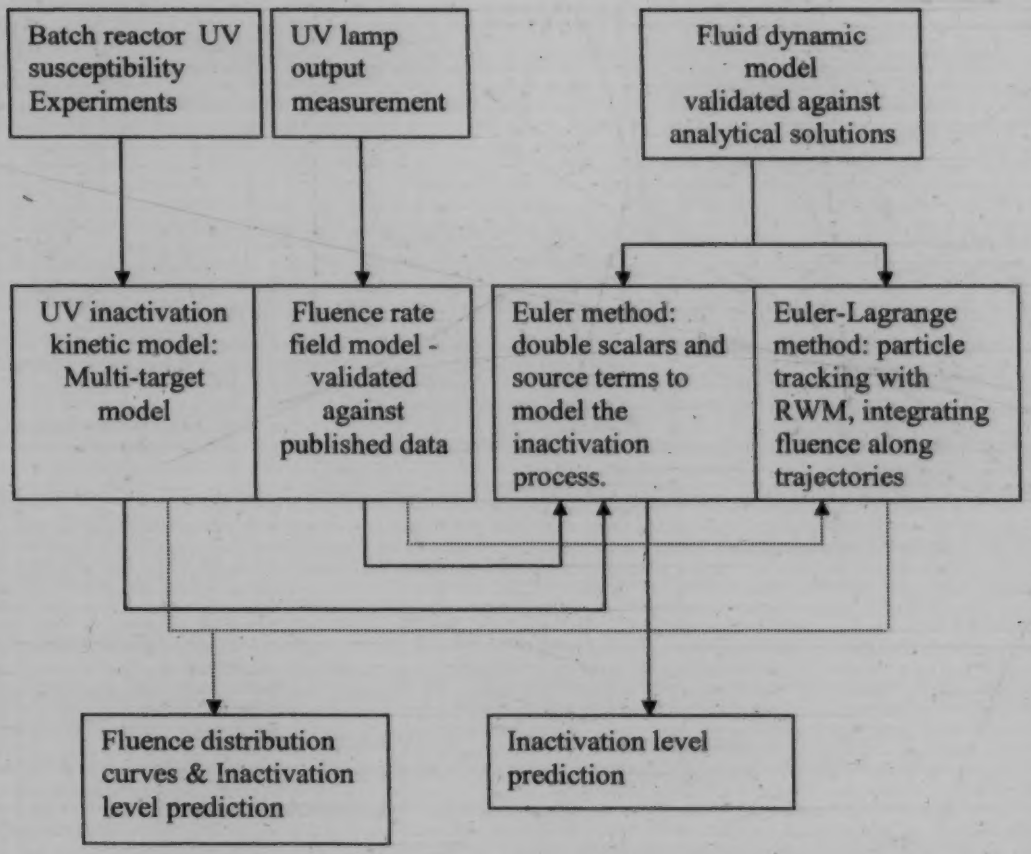
Batch reactor UV susceptibility Experiments
UV lamp output measurement
Fluid dynamic model validated against analytical solutions
UV inactivation kinetic model: Multi-target model
Fluence rate field model - validated against published data
Euler method: double scalars and source terms to model the inactivation process.
Euler-Lagrange method: particle tracking with RWM, integrating fluence along trajectories
Fluence distribution curves & Inactivation level prediction
Inactivation level prediction

Figure 5. 1. Flow chart of the development of the CFD model

The CFD model of the UVGI reactor was built on the sub-models that described the physical and biochemical behaviors of the UVGI air reactor in this study. The UV inactivation rate constants measured in the collimated beam batch reactor experiments (Chapter 3) were input into to the UV inactivation multi-target model. The UVC average output power was measured and input into the fluence rate distribution model. The velocity fields and turbulence energy fields were produced from the fluid dynamic model by using the Fluent® code. Two modeling methods, the Euler method and the Euler-

Lagrange method, utilized the velocity and turbulence energy profiles from the fluid dynamic model to predict the trajectories taken by microorganisms as they moved from the inlet to outlet of the reactor. The procedures of the two methods are distinguished by the solid lines and dashed lines in Figure 5.1.

In the Euler method, two scalars were defined to describe two important parameters in the inactivation process. One scalar was the cumulative fluence and the other is the concentration of viable microorganisms. The two scalars were defined in Fluent® according to the methods derived by Noakes et al. (2004a, 2006); see Section 2.6.3 for details. The UDF of the accumulative fluence scalar source term 'dose.c' and the UDF of viable microorganism concentration scalar source term 'disinfect.c' are presented in Appendix 5. In the UDFs, the fluence rates are embedded into the source terms of the two scalars. The solid lines beneath the second row of boxes in Figure 5.1 show how the multi-target kinetic model and the fluence rate distribution were utilized in combination with the Euler method. The final goal of the Euler method is to predict the inactivation level by comparing the concentration of the viable microorganisms at the inlet and outlet boundaries of the UVGI reactor.

In the Euler-Lagrange method, the simulation results were presented as fluence-distribution curves and inactivation levels. In this method, the microorganisms were treated as particles released from the inlet surface of the reactor. The Euler-Lagrange method is, thus, frequently called a 'particle tracking' method. Each microorganism particle that enters the reactor takes a different path and receives a different fluence by the time it exits the reactor. The dashed lines in Figure 5.1 show that the fluence rate distribution field was embedded into the Euler-Lagrange method to calculate the fluence

along the trajectories of individual microorganism particles. The fluence distribution curves from the Euler-Lagrange model can help one to understand the characteristics of the inactivation process.

To gain sufficient confidence in the model-development process, each sub-model was validated before it was embedded into the integrated model. The building processes of the UVGI reactor CFD models and its sub-models and their validation are presented in detail in the following sections.

5.2.2 Meshing and grid independency study

The UVGI air inactivation reactor was simulated with a 3-Dimensional (3D) model. A virtual prototype of the UVGI reactor built in this study was first drawn in AutoCAD® 2006 Education Version (Autodesk Inc.). The dimensions of the virtual 3D prototype were drawn according to the exact dimensions of the real UVGI reactor as shown in Figure 4.1. The 3D prototype of the UVGI air inactivation reactor was imported into Gambit® (R2.2.30, Fluent Inc.) and was divided into numerous discrete, non-overlapping finite control volumes. This process is called "meshing". The boundary types and fluid type were also assigned to the virtual prototype's elements in Gambit. The 3D prototype of the UVGI air inactivation reactor without any baffle installed is sketched in Figure 5.2. The *x*-*y*-*z* Cartesian coordination system is also shown in the figure. The duct pipe axis and the lamp axis coincide with the *y*-axis. The stainless wires which are used to hang the lamp and the power cable are not drawn in the 3D model and their effect on the aerodynamics was neglected. Note that the origin point **O**(0,0,0) is located at the upstream end of the lamp arc, not at the beginning of the electrical pin of the lamp.

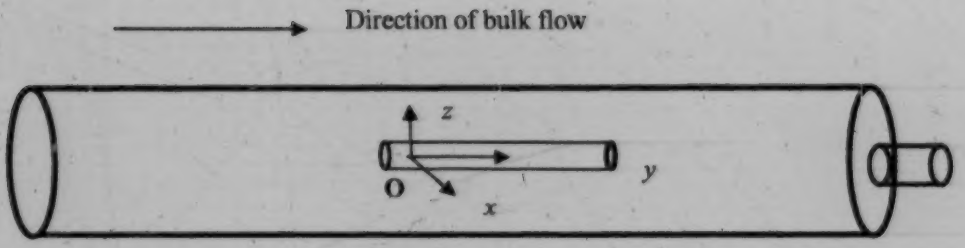

Figure 5.2. UVGI air inactivation reactor 3D model with Cartesian coordination system

A mesh independency study is a necessary step in CFD modeling and is used to determine an appropriate balance between computational accuracy and computational cost. The Fluent® (R 6.2.16 Fluent Inc.) code solves the fluid dynamics governing equations by using the finite volume method (Fluent 2005). The topologies and number of the discrete control volumes affect the discretisation and linearization of the governing equations and, therefore, determines the accuracy and computational speed of the numerical solution. Generally, when the same topologies of the control volumes and the discretisation and linearization schemes are chosen, the accuracy of the numerical solution increases as the number of the discrete control volume increases. On the other hand, a higher density meshed domain requires more computational cost than a lower density domain does. A high density mesh increases the computational time needed to reach a converged solution. In a mesh independency study, simulations are carried out using different density meshes. Typically, the mesh density is increased from lower density to higher density with each simulation to test the balance between the accuracy and the computational cost. Certain simulation outputs are chosen as criteria in order to compare the effect of different mesh densities. If the results of the simulations do not

change within a defined tolerance when the density of the mesh is increased from a lower density mesh to a higher density one, the solution is regarded as mesh independent. The lower density mesh is then used to carry out the remaining simulations.

The 3D UVGI reactor virtual prototype was imported into Gambit and then meshed with three different density grids, consequently. The numbers of cells were 37,014 (coarse mesh), 66,385 (medium density mesh), and 173,801 (fine mesh). Axial views of the three density meshes are presented in Figure 5.3. The reactor was meshed with a structured hexahedral grid. Structured grids with near wall treatments were implemented in each of the three different density grids.

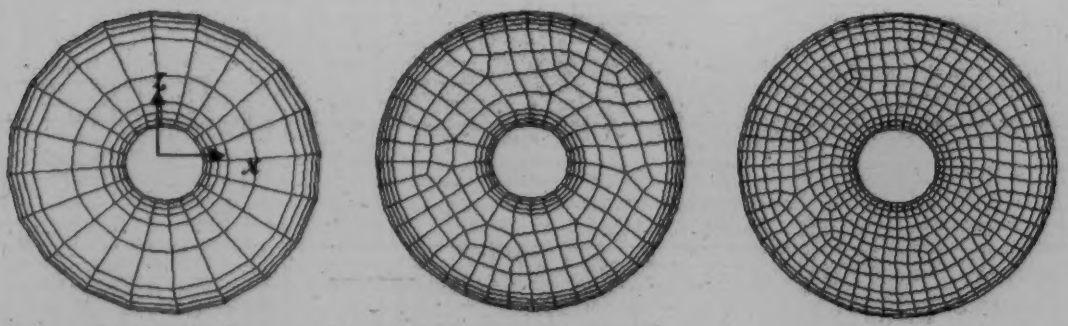

Figure 5. 3. Axial views of the three structured hexahedral grids with different density meshes

In comparison to the x and z velocity profiles, the y velocity profile has the greatest impact on the prediction of microorganism inactivation. The y-velocity profile, therefore, was chosen as the critical parameter for the mesh independency study.

The y velocity profiles were exported from Fluent® through the 'XY Plot' function. The inlet conditions of the three models were set to 'velocity inlet' and the average inlet velocities were all set to 0.023 m/s (11 L/min). The outlet boundary

conditions of the three models were also identical, with zero gauge pressure. The k-ε turbulence model was chosen to model the turbulence. After the iterations converged, two lines were drawn in the three models in Fluent®. The two lines were drawn in the z-y plane, parallel to the y-axis and at different distances from the central axis of the lamp. One line was at z = 0.035 m, the other was at z = 0.045 m. Figure 5.4 shows the computed axial (y) velocity profiles determined along the two lines using each of the three grid models. Along the y axis, at y = 0 to 43 cm where the UV lamp was located, a significant difference existed between the profiles computed using the medium density and low density meshes. In contrast, the profiles computed using the fine mesh and medium density mesh were almost identical. To balance the computational accuracy and cost, the medium density mesh was chosen in the rest UVGI reactor modeling.

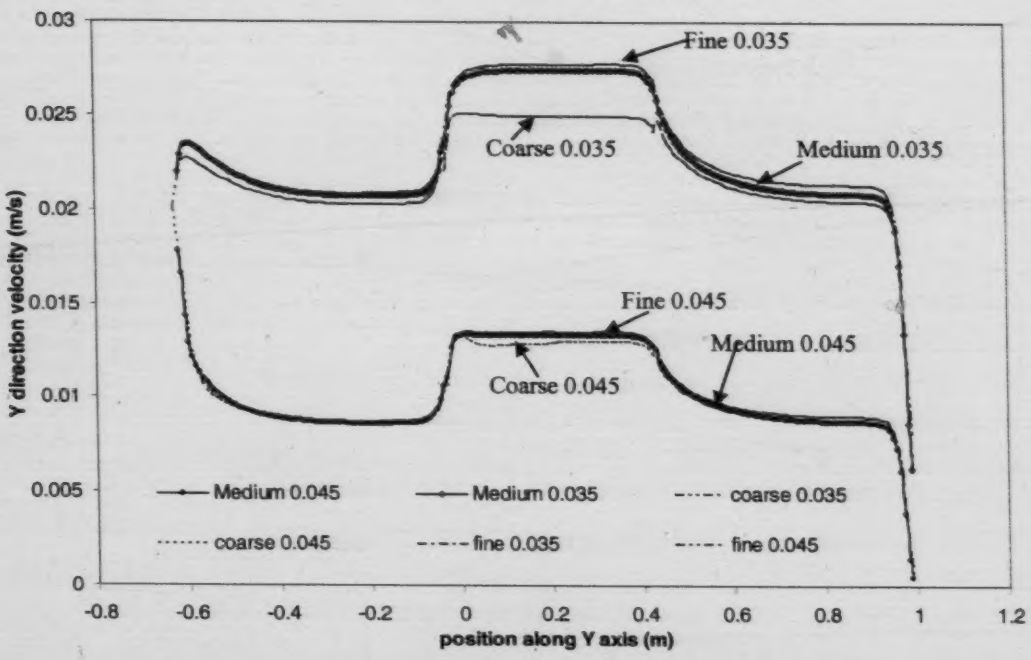

Figure 5. 4. Longitudinal y-velocity profiles computed at two z positions (z = 0.035 m and z = 0.045 m using) three different density meshes

Note that, in Figure 5.4, "Medium 0.045" means the profile was obtained at a radial distance of 0.045 m from the central y-axis using the medium density mesh grid model. Other annotations have similar meanings.

5.2.3 Air fluid modeling in the annular duct

The numerical solution of the air flow velocity profile was compared to an analytical solution. Ideally, visualization techniques such as Laser Doppler Velocimetry (LVD) or Particle Image Velocimetry (PIV) should be used to validate the velocity profiles predicted by CFD models. In this study, these expensive and time consuming velocity profile visualization techniques were not conducted. Instead, the validation of the air flow modeling was done by comparing the predicted velocity profile to one predicted by using a previously published analytical formula.

The analytical velocity magnitude profile and flow rate formulas for Newtonian flow in a concentric annulus at the midpoint of the annulus are given as the following (Chin 2001):

$$u(r) = \frac{R^2 \Delta p}{4\mu L} \times [1 - (\frac{r}{R})^2 + \frac{(1-\kappa^2)\ln(\frac{r}{R})}{\ln(1/\kappa)}] \tag{5.4}$$

$$Q = \frac{\pi R^4 \Delta p}{8\mu L} \times [1 - \kappa^4 - \frac{(1-\kappa^2)^2}{\ln(1/\kappa)}] , \tag{5.5}$$

where $u(r)$ is the local fluid velocity magnitude at radial position r (m/s); R is the outer radius of the concentric annulus (m); κ is the ratio of the inner radius to the outer radius (no units); μ is the viscosity of the fluid material (1.78×10^{-5} kg/(m·s) for air at 20°C 1 atm) ; L is the length of the annulus (m); Δp is the pressure drop between the two ends of

the annulus (Pa); Q is the flow rate of the air passing through the annulus (m^3/s). Figure 5.5 shows the concentric annulus and the location of the velocity magnitude profile.

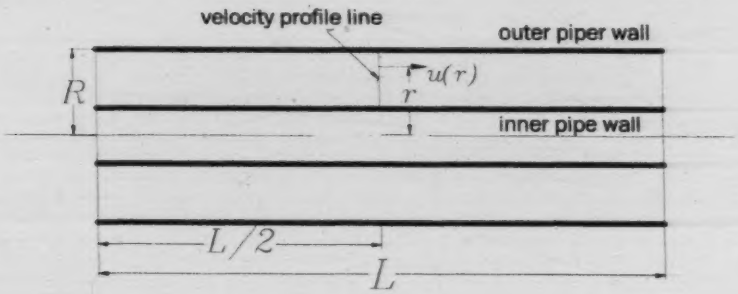

Figure 5.5. A concentric annulus and the location of the velocity profile line

By substituting the geometrical dimensions of the experimental UVGI air inactivation reactor (Figure 4.1) into the above formula, the velocity magnitude profile can be calculated. The velocity magnitude profiles computed for the flow rates of Q = 0.00018 m^3/s (11 L/min) and Q = 0.00073 m^3/s (44 L/min) are plotted in Figure 5.6. The CFD numerical solutions under the same flow rate conditions are also presented in Figure 5.6. As Figure 5.6 shows, the velocity magnitude values from CFD prediction superimpose to the analytical solutions near the wall regions, but are almost 10% higher than the analytical solutions at the peak velocity in predicting the velocity magnitude profile. The wall roughness effect on the velocity profile was not considered in analytical solutions, this might be the reason that the analytical velocity is higher that the CFD prediction.

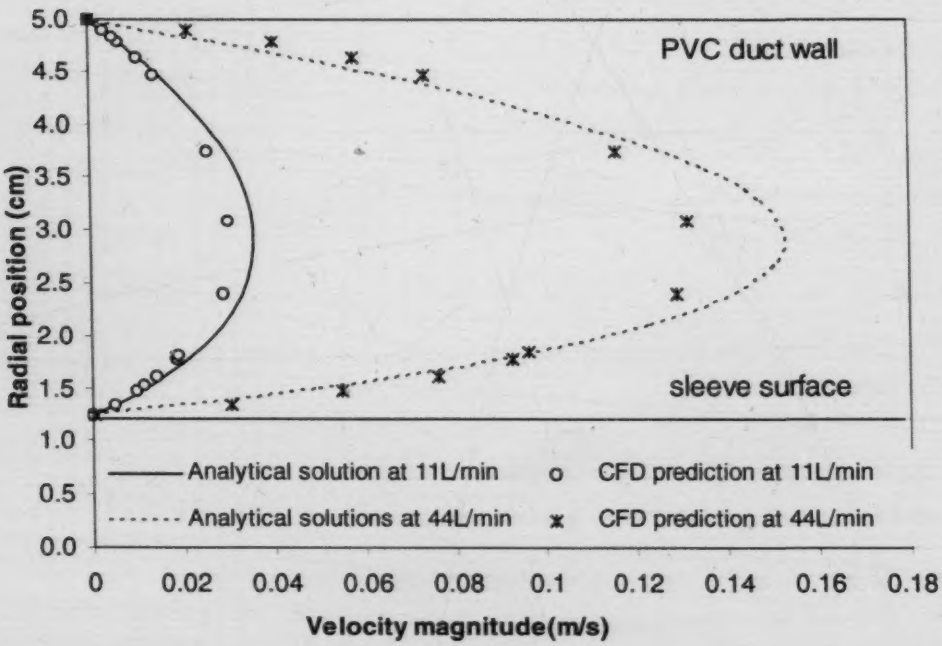

Figure 5. 6. Comparison of the radial velocity profiles calculated by using analytical formulas and computed by using CFD

5.2.4 Thermal effects of the lamp

When a UV lamp is energized, it generates heat, which is transferred away from the lamp into the surrounding air by convection and radiation. Radiation is negligible because the absorbance of air is low at the wavelength range emitted by a LP UV lamp (i.e., 254 nm). Convection caused by the thermal effects of the UV lamp may influence the air flow pattern inside the reactor. In order to account for this possibility, energy balance equations were solved in the CFD model along with the mass and momentum conservation equations.

The reactor inlet air temperature and the lamp sleeve surface temperature measured in the inactivation experiments were used as the boundary conditions in the CFD energy model. The thermal model was validated by comparing the bulk temperature

of the air measured at the outlet of the reactor to the temperature computed by the CFD model. The values of the thermal properties of the PVC pipe were adapted from the *PVC Hand Book* (Wilkes et al. 2005) and were listed as follows: density (ρ) 1390 kg/m^3, specific heat (C_p) 920 J/(kg°C) and thermal conductivity (k) 0.175 J/(m·s°C). Temperature data from the inactivation experiments and the CFD prediction are tabulated in Table 6. All the thermal data were measured without any baffles installed in the reactor.

Table 6 Comparison of measured temperature CFD predicted temperature

Inlet air flow rate (L/min)	Inlet bulk air temperature (°C)	Sleeve surface temperature (°C)	Outlet bulk air temperature	
			Measured (°C)	CFD Predicted(°C)
11	20	79	25-26	28.0
26.5	20	78	24-25	27.9
44	20	72	26-27	27.4

Table 6 shows that the measured temperature at the reactor outlet was lower than but still close to the CFD predicted temperature. The thermal effect on the velocity magnitude profile at 11 L/min is shown in Figure 5.7. The velocity profiles were extracted from the same location shown in Figure 5.6. The velocities computed when the thermal effect was accounted for were greater than those computed without considering the thermal effect. Convection caused by the thermal effect increased the velocities. Therefore, the thermal effects were modeled in all subsequent reactor simulations.

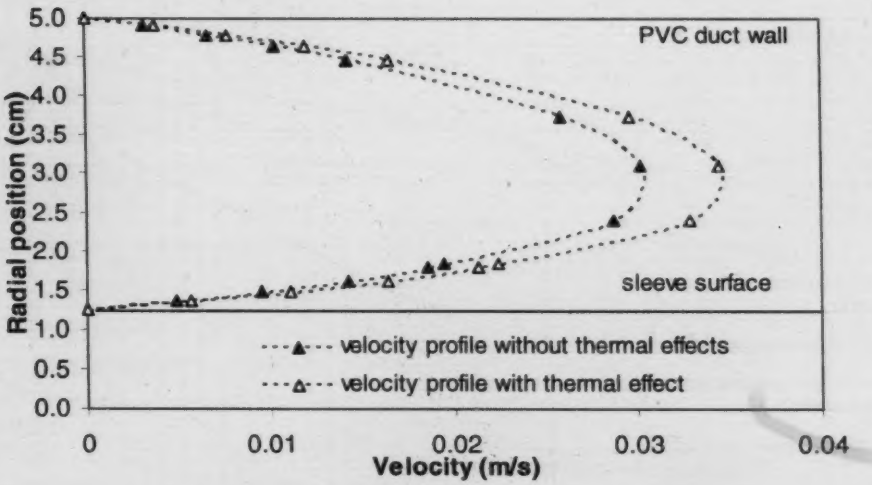

Figure 5. 7. Thermal effect on the velocity profiles

It was assumed that the temperature effect on the UV inactivation rate was negligible because of the biological stability of the *B. subtilis* spores. Hence, the UV inactivation constants of *B. subtilis* spores measured at RH = 50-60% in Chapter 3 were used in the CFD model without considering the temperature effects.

5.2.5 UVC fluence rate field modeling

Various mathematical fluence rate models have been developed by applying optical theories and radiation transportation laws. The View Factor model (Modest 2003) was used in this research because it is accurate and easy to program. The View Factor model was originally derived from radiation energy theory and is used to calculate energy transfer between two surfaces. In the View Factor model, the absorption of UV by the medium (air) at 254 nm wave length is assumed to be negligible. Kowalski (2001) embedded a View Factor model into his UVX code to predict the fluence rate inside air ducts. The View Factor formulas in this thesis were adapted from Kowalski (2001).

Unlike Kowalski's UVX program, this present study did not consider the reflection of UV radiation from the duct walls because the construction material (clear PVC) has a very low reflection factor (<3.4 %) at 254 nm. A C++ program 'VFfluence.cpp' was written to calculate the fluence rate around the UV lamp using the View Factor method. See Appendix 5 for the 'VFfluence.cpp' source code. The VFfluence.cpp can calculate the fluence rate at a given point. In CFD modeling, the control volumes are so small that the fluence rate in any control volume can be represented by using the fluence rate calculated at the centroid point of the control volume.

The View Factor method was validated by comparing the fluence rate profile computed using the program 'VFfluence.cpp' with that computed using UVCalc2D v2.3.0 (Bolton Photosciences Inc., Edmonton, Alberta). Liu et al. (2004) validated the latter model against a spherical actinometry method. The UVCalc2D predictions were close to the spherical actinometry results. Figure 5.8. compares the longitudinal fluence rate profiles at a radial distance of 5 cm from the central axis of the UV lamp predicted by UVCalc2D and the View Factor method (VFfluence.cpp).

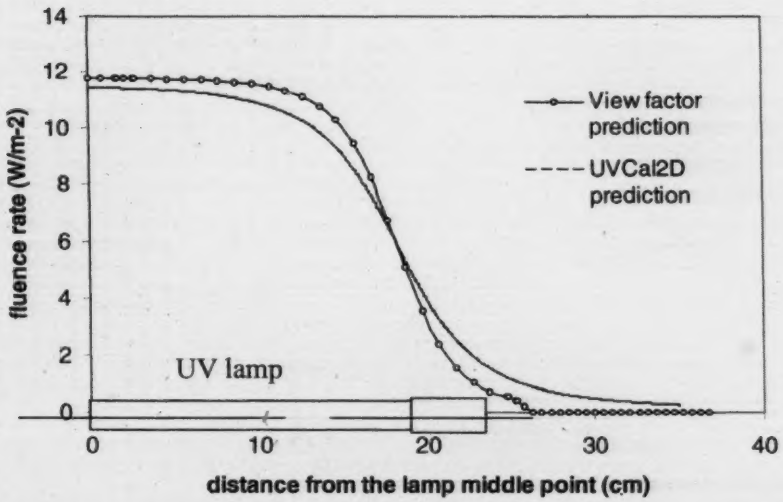

Figure 5.8. Fluence rate profiles predicted at a radial distance of 5 cm from the central axis of the lamp using two models: the View Factor method and UVCal2D

Figure 5.8 reveals the discrepancies between the two predictions. The fluence rates predicted by using the View Factor method are higher in the middle section of the lamp than those predicted using UVCalc2D, while the fluence rates calculated by View Factor near and beyond the lamp ends are lower than the UVCalc2D predictions. However, most of the difference in two models' predictions was less than 0.1 mW/cm^2. It was, therefore, concluded that the View Factor method (VFfluence.cpp program) can generate satisfactory fluence rate field predictions for UV inactivation modeling. Figure 5.9 shows the contour maps of the fluence rate fields inside the UVGI section of the reactor generated by the View Factor model (VFfluence.cpp program). The fluence rates for each centroid point were imported from 'VFfluence.cpp' output data file and were stored in a User Define Memory (UDM) through a User Define Function (UDF) 'addfluence.c' listed in Appendix 5.

Figure 5. 9. Contour map of the fluence rates field of the UVGI reactor section Numbers in the contour lines are the fluence rates in (W m^{-2}), numbers along the axes are the positions in (m)

5.2.6 Euler method: Spore concentration as a scalar

Since the aerodynamic diameter of aerosolized spores is on the order of one micrometer, the effect of gravity on the spore particles was assumed to be negligible during the UV inactivation process. The spore particles are unlikely to have trajectories that differ significantly from the bulk air flow in the reactor. The viable spore concentration in a volume of air was treated as a passive scalar; i.e., the microorganism particle trajectories were assumed to be determined totally by the air flow. Transport of the microorganisms through the reactor is determined by mass transport of the bulk air and the concentration gradient of microorganisms. Microorganism particles were assumed to be distributed homogenously in each finite control volume.

For a control volume in the modeling domain, let the scalar φ represent the concentration of viable spores, and let S_φ be the source term of the scalar φ. The transportation equation for the scalar can be written as

$$\frac{\partial \varphi}{\partial t} + div(\vec{U}\varphi) - div[\Gamma\, grad(\varphi)] - S_\varphi = 0\,. \qquad \textbf{(5.6)}$$

At steady state, $\frac{\partial \varphi}{\partial t} = 0$. The diffusion coefficient Γ for spore particles with an average 0.9 μm aerodynamic diameter can be estimated theoretically to be 2.7×10^{-11} m^2/s (Baron and Willeke 2001) .

The viable spore concentration in the bulk air was defined as a Fluent® User Defined Scalar (UDS) in the UVGI CFD model. The UDS was named 'spore_CFU/m^3', with a unit of CFU/m^3. The average concentrations of the spores at the reactor inlet surface (φ_{in}) and reactor outlet surface (φ_{out}) were calculated by using the 'Mass-weight average' report function in Fluent®. The log inactivation level achieved in the reactor as computed by the model was calculated as

$$-\log S = -\log \frac{\varphi_{in}}{\varphi_{out}} . \qquad (5.7)$$

5.2.7 Euler method: Source terms in the scalar transportation equations

In the Euler model, the source term S_φ was defined to describe the UV inactivation effect of the viable spores in the UVGI air inactivation reactor. S_F was defined as the cumulative fluence scalar source.

Definition of S_φ

In equation (5.6), the source term for a control volume is the UV inactivation kinetics. The kinetics will define the rate of the inactivation process. If the first-order kinetic model is chosen, the source term in (5.6) can be written as

$$S_\varphi = \frac{d\varphi}{dt} = -kE' \qquad (5.8)$$

where k is the first-order UV inactivation constants (in cm^2/mJ) of the aerosolized spores. E is the local fluence rate of the control volume (in mJ/cm^2). The k value for aerosolized *B. subtilis* spores was calculated by linear regression of the inactivation curve experimental data at RH 50-60% in (Figure 3.5, Chapter 3) and by forcing the y-intercept to be 0.

When the air flow velocity is high and the fluence rate is low, the shoulder section in the response curve should be taken into account for better modeling results. In Fluent®, the source term is defined by an internal 'DEFINE_SOURCE' macro in which a derivative form $(\frac{dS_\varphi}{d\varphi})$ of the source term is required. Since the multi-target model's derivative form is hard to write, the multi-target model was described by two linear sections in order to embed it into the CFD model. Graphically, the semi-log form of the multi-target fluence-inactivation level curve can be divided into two sections: a shoulder section at low fluence and a linear section at high fluence. The linearization process is demonstrated in the following Figure 5.10.

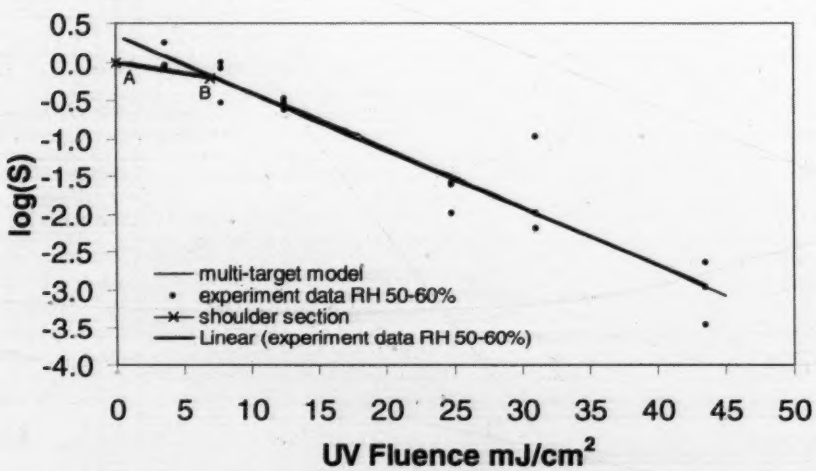

Figure 5.10. Linearization of the multi-target model

In Figure 5.10, the multi-target model is divided into two sections. Experimental data from Chapter 3 'inactivation constants measurement' were used as the raw data. The linear section in the semi-log graphic was derived by applying linear regression to all of the data points. The intersection *B* of the multi-target model curve and the linear line was the beginning of the linear section. The linearization of the shoulder section can be obtained by linking the 100% survival rate point *A* (log S =0) with point *B*. According to the multi-target model theory, there is little or no inactivation at low fluence; the rate of inactivation increases until the fluence increases beyond a threshold certain level (Harm 1980). Similar treatments to the shouldered multi-target models can be found in Kowalski (2001). Hence, the shoulder section has a lower inactivation constant than the linear section does. The mathematical description for these two sections can be written as

$$S_\varphi = \frac{d\varphi}{dt} = \begin{cases} -k_s E' & Shoulder\ \ Section \\ -k_l E' & Linear\ \ Section \end{cases}, \qquad (5.9)$$

where k_s is the inactivation constant for the line AB section and its value is 0.066 cm^2/mJ; k_l is the linear inactivation constant, and k_l = 0.174 cm^2/mJ. A fluence of F = 6 mJ/cm^2 was selected to define the dividing point of the two sections in the multi-target model. The source term was embedded into the CFD model by writing a UDF 'disinfect.c' (See Appendix 5) and loading it into the model.

Definition of S_F

A scalar, the cumulative fluence *F*, was introduced into the reactor CFD model to calculate the fluence received by the air streams as they passed through the UVGI air reactor. The cumulative fluence *F* was used to flag the dividing point of the linear and

shoulder section in CFD modeling. The source term of the cumulative fluence scalar was given by $S_F = dF/dt = E'$. The transportation of the accumulative fluence F is given by

$$\frac{\partial F}{\partial t} + div(\vec{U}F) - E' = 0 \qquad \textbf{(5.10)}$$

The meanings of the symbols in Equation 5.10 were provided in Equation 2.3 in Chapter 2.

Validation of the source term

Because published CFD papers do not discuss embedment of the multi-target model into the source term of a CFD model, the model had to be validated. A hypothetical batch reactor in the shape of a column was built in Fluent®. The fluence rate, $E' = 0.1$ mW/cm^2, was set to be spatially uniform throughout the batch reactor. The cumulative fluence scalar F was defined in Fluent® to calculate the cumulative fluence of the bulk air inside the column. Equation (5.8) was used to define the source term, S_H, of the cumulative fluence scalar. The local fluence rate at the centroid of a control volume was defined as the source term of the cumulative fluence scalar, that is $S_F = E'$.

Unsteady-state simulations were carried out by using one-second step intervals and 500 time steps. The average concentration of viable spores inside the column volume was calculated at the end of each time step. The UV inactivation rate was calculated for every step with the formula:

$$k_i = \frac{\log(\varphi_i / \varphi_{i-1})}{F_i} \qquad \textbf{(5.11)}$$

where k_i (cm^2/mJ) is the step-wise inactivation rate constant at i^{th} second; φ_i and φ_{i-1} (CFU/m^3) are the average viable spore concentrations at i^{th} and $(i\text{-}1)^{th}$ second; F_i (mJ/cm^2) is the volume average fluence in the batch reactor at i^{th} second. See Appendix 5

for the C code 'stepUDS.c' that was used for the calculations. In order to compare the first-order inactivation model with the multi-target model, both formulas (5.8) and (5.9) were assigned to the source term of the viable spore concentration scalar respectively. Figure 5.11 shows the results of the model validation in semi-log form. The slopes of the lines yield the inactivation rates.

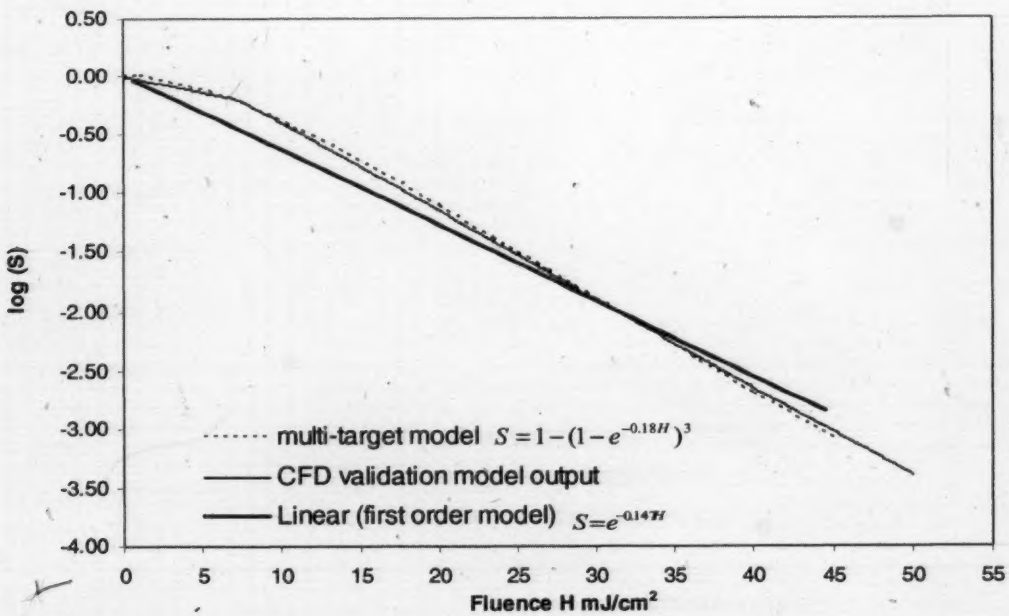

Figure 5. 11. CFD output of the validation model for the double scalar source terms

Figure 5.11 shows that when the fluence is less than 30 mJ/cm^2, the first-order inactivation model resulted in a higher inactivation level than the multi-target model in the shoulder region. Hence, when the fluence is low, the use of the first-order inactivation model can overestimate the inactivation level. In order to generate a conservative prediction, the multi-target model was divided into two linear section and was used in the UVGI reactor CFD models.

5.2.8 Euler-Lagrange model and the fluence distribution curves

Although the inactivation level in the UVGI reactor can be predicted by using the Euler method (the scalar transportation model), the Euler-Lagrange method (the particle tracking method) is widely used in UV reactor modeling to calculate the distribution of fluence rate received by many microorganisms as they pass through the reactor (Chiu and Lyn 1999; Chiu et al. 1999; Munoz 2004). The particle tracking method provides another way of simulating the performance of a UV reactor. Two papers (Ducoste et al. 2005; Sozzi and Taghipour 2006) compared the Euler method with the Euler-Lagrange method for simulating UV reactors in water and wastewater treatment. Both studies concluded that the two methods generate very similar predictions of UV reactor inactivation efficiency. Both methods were valuable in understanding the UV disinfection process and providing the designer with information on different aspects of the UV disinfection process. In this study, the particle-tracking method was used to help understand the effects of internal baffles on the UV inactivation performance of the UVGI reactor. A user defined function 'dose_out.c' was defined in the particle tracking model to store the fluence received by microorganism particles traveling through the UV radiation field. Descriptions and validations of the UDFs used in particle tracking can be found in Munoz (2004).

The average log reduction levels $(-\log S)_{average}$ were computed by:

$$(-\log S)_{average} = -\log \frac{\sum_{i=1}^{N} S_i}{N} = -\log \frac{\sum_{i=1}^{N} (1-(1-e^{-0.018F_i})^3)}{N}, \qquad \textbf{(5.12)}$$

where F_i is the fluence received by the i^{th} particle. S_i is the survival ratio of the particle after receiving F_i fluence predicted by the multi-target model developed in the batch

reactor experiments (Chapter 3); and N is the number of particles released at the inlet surface. The Random Walk Model (RWM) was selected to simulate the uncertainties in the trajectories caused by turbulence.

5.2.9 Boundary conditions of CFD models

The boundary conditions of a CFD model supply the initial boundaries conditions to the serial conservation partial differential equations. The partial differential equations are solved based on the boundary conditions. Hence, the boundary conditions are critical in CFD modeling. However, the boundary conditions are normally unknown before the physical model of interest is built, even after it is built, measurements of the boundary conditions (e.g. kinetic energy k at the inlet) are too difficulty or too expensive. Estimations based on the available parameters are helpful to supply the initial boundary conditions, which were derived from the known parameters in this research.

Inlet and outlet

The inlet boundary condition of the UVGI reactor was set to the 'velocity inlet' type. The inlet velocity was set to be normal to the inlet face with uniform velocity magnitude, and the velocity magnitude was the average value given by $V = Q/A$. Where V is the velocity in m/s; and A is the cross sectional area of the reactor in m^2; and Q is the volumetric flow rate of the air entering the reactor in m^3/s. The outlet boundary condition of the UVGI reactor was set to be the 'pressure outlet' boundary condition. The k and ε values at the inlet boundary were estimated by specifying the turbulence intensity I and turbulence length scale ℓ (Fluent 2005). The values of the turbulence intensity I and turbulence length scale ℓ in duct flow were estimated by using the empirical formulas:

$$I = 0.16(\mathrm{Re})^{\frac{1}{8}} \tag{5.13}$$

$$\ell = 0.07L \ , \tag{5.14}$$

where Re is the Reynolds number, and L is the characteristic dimension of the pipe, which in this case was the diameter of the pipe. The turbulence intensity, I, was estimated to be 6 % by substituting the relevant Reynolds numbers into (5.13) at the inlet boundary. The turbulence length scale, ℓ, was estimated as 0.007 m. The CFD solution would be more accurate if the true velocity and turbulence profiles at the inlet of the reactor were known.

The outlet boundary was set to 'pressure outlet' type, which required the pressure value at the outlet face. At the experimental flow rate of 11 L/min, the sampling impinger caused a positive backpressure at the reactor outlet. The pressure was measured at another place in the outlet section of the UVGI reactor other than at the outlet face (Figure 4.1.). At such a low velocity and low pressure conditions, the air flow in the UVGI reactor can be assumed to be incompressible flow. The gauge pressure at the outlet face was estimated to be close to the measured value at the outlet section which was 10,480 Pascal. For flow rates other than 11 L/min, the outlet gauge pressures were measured to be 0 Pascal. The gauge readings were input into the CFD models as the pressure values for the 'pressure outlet' boundary conditions.

Walls

All walls were set to the 'no-flip' boundary condition in the flow model by default. In the particle tracking model, all the walls are set to be the 'reflect' type with the normal reflecting coefficient equal to 0.

Scalars

The cumulative fluence scalar F was set to be 0 J/m^2 at the reactor inlet face. The viable microorganism concentration scalar φ was set to be a fixed value of 1×10^6 CFU/m^3 at the reactor inlet at was assumed to be spatially uniform at the inlet. The source terms of the two scalars were implemented by defining the relevant UDFs in the fluid boundary conditions. The source codes are 'dose.c' for the cumulative fluence scalar and 'inactive.c' for the viable spore concentration scalar.

Particle tracking model boundary conditions

Microorganism particles were injected at the reactor inlet boundary and were sampled at the reactor outlet boundary. The injection type was the 'surface' type with one particle released from each facet in the inlet surface, which consisted of 313 facets. All microorganism particles were assumed to be spherical and to have a diameter of 1 μm.

In the particle tracking model, the 'inlet' boundary condition was set to the 'reflect' type discrete phase boundary condition, and the 'outlet' boundary condition was set to the 'escape' type boundary condition.

5.3 Results and discussion

So far, the reactor models were built according to the flow chart in Figure 5.1. The sub-models were validated against experimental measurements or analytical solutions. The process of model building is a process of validation and verification. A model built in this way gives the modeler confidence in the model. Based on the studies in water-based modeling (Ducoste et al. 2005; Sozzi and Taghipour 2006), the inactivation level predictions generated by the Euler and Euler-Lagrange models are expected to be close to each other.

5.3.1 Results from the Euler models

The experimental results and CFD predictions for the inactivation levels from the Euler model are presented in Figure 5.12 for three arrangements of baffles: no baffles, a baffle at the inlet of the reactor (head baffle) and a baffle at the middle of the reactor (mid baffle). See Figure 4.1 for the baffle locations. The columns with error bars are the mean of the replicate experimental runs (described in Chapter 4). The error bars represent the 95% confidence interval of the triplicate runs. The columns without error bars represent the log inactivation levels predicted by the CFD model.

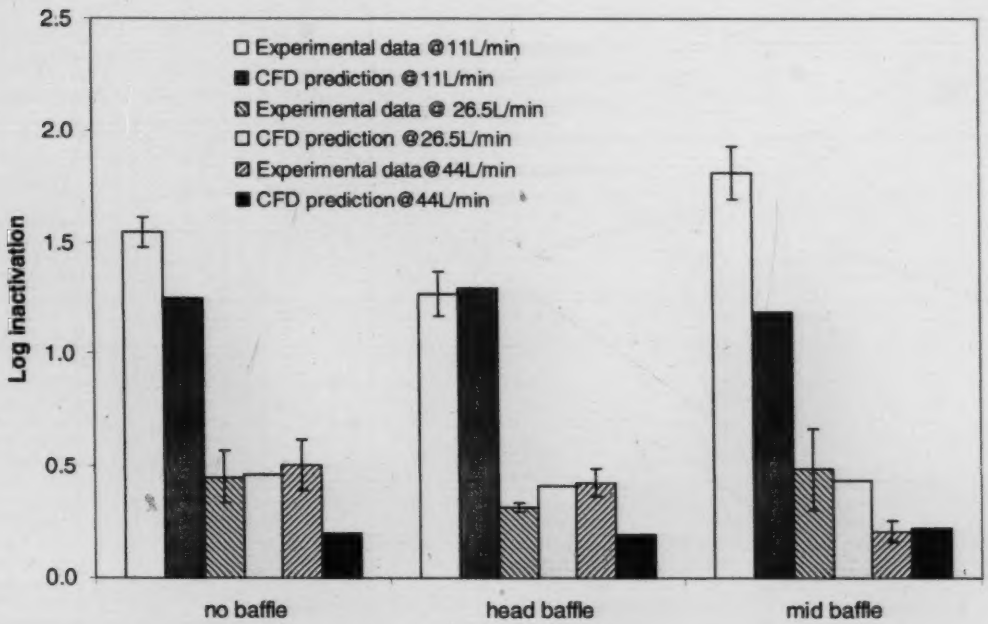

Figure 5. 12. UVGI air disinfection reactor log inactivation levels Experimental results vs. CFD predictions

Figure 5.12 shows that the inactivation levels predicted by the Euler CFD model were generally lower than the experimentally measured inactivation. The exception was

that at the 26 L/min flow rate, with the inlet baffles (head baffle) in place, the experimental log reduction level was lower than the CFD predicted value.

Unlike the experimental results, the CFD predicted inactivation levels were almost the same for a given flow rate, regardless of the baffle arrangement. The effect of the baffles on fluence was negligible in the CFD models. The effect of the baffles in the CFD models can be examined by looking at the velocity profiles. Figure 5.13 shows the effect of baffles on the z velocity (U_z) profiles at the flow rate condition of 44 L/min. The profile line is located in the y-z plane at $z = 0.02$ m.

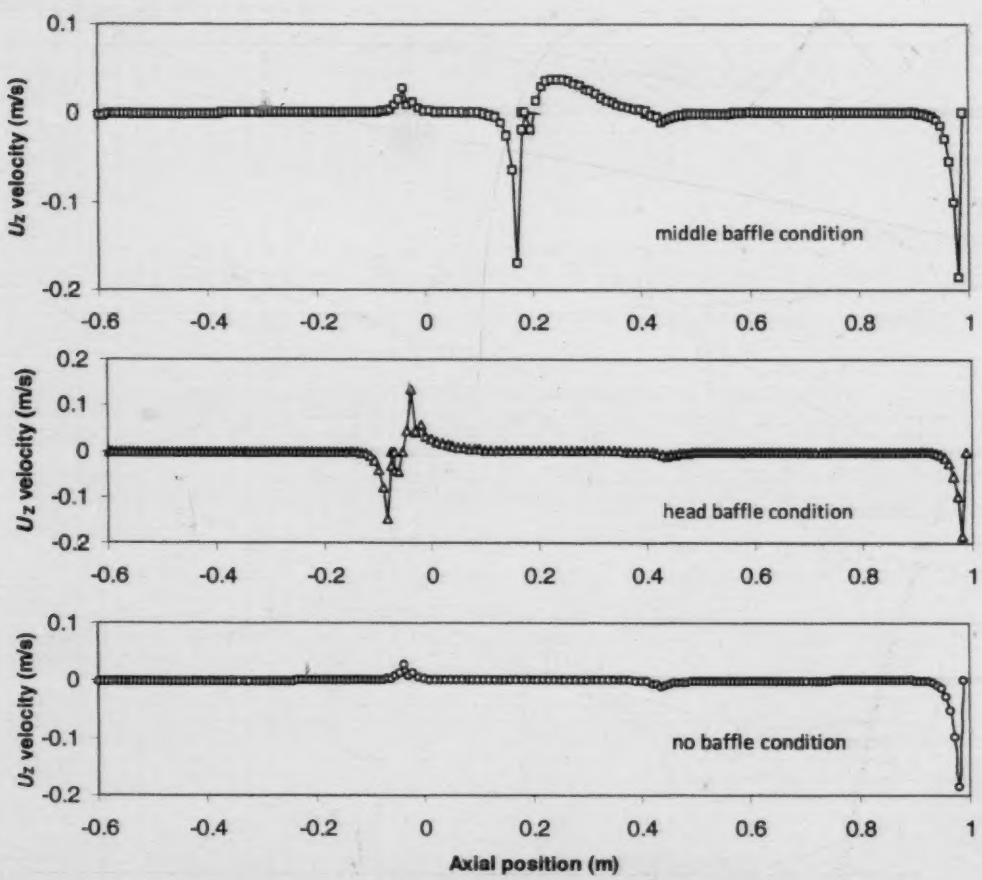

Figure 5.13. U_z profiles at $z = 0.02$ m at flow rate = 44 L/min along the UVGI reactor longitudinal axis with different baffle conditions

In Figure 5.13., the z direction velocity profiles show how the baffles at the head and middle positions affect the mixing of the flow by increasing the U_Z direction velocity. The most prominent mixing effects occur at the baffle locations. The 'middle baffle' causes more mixing in the z direction than the 'head baffle' does. However, the increase in the mixing did not result in an increase in the predicted overall reactor fluence and predicted microorganism inactivation. In order to examine the baffle effects on the cumulative fluence, the cumulative fluence profiles were drawn in Figure 5.14. The profile line is located at the y-z plan at z= 0.02 m, the same position as that of U_Z profiles in Figure 5.13. The air flow rate is also at 44 L/min.

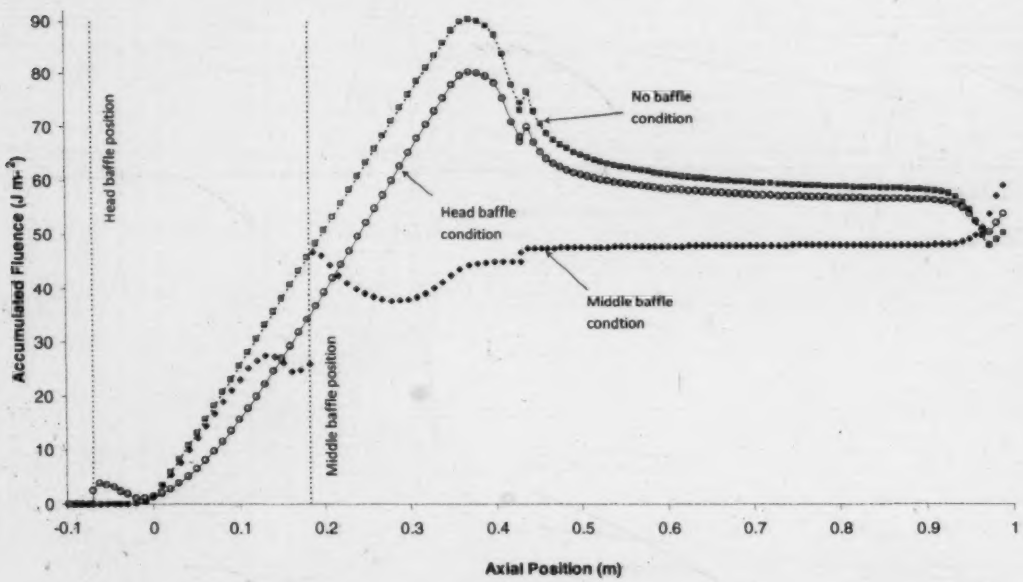

Figure 5.14. Cumulative fluence profiles under three baffle arrangements

Figure 5.14 shows that when no baffle is installed, the cumulative fluence increases linearly along the axial length in the UVGI field. The small bump in the 'head baffle' condition profile after the head baffle position indicates that the baffle effect on

cumulative fluence was small and negligible. Under the 'middle baffle' condition, the cumulative fluence first jumped from 25 to 45 J m^{-2} as a result of the mixing effect, but afterwards the cumulative fluence dropped continuously to the $y = 0.27$ m position. The decrease in the cumulative fluence might be explained by the change of the U_y velocity. Immediately after the baffle, the Uy velocity increased due to the sudden decrease of the baffle's cross section area. The increase of U_y velocity shortened the time length in which the spore particles were exposed to the UV light. The fluence increase from the mixing effects was offset by the fluence decrease caused by the shorter radiation time.

5.3.2 Results from Euler-Lagrange models

Fluence distribution curves were generated by using the data generated by the 'dose_out.c' UDF in the Euler-Lagrange (particle tracking) CFD model. In the particle tracking simulation, a total of 313 (the number of facets at the reactor inlet surface) particles were released at the reactor inlet face. The fluence was calculated for each particle as it moved along its unique trajectory to the reactor outlet face. The computed fluence distribution histograms for the three simulated flow rates and for each of three baffle arrangements are shown in Figure 5.15. The inactivation levels were computed with equation (5.12).

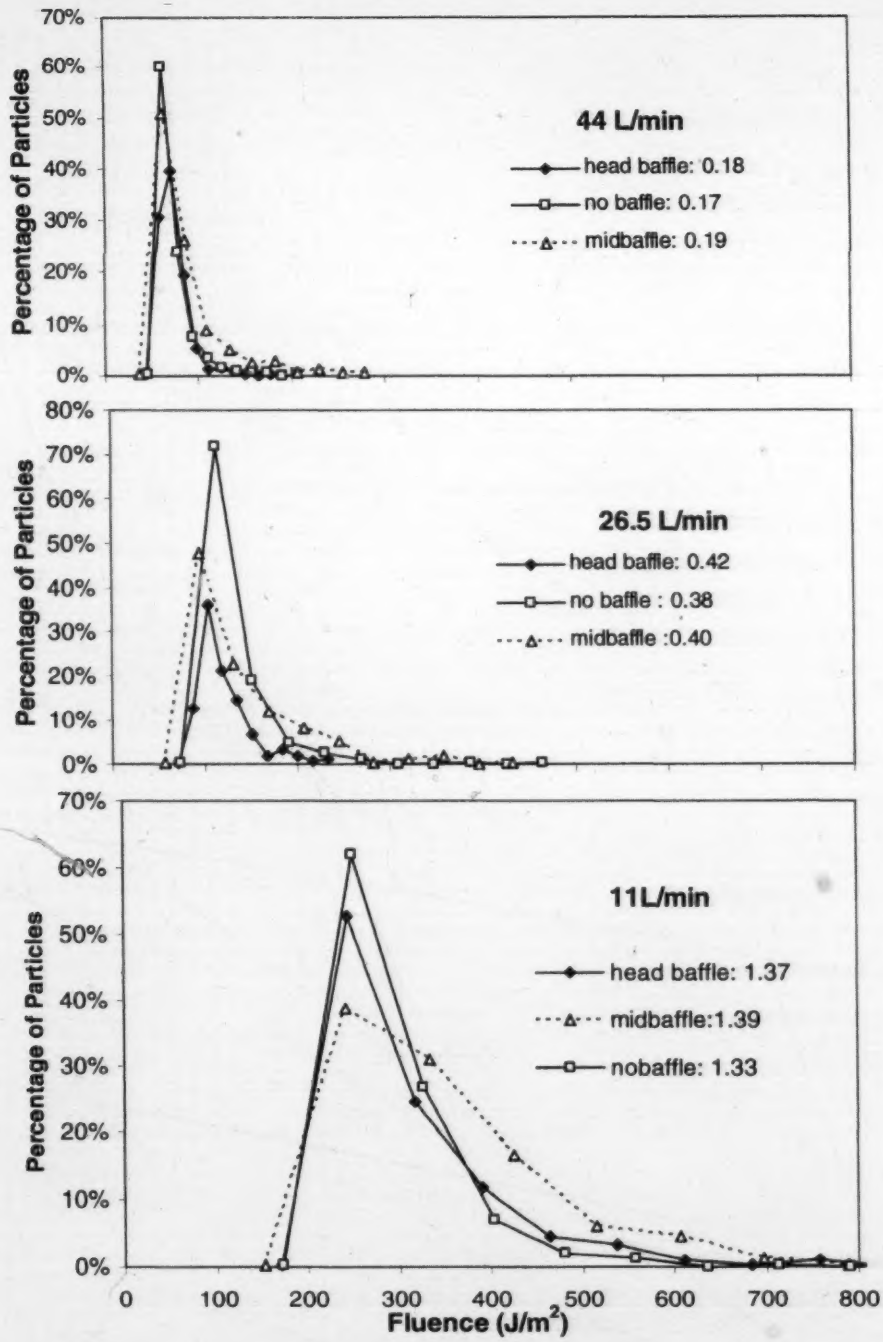

Figure 5. 15. Fluence distributions generated from the particle tracking CFD models for the three flow rate conditions and the three baffle arrangements; numbers to the right of baffle arrangements in the legend are the computed inactivation levels

The single peak and narrow shaped curves in Figure 5.15 reveal that the flow inside the UVGI reactor behaves, superficially, very much like ideal plug flow, in which all the particles receive identical fluence. This explains why the ideal plug flow model predicted the inactivation efficiency so well at 26.5 and 44 L/min, but it doesn't mean that the flow inside the UVGI reactor actually reaches a state of perfect radial mixing with little or no axial mixing. Stratification of the flow likely occurred to some extent, especially at the lower flow rate conditions when the Reynolds number where in the laminar range (625 for 11 L/min). The narrow shape and single peaks shape of the computed fluence distribution curves may have been a result of the relatively small annular space of the UVGI air reactor and absorption and scattering of the UV light at 254 nm in air was negligible. Given a larger UVGI duct or a UVGI duct with curvature features, the fluence distribution curves may have been broader.

As the flow rate of air through the reactor increased, the mode and mean values of the fluence distribution curves decreased (Figure 5.15.). Shifting of the curves mode and mean values under three flow rate conditions reveals that the flow rate was the most significant factor affecting the fluence received by the particles. Hence, the air flow rate was the most significant factor determining the inactivation efficiency of the UVGI reactor. As well, the fluence distribution curves became narrower when the flow rate increased from 11 to 44 L/min. The narrower shapes of the fluence curves suggest that at the higher flow rates, the flow regime in the UVGI reactor approached ideal plug flow more closely. The higher flow velocity caused more turbulence in the fluid and, hence, increased mixing in the radial direction.

Introducing the baffles did not cause significant changes in the shapes of the fluence distribution curves. Figure 5.15 shows that the addition of the baffles resulted in a decrease in the mode values to the fluence curves and an increase in tail area thus increasing the mean of the distribution. These changes to the curves should result in a higher fluence. However, these changes were so small that statistically significant improvements in the disinfection efficiency were not observed.

5.3.3 Discussion

The inactivation levels predicted using the ideal plug flow model and the CFD models, along with the corresponding bioassay experimental results, are presented in Table 7. For the experimental results, the upper and lower 95% confidence limits are provided. Comparisons of the models are based on the values presented in Table 7.

Table 7. Inactivation levels from the models and bioassay experiments

Baffle arrangement	Flow rate (L/min)	Experimental results	Ideal plug flow model	CFD Euler-model	CFD Euler-Lagrange model
no baffle	11	1.48-1.62	1.65	1.25	1.33
	26	0.33-0.57	0.47	0.46	0.38
	44	0.39-0.61	0.19	0.17	0.17
head baffle	11	1.17-1.37	1.65	1.30	1.37
	26	0.30-0.34	0.47	0.41	0.42
	44	0.36-0.48	0.19	0.19	0.18
mid baffle	11	1.69-1.93	1.65	1.19	1.39
	26	0.30-0.66	0.47	0.44	0.40
	44	0.16-0.26	0.19	0.19	0.19

With no baffle in place, the CFD model predictions are consistently lower than the both the experimental results and the ideal plug flow model predictions. The ideal plug flow model predicted higher log inactivation levels than the CFD models did at the

two lower flow rates, 11 L/min and 26 L/min. At the 44 L/min flow rate, the log inactivation level predicted by the plug flow model (0.19) was close to the inactivation predicted by the CFD model (0.17). The discrepancies and agreement between the ideal plug flow model and the CFD model can be explained by the mechanisms involved. In the ideal plug model, all the spore particles passing through the UVGI reactor receive identical fluence, regardless of their individual trajectories. It is well known that an ideal plug flow reactor is a perfect reactor for the UV disinfection process. The UV inactivation efficiency is maximized in an ideal plug flow reactor, in which air mixes in the radial direction completely and axial mixing does not occur. On the contrary, in the CFD models, the flow is not assumed to be ideal plug flow. At the 11 L/min and 22 L/min flow rates, the flow is mainly in the laminar flow regime. The fluid is not completely mixed in the radial direction. Therefore, the plug flow model predicts higher inactivation level than the CFD model does at these two flow rates. When the flow rate reaches 44 L/min and the Reynolds number reaches 2526, the level of flow stratification inside the UVGI reactor decreases and the radial mixing increases due to greater turbulence. Hence, the predictions from the ideal plug flow model and CFD models are close to each other at the flow rate of 44 L/min.

Neither the CFD models nor the ideal plug flow model predicted the difference in inactivation that was observed between the 'no baffle' condition and baffled conditions. At 26 L/min, with the head baffle installed, the measured inactivation level was lower than the inactivation predicted by both the CFD models and the ideal plug flow model. Except for that condition, the inactivation levels predicted by the CFD models were lower

than the measured inactivation. Overall, the installation of the baffles did not result in an increase in the inactivation levels. Hence, baffles need to be designed carefully.

The ability to account for the shoulder section is very important in modeling the UVGI air inactivation process because many airborne microorganisms, such as some fungi, bacteria spores and molds, exhibit shoulder effects in their UV inactivation kinetics. Compared to other Euler models built by other researchers (Noakes et al. 2004a; Noakes et al. 2004b) in UVGI air disinfection modeling, the Euler model with the double-scalar can account for the shoulder section of the UV response curve. A first-order kinetic model cannot describe the shoulder section in the inactivation process for these species. This simplification may result in overestimation of the UV inactivation levels at lower fluences. The Euler model with double scalars can also be easily modified to account for the tailing effects in UV inactivation curves by defining the threshold fluence for the tailing section. The shoulder section of the UV inactivation was also accounted for in the Euler-Lagrange model. In Euler-Lagrange model, the inactivation levels were computed in the post-processing calculations by substituting the fluence into the multi-target model.

Both the Euler and Euler-Lagrange models are valuable for modeling the in-duct UVGI air inactivation reactor. In the Euler method, with the help of various tools in the Fluent® code, the local flow condition and local fluence can actually be 'seen' through contour maps and other plot functions. Although it was not demonstrated in this study due to the simple geometry of the UVGI reactor, the visualization functions will give a UVGI reactor designer an opportunity to visualize the air flow pattern within the reactor and to use this to design baffle arrangements that will improve the efficiency of the

reactor. The Euler-Lagrange method produces fluence distribution curves that can enable the designer to understand on how the mixing effects can affect the fluence distribution received by the target microorganisms.

In this study, numerical predictions of inactivation generated with the two CFD models were close to or lower than experimentally measured inactivation except at the 26 L/min flow rate when the head baffle was installed. Conservative results in modeling, especially in pathogen microorganism control practice, are beneficial since the public health protection is the primary goal. Gradual build up of dust on the sleeve or lamp surface, and the aging of the lamp or the ballast may decrease the fluence rate level inside a induct UVGI air disinfection reactor (IUVA 2005b). Hence, the sizing of the UV lamp power based on numerical modeling should be conservative.

In CFD modeling of the in-duct annular UVGI air disinfection reactor, both Euler and Euler-Lagrange methods have been applied. The two methods produced similar results in predicting the inactivation efficiency of the UVGI reactor. However, due to potential experimental bias and the uncertainty in numerical model, discrepancies exist between the experiment data and the numerical simulation. Experimental bias can come from and accumulate in the process of controlling the experimental factors, such as the flow rate control, and spores' culture and enumeration procedures. On the other hand, the accuracy of numerical modeling may be affected by assumptions made regarding to boundary conditions, the approximations in the solutions of Navier-Stokes equations, and simplifications in the turbulence model and the fluence rate field sub-model. In order to get sufficient confidence in CFD modeling, the verification of the overall CFD model predictions by using experimental results is necessary. Validations of the sub-models in

the lower hierarchy of the overall model are also necessary in order to gain confidence in the overall model (Oberkampf and Trucano 2002). Validations of the sub-models are also very helpful in trouble-shooting when a large difference exists between the model predictions and the experimental results.

B. subtilis spore is an important surrogate challenge microorganism that has been used in water-based UV reactor testing and validation practice. *B. subtilis* spore can also be a valuable surrogate in air-based UVGI disinfection system testing and validation. Note that in Table 7, the experimental results for the high flow rate (44L/min) are higher than the ideal plug flow model predictions in the 'no baffle' and 'head baffle' cases, which is impossible according to reactor modeling theory. However, the fluence (6.8 mJ/cm^2) for this high flow rate is in the shoulder section of the inactivation curve, see Figure 3.5. This means that the inactivation level is very insensitive to the fluence in the shoulder section and that one can not estimate the inactivation level with confidence. Hence, when *B. subtilis* spores are used in a biodosmetry test, the fluence should reach a level that shoulder section can be avoided.

6 Conclusions

In this study, an annular UVGI air inactivation reactor was built, and its microorganism inactivation efficiency was measured experimentally. Also, a preliminary attempt was carried out to use CFD techniques to model the inactivation efficiency in the reactor. In order to supply reliable inactivation constants for the modeling, a new method to measure the UV inactivation constants of aerosolized *B. subtilis* spores was developed.

The collimated beam well-mixed batch reactor system used in this study to measure the UV inactivation rate constants has some advantages in terms of fluence rate measurement and operational control over methods used by previous researchers. The standard protocol widely accepted in water-based UV inactivation studies was adapted to build the collimated beam batch reactor. However, before the collimated beam well-mixed batch reactor system can became a standard method, more experiments should be done on other aerosolized species microorganisms such as vegetative cells and viruses. The same collimated beam system used in this study was used by other students for measuring UV inactivation of microorganisms in water, except that the well-mixed batch reactor was replaced with a small Petri dish. The dimensions of the collimated beam limit the volume of the well-mixed batch reactor. In order to extend the inactivation level beyond 3 log reduction, a larger well-mixed batch reactor is needed. A collimated beam system should be designed and built for this specific purpose. Because the flow rate for sampling is not limited to a specific value, air samplers other than impingers, such as a single stage Anderson impactor, can be used to collect larger samples of the aerosolized microorganisms trapped in the well-mixed batch reactor.

Bioassay experiments were conducted to test the efficiency of the annular UVGI air disinfection reactor in the single-pass mode. It was found that, without any baffles installed in the UVGI reactor, the inactivation level predicted by a perfect plug flow model in combination with a multi-target kinetic model was higher than the experimental result at a low flow rate 11 L/min. For a UVGI reactor with such a simple geometry, the use of ideal plug flow assumption and multi-target model to predict inactivation level, which was proposed by Kowalski (2001), was valid at higher flow rate at 26.5 L/min and 44 L/min flow rate.

In the CFD modeling, the Euler and Euler-Lagrange methods were both investigated for their ability to predict the inactivation level in the UVGI reactor. The predictions of inactivation generated by using the two CFD models were close to each other. The CFD predictions of the inactivation levels for the three flow rate conditions were, in general, conservative in comparison to the prediction from the perfect plug flow model. The CFD predictions agree with the experimental results for four conditions, and lower than experimental results under other four conditions. Only under one out of the nine experimental conditions, the CFD model predictions are slightly higher than the experimental result. Therefore, the CFD models can predict valuable inactivation levels for the UVGI designer.

7. Recommendations

Although the CFD simulation results from this research agree well with the parallel bench-scale experimental results, additional studies need to be done before CFD simulation can be used to aid the design process. In this preliminary research, a sensitivity study on how changes of modeling parameters affect inactivation levels was not conducted. The important parameters include the inactivation rate constants, the lamp's UVC output value, the value of the Lagrangian empirical constant (C_L) in the Lagrange model. A sensitivity study on how these parameters affect the power consumption should also be done.

The UV reactor model components and the validation process also need improvements. A more sophisticated fluence rate distribution model is needed. In a complex geometry with curvature and elbow features, UV radiation shadows occur. A fluence rate model must be developed to account for this shadowing effect. Otherwise, the inactivation level will be over-estimated. When materials of high reflectivity are used in UVGI system construction, failure to account for the reflected UV radiation will lead to under-estimation of the inactivation level. Ray-tracing software may be a solution for the fluence rate distribution model in a UVGI system with complex geometry and high reflection materials. In a UVGI system with complex geometry, the velocity profiles can be very complicated, and the analytical solutions are not available. Under such situations, Laser Doppler Velocimetry (LVD) or Particle Image Velocimetry (PIV) techniques can be used to validate the velocity profiles predicted by CFD models.

References

ACGIH. (1999). Bioaerosols: assessment and control Conference of Governmental Industrial Hygienists. Cincinnati, OH, USA

Alani, A., Barton, I. E., Seymour, M. J., and Wrobel, L. C. (2001). Application of Lagrangian particle transport model to tuberculosis (TB) bacteria UV dosing in a ventilated isolation room. *International Journal of Environmental Health Research, 11*(3), 219-228.

Baron, P. A. and Willeke, K. (2001). *Aerosol Measurement - Principles, Techniques, and Applications* (2nd ed.): John Wiley and Sons. Online version available at:http://www.knovel.com/knovel2/Toc.jsp?BookID=1080&VerticalID=0.

Beggs, C. B. (2003). The airborne transmission of infection in hospital buildings: Fact or fiction? *Indoor and Built Environment, 12*(1-2), 9-18.

Blatchley, E. R. (1997). Numerical modelling of UV intensity: Application to collimated-beam reactors and continuous-flow systems. *Water Research, 31*(9), 2205-2218.

Bolton, J. R. (2001). *Ultraviolet Applications Handbook* (2nd ed.). Bolton Photosciences Inc. Edmonton, AB, Canada.

Bolton, J. R., and Linden, K. G. (2003). Standardization of methods for fluence (UV dose) determination in bench-scale UV experiments. *Journal of Environmental Engineering-ASCE, 129*(3), 209-215.

Burge, H. A. (1995). *Bioaerosols*. CRC Press. Boca Raton, Florida, USA

CDC. (2007). Public Health investigation seeks people who may have been exposed to extensively drug resistant tuberculosis (XDR TB) infected person.

Chin, W. C. (2001). *Computational Rheology for Pipeline and Annular Flow*. Butterworth-Heinemann. Boston, MA, USA

Chiu, K.-p., and Lyn, D. A. (1999). Effect of UV System Modifications on Disinfection Performance. *Journal of Environmental Engineering, 125*(5), 459.

Chiu, K., Lyn, D. A., Savoye, P., and Blatchley, E. R. (1999). Integrated UV disinfection model based on particle tracking. *Journal of Environmental Engineering-ASCE, 125*(1), 7-16.

Ducoste, J. J., Liu, D., and Linden, K. (2005). Alternative approaches to modeling fluence distribution and microbial inactivation in ultraviolet reactors: Lagrangian versus Eulerian. *Journal of Environmental Engineering-ASCE, 131*(10), 1393-1403.

Ehrlich, R., Miller, S., and Walker, R. L. (1970a). Effects of Atmospheric Humidity and Temperature on Survival of Airborne Flavobacterium. *Applied Microbiology, 20*(6), 884-887.

Ehrlich, R., Miller, S., and Walker, R. L. (1970b). Relationship between Atmospheric Temperature and Survival of Airborne Bacteria. *Applied Microbiology, 19*(2), 245-249.

Fletcher, L. A., Noakes, C. J., Beggs, C. B., Sleigh, P. A., Donnelly, J., and Kerr, K. (2003). *The Ultraviolet Susceptibilty of Aerosolised Microorganisms and the Role of Photoreactivation.* Paper presented at the 2nd International Congress on Ultraviolet Technologies, Vienna, Austria.

Fluent. (2005). *Fluent 6.2 User's Guide*. Fluent Inc. Lebanon, NH, USA

Griffiths, W. D., Bennett, A., Speight, S., and Parks, S. (2005). Determining the performance of a commercial air purification system for reducing airborne contamination using model micro-organisms: a new test methodology. *Journal of Hospital Infection, 61*(3), 242-247.

Harm, W. (1980). *Biological Effects of Ultraviolet Radiation*. Cambridge University Press, New York, NY, USA

IUVA. (2005a). General Guideline for UVGI Air and Surface Disinfection System (Vol. IUVA-G01A-2005): IUVA.

IUVA. (2005b). Guideline for Design and Installation of UVGI In-Duct Air Disinfection System (Vol. IUVA Draft Guideline IUVA-G03A-2005).

Keitz, H. A. E. (1971). *Light Calculations and Measurements* (2nd ed.). N.V. Philips. Eindhoven, Netherlands.

Ko, G., First, M. W., and Burge, H. A. (2000). Influence of relative humidity on particle size and UV sensitivity of *Serratia marcescens* and *Mycobacterium bovis* BCG aerosols. *Tubercle and Lung Disease, 80*(4-5), 217-228.

Kowalski, W. B. (2001). *Design and Optimization of UVGI Air Disinfection Systems.* PhD Thesis, Department of Architecture, The Pennsylvania State University. State College, PA, USA.

Kowalski, W. J., and Bahnfleth, W. P. (2000). UVGI Design Basics for Air and Surface Disinfection. *Heating/Piping/Air Conditioning*, January, 100-110

Kowalski, W. J., Bahnfleth, W.P., and Mistrick, R.G. (2005). A Specular Model for UVGI Air Disinfection Systems. *IUVA News, 7*(1), 19-26.

Kowalski, W. J. and Bahnfleth,W. P. (2003). Immune-Building Technology - The effectiveness of dilution ventilation, filtration, and UVG1 in mitigating five biological-weapon agents. *HPAC Engineering, 75*(1), 57-62.

Marthi, B., Fieland, V. P., Walter, M., and Seidler, R. J. (1990). Survival of Bacteria During Aerosolization. *Applied and Environmental Microbiology, 56*(11), 3463-3467.

May, K. R. (1973). The collison nebulizer: Description, performance and application. *Journal of Aerosol Science, 4*(3), 235-238.

Miller, S. L. M., Janet M. (2000). Evaluation of a Methodology for Quantifying the Effect of Room Air Ultraviolet Germicidal Irradiation on Airborne Bacteria *Aerosol Science and Technology, v.33*(n3), 274-294.

Miller, W. S., Idoine, L. S., Scherff, R. A., and Piepoli, C. R. (1961). Physical Tracers for Bacterial Aerosols. *Applied Microbiology, 9*(3), 248-251.

Modest, M. F. (2003). *Radiative Heat Transfer* (2nd ed.). Elsevier Science. San Diego, CA, USA.

Munoz, A. (2004). *Development of a CFD Model for Predicting Disinfection in a Large UV Reactor.* MSc Thesis, Department of Civil and Environmental Engineering, University of Alberta, Edmonton, AB, Canada.

Nicas, M., and Miller, S. L. (1999). A Multi-Zone Model Evaluation of the Efficacy of Upper-Room Air Ultraviolet Germicidal Irradiation. *Applied Occupational and Environmental Hygiene, 14*, 317-328.

Noakes, C. J., Beggs, C. B., and Sleigh, P. A. (2004a). Modeling the performance of upper room ultraviolet germicidal irradiation devices in ventilated rooms:

Comparison of analytical and CFD methods. *Indoor and Built Environment, 13*(6), 477-488.

Noakes, C. J., Fletcher, L. A., Beggs, C. B., Sleigh, P. A., and Kerr, K. G. (2004b). Development of a numerical model to simulate the biological inactivation of airborne microorganisms in the presence of ultraviolet light. *Journal of Aerosol Science, 35*(4), 489-507.

Noakes, C. J., Sleigh, P. A., Fletcher, L. A., and Beggs, C. B. (2006). Use of CFD Modelling to Optimise the Design of Upper-room UVGI Disinfection Systems for Ventilated Rooms. *Indoor and Built Environment, 15*(4), 347-356.

Oberkampf, W. L., and Trucano, T. G. (2002). Verification and validation in computational fluid dynamics. *Progress in Aerospace Sciences, 38*(3), 209-272.

Peccia, J., and Hernandez, M. (2001). Photoreactivation in airborne Mycobacterium parafortuitum. *Applied and Environmental Microbiology, 67*(9), 4225-4232.

Peccia, J., and Hernandez, M. (2004). UV Induced Inactivation Rates for Airborne Mycobacterium bovis BCG. *Journal of Occupational and Environmental Hygiene, 1*(7), 430-435.

Peccia, J., Werth, H. M., Miller, S., and Hernandez, M. (2001). Effects of relative humidity on the ultraviolet induced inactivation of airborne bacteria. *Aerosol Science and Technology, 35*(3), 728-740.

Sasges, M., and Robinson, J. (2005). Accurate Measurement of UV Lamp Output. *IUVA News, 7*(3), 21-24.

Setlow, P. (2006). Spores of *Bacillus subtilis*: their resistance to and killing by radiation, heat and chemicals. *Journal of Applied Microbiology, 101*(3), 514-525.

Severin, B. F., and Roessler, P. F. (1998). Resolving UV photometer outputs with modeled intensity profiles. *Water Research, 32*(5), 1718-1724.

Severin, B. F., Suidan, M. T., and Engelbrecht, R. S. (1983). Effects of Temperature on Ultraviolet-Light Disinfection. *Environmental Science & Technology, 17*(12), 717-721.

Severin, B. F., Suidan, M. T., and Engelbrecht, R. S. (1984). Mixing Effects in UV Disinfection. *Journal Water Pollution Control Federation, 56*(7), 881-888.

Sozzi, D. A., and Taghipour, F. (2006). UV reactor performance modeling by Eulerian and Lagrangian methods. *Environmental Science & Technology, 40*(5), 1609-1615.

Uvbiama, R. D. (2005). *The Effect Of Upstream Treatment Processes On UV Inactivation Of Microorganisms in Filtered Drinking Water.* University of Alberta, Edmonton, AB, Canada.

VanOsdell, D., and Foarde, K. (2002). *Defining the effectiveness of UV lamps installed in circulating air ductwork* (No. ARTI-21CR/610-40030-01).Air Conditioning and Refriguration Technology Institute, Arlington, VA, USA.

Versteeg, H. K., and Malalasekera, W. (1995). *An introduction to computational fluid dynamics : the finite volume method* Pearson Education Ltd. Harlow, Essex, England.

Wilkes, C. E., Summers, J. W., and Daniels, C. A. (2005). *PVC Handbook.* Cincinnati, OH, USA.

Xu, P., Peccia, J., Fabian, P., Martyny, J. W., Fennelly, K. P., Hernandez, M., Miller, S.L. (2003). Efficacy of ultraviolet germicidal irradiation of upper-room air in inactivating airborne bacterial spores and mycobacteria in full-scale studies. *Atmospheric Environment, 37*(3), 405-419.

APPENDIXES

Appendix 1. Raw data from B. Subtilis Spores UV inactivation constants measurement experiments

RH=50-60% Fluence: 3.66 mJ/cm2

Run #	Without UV Exposure (N0)						With UV Exposure (N)						Log N/N0
1	Dilution	Plate 1	Plate 2	Plate 3	Geomean	CFU/ml	Dilution	Plate 1	Plate 2	Plate 3	Geomean	CFU/ml	-0.045455
	1.00E-02	171	174	158	167.5	1.68E+04	1.00E-02	143	158	152	150.9	1.51E+04	
	1.00E-03	23	20	18			1.00E-03	14	14	11			
2	Dilution	Plate 1	Plate 2	Plate 3	Geomean	CFU/ml	Dilution	Plate 1	Plate 2	Plate 3	Geomean	CFU/ml	-0.077884
	1.00E-02	173	217	222	202.7	2.03E+04	1.00E-02	176	175	158	169.5	1.69E+04	
	1.00E-03	21	20	27			1.00E-03	14	18	14			
3	Dilution	Plate 1	Plate 2	Plate 3	Geomean	CFU/ml	Dilution	Plate 1	Plate 2	Plate 3	Geomean	CFU/ml	0.246693
	1.00E-02	151	149	147	149.0	1.49E+04	1.00E-02	263	256	270	262.9	2.63E+04	
	1.00E-03	15	17	14			1.00E-03	25	29	19			
Control	Dilution	Plate 1	Plate 2	Plate 3	Geomean	CFU/ml							
	1.00E-06	109	114	103	108.6	1.09E+08							
	1.00E-07	15	7	13									

RH=50-60% Fluence 7.77mJ/cm2

Run #	Without UV Exposure (N0)						With UV Exposure (N)						Log N/N0
1	Dilution	Plate 1	Plate 2	Plate 3	Geomean	CFU/ml	Dilution	Plate 1	Plate 2	Plate 3	Geomean	CFU/ml	0.002873
	1.00E-01	tdtc	tdtc	tdtc		-	1.00E-01	tdtc	tdtc	tdtc		7.09E+03	
	1.00E-02	62	75	75	70.4	7.04E+03	1.00E-02	70	77	66	70.9		
2	Dilution	Plate 1	Plate 2	Plate 3	Geomean	CFU/ml	Dilution	Plate 1	Plate 2	Plate 3	Geomean	CFU/ml	-0.078763
	1.00E-01	tdtc	tdtc	tdtc		-	1.00E-01	tdtc	tdtc	tdtc			
	1.00E-02	81	84	76	80.3	8.03E+03	1.00E-02	69	63	70	67.3	6.73E+03	
3	Dilution	Plate 1	Plate 2	Plate 3	Geomean	CFU/ml	Dilution	Plate 1	Plate 2	Plate 3	Geomean	CFU/ml	-0.532423
	1.00E-01	tdtc	tdtc	tdtc		-	1.00E-01	tdtc	tdtc	tdtc			
	1.00E-02	232	239	229	233.3	2.33E+04	1.00E-02	59	64	85	68.5	6.85E+03	
Control	Dilution	Plate 1	Plate 2	Plate 3	Geomean	CFU/ml							
	1.00E-06	78	78	89	81.5	8.15E+07							
	1.00E-07	10	8	7									

RH=50-60% Fluence: 12.43 mJ/cm2

Run #	Without UV Exposure (N0)						With UV Exposure (N)						Log N/N0
1	Dilution	Plate 1	Plate 2	Plate 3	Geomean	CFU/ml	Dilution	Plate 1	Plate 2	Plate 3	Geomean	CFU/ml	-0.475607
	1.00E-02	50	71	47	55.1	5.51E+03	1.00E-01	173	188	192	184.1	1.84E+03	
	1.00E-03	3	4	6			1.00E-02	20	20	22			
2	Dilution	Plate 1	Plate 2	Plate 3	Geomean	CFU/ml	Dilution	Plate 1	Plate 2	Plate 3	Geomean	CFU/ml	-0.537573
	1.00E-02	75	63	68	68.5	6.85E+03	1.00E-01	221	173	205	198.6	1.99E+03	
	1.00E-03	4	7	6			1.00E-02	6	4	7			
3	Dilution	Plate 1	Plate 2	Plate 3	Geomean	CFU/ml	Dilution	Plate 1	Plate 2	Plate 3	Geomean	CFU/ml	-0.629795
	1.00E-02	65	87	74	74.8	7.48E+03	1.00E-01	180	163	184	175.4	1.75E+03	
	1.00E-03	4	6	6			1.00E-02	27	16	13			
Control	Dilution	Plate 1	Plate 2	Plate 3	Geomean	CFU/ml							
	1.00E-06	91	107	80	92.0	9.20E+07							
	1.00E-07	5	13	8									

RH=50-60% Fluence: 24.86 mJ/cm2

Run #	Without UV Exposure (N0)						With UV Exposure (N)						Log N/N0
	Dilution	Plate 1	Plate 2	Plate 3	Geomean	CFU/ml	Dilution	Plate 1	Plate 2	Plate 3	Geomean	CFU/ml	
1	1.00E-01	tdtc	tdtc	tdtc			1.00E+00	102	93	104	99.5	9.95E+01	-1.958965
	1.00E-02	86	96	90	90.6	9.06E+03	1.00E-01	6	6	6			
	Dilution	Plate 1	Plate 2	Plate 3	Geomean	CFU/ml	Dilution	Plate 1	Plate 2	Plate 3	Geomean	CFU/ml	
2	1.00E-01	279	255	292	274.9	2.75E+03	1.00E+00	63	91	63	71.2	7.12E+01	-1.586602
	1.00E-02	30	23	25			1.00E-01	58	8	8			
	Dilution	Plate 1	Plate 2	Plate 3	Geomean	CFU/ml	Dilution	Plate 1	Plate 2	Plate 3	Geomean	CFU/ml	
3	1.00E-01	302	281	294	292.2	2.92E+03	1.00E+00	73	70	74	72.3	7.23E+01	-1.606469
	1.00E-02	27	28	30			1.00E-01	5	5	6			
	Dilution	Plate 1	Plate 2	Plate 3	Geomean	CFU/ml							
Control	1.00E-06	88	107	102	98.7	9.87E+07							
	1.00E-07	15	7	11									

RH=50-60% Fluence 31.08 mJ/cm2

Run #	Without UV Exposure (N0)						With UV Exposure (N)						Log N/N0
	Dilution	Plate 1	Plate 2	Plate 3	Geomean	CFU/ml	Dilution	Plate 1	Plate 2	Plate 3	Geomean	CFU/ml	
1	1.00E-01	33	27	38	32.4	3.24E+02	1.00E+00	3	2	6	3.3	3.30E+00	-1.99112
	1.00E-02	2	7	2	3.0		1.00E-01	0	1	0			
	Dilution	Plate 1	Plate 2	Plate 3	Geomean	CFU/ml	Dilution	Plate 1	Plate 2	Plate 3	Geomean	CFU/ml	
2	1.00E-01	189	166	128	158.9	1.59E+03	1.00E+00	9	10	12	10.3	1.03E+01	-2.190119
	1.00E-02	18	17	19			1.00E-01	0	1	1			
	Dilution	Plate 1	Plate 2	Plate 3	Geomean	CFU/ml	Dilution	Plate 1	Plate 2	Plate 3	Geomean	CFU/ml	
3	1.00E-01	tdtc	tdtc	tdtc			1.00E+00	tdtc	tdtc	tdtc			-0.977684
	1.00E-02	24	31	30	28.2	2.82E+03	1.00E-01	24	31	35	29.64015	2.96E+02	
	Dilution	Plate 1	Plate 2	Plate 3	Geomean	CFU/ml							
Control	1.00E-06	118	86	100	100.5	1.00E+08							
	1.00E-07	12	7	12									

RH=50-60% Fluence 43.51 mJ/cm2

Run #	Without UV Exposure (N0)						With UV Exposure (N)						Log N/N0
	Dilution	Plate 1	Plate 2	Plate 3	Geomean	CFU/ml	Dilution	Plate 1	Plate 2	Plate 3	Geomean	CFU/ml	
1	1.00E-01	tdtc	tdtc	tdtc		0.00E+00	1.00E+00	2	1	1	1.3	1.26E+00	-3.444818
	1.00E-02	36	40	30	35.1	3.51E+03	1.00E-01	0	0	0			
	Dilution	Plate 1	Plate 2	Plate 3	Geomean	CFU/ml	Dilution	Plate 1	Plate 2	Plate 3	Geomean	CFU/ml	
2	1.00E-01	134	141	148	140.9	1.41E+03	1.00E+00	2	8	2	3.2	3.17E+00	-2.647145
	1.00E-02	18	19	11			1.00E-01	0	0	0			
	Dilution	Plate 1	Plate 2	Plate 3	Geomean	CFU/ml	Dilution	Plate 1	Plate 2	Plate 3	Geomean	CFU/ml	
3	1.00E-01	121	119	115	118.3	1.18E+03	1.00E+00	1	1	2	1.3	1.26E+00	-2.972687
	1.00E-02	15	6	12			1.00E-01	0	0	0			
	Dilution	Plate 1	Plate 2	Plate 3	Geomean	CFU/ml							
Control	1.00E-06	156	164	152	157.3	1.57E+08							
	1.00E-07	29	17	13									

RH=70-83% Fluence 3.74 mJ/cm2

Run #	Without UV Exposure (N0)						With UV Exposure (N)						Log N/N0
	Dilution	Plate 1	Plate 2	Plate 3	Geomean	CFU/ml	Dilution	Plate 1	Plate 2	Plate 3	Geomean	CFU/ml	
1	1.00E-02	tdtc	tdtc	tdtc			1.00E-02	179	171	176	175.3	1.75E+04	-0.326353
	1.00E-03	36	46	31	37.2	3.72E+04	1.00E-03	17	31	24			
	Dilution	Plate 1	Plate 2	Plate 3	Geomean	CFU/ml	Dilution	Plate 1	Plate 2	Plate 3	Geomean	CFU/ml	
2	1.00E-02	191	196	221	202.3	2.02E+04	1.00E-02	306	292	310	302.6	3.03E+04	0.174928
	1.00E-03	19	23	18			1.00E-03	22	32	23			
	Dilution	Plate 1	Plate 2	Plate 3	Geomean	CFU/ml	Dilution	Plate 1	Plate 2	Plate 3	Geomean	CFU/ml	
3	1.00E-02	222	215	221	219.3	2.19E+04	1.00E-02	150	164	165	159.5	1.60E+04	-0.138255
	1.00E-03	29	28	19			1.00E-03	18	30	15			
	Dilution	Plate 1	Plate 2	Plate 3	Geomean	CFU/ml							
Control	1.00E-06	87	94	116	98.3	9.83E+07							
	1.00E-07	3	10	13									

RH=70-83% Fluence 7.47

Run #	Without UV Exposure (N0)						With UV Exposure (N)						Log N/N0
	Dilution	Plate 1	Plate 2	Plate 3	Geomean	CFU/ml	Dilution	Plate 1	Plate 2	Plate 3	Geomean	CFU/ml	
1	1.00E-02	222	214	233	222.9	2.23E+04	1.00E-01	tdtc	tdtc	tdtc			-0.082247
	1.00E-03	29	20	19			1.00E-02	198	175	181	184.4	1.84E+04	
	Dilution	Plate 1	Plate 2	Plate 3	Geomean	CFU/ml	Dilution	Plate 1	Plate 2	Plate 3	Geomean	CFU/ml	
2	1.00E-02	163	164	152	159.6	1.60E+04	1.00E-01	tdtc	tdtc	tdtc			-0.276127
	1.00E-03	24	10	21			1.00E-02	79	92	83	84.5	8.45E+03	
	Dilution	Plate 1	Plate 2	Plate 3	Geomean	CFU/ml	Dilution	Plate 1	Plate 2	Plate 3	Geomean	CFU/ml	
3	1.00E-02	278	291	294	287.6	2.88E+04	1.00E-01	tdtc	tdtc	tdtc			-0.223473
	1.00E-03	31	40	29			1.00E-02	165	172	179	171.9	1.72E+04	
	Dilution	Plate 1	Plate 2	Plate 3	Geomean	CFU/ml							
Control	1.00E-06	101	94	110	101.5	1.01E+08							
	1.00E-07	8	7	6									

RH=70-83% Fluence 14.41 mJ/cm2

Run #	Without UV Exposure (N0)						With UV Exposure (N)						Log N/N0
	Dilution	Plate 1	Plate 2	Plate 3	Geomean	CFU/ml	Dilution	Plate 1	Plate 2	Plate 3	Geomean	CFU/ml	
1	1.00E-02	177	161	168	168.5	1.69E+04	1.00E-01	180	168	204	183.4	1.83E+03	-0.963299
	1.00E-03	12	12	11			1.00E-02	20	30	24			
	Dilution	Plate 1	Plate 2	Plate 3	Geomean	CFU/ml	Dilution	Plate 1	Plate 2	Plate 3	Geomean	CFU/ml	
2	1.00E-02	230	245	207	226.8	2.27E+04	1.00E-01	tdtc	tdtc	tdtc			-0.759919
	1.00E-03	23	28	27			1.00E-02	25	70	35	39.4	3.94E+03	
	Dilution	Plate 1	Plate 2	Plate 3	Geomean	CFU/ml	Dilution	Plate 1	Plate 2	Plate 3	Geomean	CFU/ml	
3	1.00E-02	151	142	144	145.6	1.46E+04	1.00E-01	tdtc	tdtc	tdtc			-0.467765
	1.00E-03	17	16	12			1.00E-02	46	51	52	49.6	4.96E+03	
	Dilution	Plate 1	Plate 2	Plate 3	Geomean	CFU/ml							
Control	1.00E-06	70	60	88	71.8	7.18E+07							
	1.00E-07	13	9	7									

RH=70-83% Fluence 31.08 mJ/cm2

Run #	Without UV Exposure (N0)						With UV Exposure (N)						Log N/N0
	Dilution	Plate 1	Plate 2	Plate 3	Geomean	CFU/ml	Dilution	Plate 1	Plate 2	Plate 3	Geomean	CFU/ml	
1	1.00E-01	tdtc	tdtc	tdtc			1.00E+00	tdtc	tdtc	tdtc			-1.576955
	1.00E-02	142	167	149	152.3	1.52E+04	1.00E-01	32	36	57	40.3	4.03E+02	
	Dilution	Plate 1	Plate 2	Plate 3	Geomean	CFU/ml	Dilution	Plate 1	Plate 2	Plate 3	Geomean	CFU/ml	
2	1.00E-01	tdtc	tdtc	tdtc			1.00E+00	137	140	154	143.5	1.43E+02	-1.613371
	1.00E-02	50	73	56	58.9	5.89E+03	1.00E-01	7	16	13			
	Dilution	Plate 1	Plate 2	Plate 3	Geomean	CFU/ml	Dilution	Plate 1	Plate 2	Plate 3	Geomean	CFU/ml	
3	1.00E-01	tdtc	tdtc	tdtc			1.00E+00	282	279	299	286.5	2.87E+02	-1.740493
	1.00E-02	159	127	194	157.6	1.58E+04	1.00E-01	24	28	26			
	Dilution	Plate 1	Plate 2	Plate 3	Geomean	CFU/ml							
Control	1.00E-06	97	148	105	114.7	1.15E+08							
	1.00E-07	7	6	8									

RH=70-83% Fluence 52.32 mJ/cm2

Run #	Without UV Exposure (N0)						With UV Exposure (N)						Log N/N0
	Dilution	Plate 1	Plate 2	Plate 3	Geomean	CFU/ml	Dilution	Plate 1	Plate 2	Plate 3	Geomean	CFU/ml	
1	1.00E-02	45	56	60	53.3	5.33E+03	1.00E+00	3	2	1	1.8	1.82E+00	-3.467134
	1.00E-03	5	5	3			1.00E-01	1	0	0			
	Dilution	Plate 1	Plate 2	Plate 3	Geomean	CFU/ml	Dilution	Plate 1	Plate 2	Plate 3	Geomean	CFU/ml	
2	1.00E-02	63	53	55	56.8	5.68E+03	1.00E+00	35	35	37	35.7	3.57E+01	-2.202547
	1.00E-03	3	20	9			1.00E-01	3	7	6			
	Dilution	Plate 1	Plate 2	Plate 3	Geomean	CFU/ml	Dilution	Plate 1	Plate 2	Plate 3	Geomean	CFU/ml	
3	1.00E-02	36	47	46	42.7	4.27E+03	1.00E+00	1	2	2	1.6	1.59E+00	-3.429699
	1.00E-03	3	5	4			1.00E-01	0	0	0			
	Dilution	Plate 1	Plate 2	Plate 3	Geomean	CFU/ml							
Control	1.00E-06	86	93	90	89.6	8.96E+07							
	1.00E-07	7	8	6									

Appendix 2. Raw data in Lamp UVC output measurement

UV Lamp Output Measurement using the Goniometric method

Sasages and Robinson (2005)

$$P = \int_{-\pi/2}^{\pi/2} E_\theta dA = \sum_{i=1}^{19} E_i \Delta A = \sum_{i=1}^{19} 2\pi r^2 E_i \cos\theta \Delta\theta$$

Distance/m 2.990

Lamp Temp 102 C

Angle	-90.0	-80.0	-70.0	-60.0	-50.0	-40.0	-30.0	-20.0	-10.0	0.0
Angle in rad	-1.571	-1.396	-1.222	-1.047	-0.873	-0.698	-0.524	-0.349	-0.175	0.000
Irradiance/uWcm-2	0.031	0.168	0.492	0.786	1.013	1.226	1.356	1.475	1.516	1.542
Irradiance/Wm-2	0.000	0.002	0.005	0.008	0.010	0.012	0.014	0.015	0.015	0.015
2*PI*R^2*con(thita)	0.000	9.754	19.212	28.086	36.107	43.030	48.647	52.785	55.319	56.172
dA	0.000	1.702	3.353	4.902	6.302	7.510	8.490	9.213	9.655	9.804
dP/W	0.000	0.003	0.016	0.039	0.064	0.092	0.115	0.136	0.146	0.151
Angle	10.0	20.0	30.0	40.0	50.0	60.0	70.0	80.0	90.0	
Angle in rad	0.175	0.349	0.524	0.698	0.873	1.047	1.222	1.396	1.571	
Irradiance/uWcm-2	1.495	1.458	1.385	1.209	1.056	0.784	0.454	0.104	0.052	
Irradiance/Wm-2	0.015	0.015	0.014	0.012	0.011	0.008	0.005	0.001	0.001	
2*PI*R^2*con(thita)	55.319	52.785	48.647	43.030	36.107	28.086	19.212	9.754	0.000	
dA	9.655	9.213	8.490	7.510	6.302	4.902	3.353	1.702	0.000	
dP/W	0.144	0.134	0.118	0.091	0.067	0.038	0.015	0.002	0.000	

Total UVC Power 1.371

UV Lamp Output Measurement using the Keitz Formula

Reference: H. A. E. Keitz, Light Calculations and Measurements, Macmillan and Co Ltd, London, 1971, Chap. IX.

The Keitz formula is $$P = \frac{E 2\pi^2 DL}{2\alpha + \sin 2\alpha}$$

where E is the irradiance (W/m^2) at a distance of D m from the lamp center
L is the lamp arc length (m)
α is the half angle (in radians) subtended by the lamp at the sensor position, that is tan $\alpha = L/(2D)$.

UV lamp WYCKOMAR Inc. M1-G1-15 US patent NO.4,700,101
Measurement of the LP lamp UVC output

Quartz sleeve on
L = 0.365 m

D / m	E /W m^{-2}	α	P / W
Gigahertz			
1.0	0.119	0.180513	1.200
1.5	0.054	0.121072	1.211
2.0	0.031	0.090998	1.231
2.5	0.018	0.072871	1.114
3.0	0.013	0.060758	1.158
3.5	0.012	0.052096	1.453
4.0	0.007	0.045593	1.107
4.5	0.006	0.040533	1.200
5.0	0.006	0.036484	1.482

UV output 1.311 W

Quartz sleeve off
L = 0.365 m

D / m	E /W m^{-2}	α	P / W
Gigahertz			
1.0	0.691	0.180513	6.970167
1.5	0.309	0.121072	6.929326
2.0	0.177	0.090998	7.026394
2.5	0.110	0.072871	6.809429
3.0	0.086	0.060758	7.657904
3.5	0.061	0.052096	7.388421
4.0	0.049	0.045593	7.748503
4.5	0.038	0.040533	7.602985
5.0	0.032	0.036484	7.902694

UV output 7.660651 W

Appendix 3. Raw data from bioassay on UVGI air inactivation reactor

Flow rate : 11LPM Baffle treatment : no baffle

Sample	Colony counts			dilution	geomean	airvolum	CFU/L
UV on 1	251	267	253	1.00E-01	256.90	11	1.17E+03
UV on 2	55	28	53	1.00E-02	43.38	11	1.97E+03
UV on 3	28	28	29	1.00E-02	28.33	11	1.29E+03
UV off 1	92	84	93	1.00E-03	89.57	11	4.07E+04
UV off 2	120	162	129	1.00E-03	135.86	11	6.18E+04
UV off 3	125	104	120	1.00E-03	115.98	11	5.27E+04

Flow rate : 11LPM Baffle treatment : head baffle

Sample	Colony counts			dilution	geomean	airvolum	CFU/L
UV on 1	139	160	132	1.00E-02	143.19	11	6.51E+03
UV on 2	100	110	107	1.00E-02	105.58	11	4.80E+03
UV on 3	75	73	99	1.00E-02	81.53	11	3.71E+03
UV off 1	152	160	145	1.00E-03	152.21	11	6.92E+04
UV off 2	295	233	286	1.00E-03	269.89	11	1.23E+05
UV off 3	183	189	199	1.00E-03	190.22	11	8.65E+04

Flow rate : 11LPM Baffle treatment : mid baffle

Sample	Colony counts			dilution	geomean	airvolum	CFU/L
UV on 1	40	43	38	1.00E-02	40.28	11	1.83E+03
UV on 2	37	28	28	1.00E-02	30.73	11	1.40E+03
UV on 3	132	120	119	1.00E-01	123.53	11	5.61E+02
UV off 1	219	203	207	1.00E-03	209.56	11	9.53E+04
UV off 2	158	169	141	1.00E-03	155.57	11	7.07E+04
UV off 3	134	122	135	1.00E-03	130.20	11	5.92E+04

Flow rate : 26.5LPM Baffle treatment : no baffle

Sample	Colony counts			dilution	geomean	airvolum	CFU/L
UV on 1	47	52	37	1.00E-02	44.88	8	2.81E+03
UV on 2	70	58	70	1.00E-02	65.75	8	4.11E+03
UV on 3	56	52	42	1.00E-02	49.64	8	3.10E+03
UV off 1	189	233	209	1.00E-02	209.57	8	1.31E+04
UV off 2	105	106	103	1.00E-02	104.66	8	6.54E+03
UV off 3	156	137	152	1.00E-02	148.10	8	9.26E+03

Flow rate : 26.5LPM Baffle treatment : head baffle

Sample	Colony counts			dilution	geomean	airvolum	CFU/L
UV on 1	117	125	113	1.00E-02	118.23	8	7.39E+03
UV on 2	133	138	130	1.00E-02	133.63	8	8.35E+03
UV on 3	127	133	132	1.00E-02	130.64	8	8.17E+03
UV off 1	255	264	282	1.00E-02	266.77	8	1.67E+04
UV off 2	253	255	273	1.00E-02	260.18	8	1.63E+04
UV off 3	278	248	272	1.00E-02	265.68	8	1.66E+04

Flow rate : 26.5LPM Baffle treatment : mid baffle

Sample	Colony counts			dilution	geomean	airvolum	CFU/L
UV on 1	155	170	179	1.00E-02	167.70	8	1.05E+04
UV on 2	52	63	53	1.00E-02	55.79	8	3.49E+03
UV on 3	77	101	87	1.00E-02	87.79	8	5.49E+03
UV off 1	45	41	33	1.00E-03	39.34	8	2.46E+04
UV off 2	238	257	250	1.00E-02	248.21	8	1.55E+04
UV off 3	262	245	208	1.00E-02	237.23	8	1.48E+04

Flow rate : 44LPM Baffle treatment : no baffle

Sample	Colony counts			dilution	geomean	airvolum	CFU/L
UV on 1	105	92	119	1.00E-02	104.75	8	6.55E+03
UV on 2	151	153	152	1.00E-02	152.00	8	9.50E+03
UV on 3	82	68	86	1.00E-02	78.27	8	4.89E+03
UV off 1	43	45	34	1.00E-03	40.37	8	2.52E+04
UV off 2	30	41	39	1.00E-03	36.33	8	2.27E+04
UV off 3	24	29	30	1.00E-03	27.54	8	1.72E+04

Flow rate : 44LPM Baffle treatment : head baffle

Sample	Colony counts			dilution	geomean	airvolum	CFU/L
UV on 1	197	228	195	1.00E-02	206.13	8	1.29E+04
UV on 2	31	26	34	1.00E-03	30.15	8	1.88E+04
UV on 3	221	229	204	1.00E-02	217.75	8	1.36E+04
UV off 1	63	74	59	1.00E-03	65.03	8	4.06E+04
UV off 2	48	77	69	1.00E-03	63.42	8	3.96E+04
UV off 3	57	63	65	1.00E-03	61.57	8	3.85E+04

Flow rate : 44LPM Baffle treatment : mid baffle

Sample	Colony counts			dilution	geomean	airvolum	CFU/L
UV on 1	225	223	214	1.00E-02	220.61	8	1.38E+04
UV on 2	222	207	227	1.00E-02	218.50	8	1.37E+04
UV on 3	231	211	202	1.00E-02	214.33	8	1.34E+04
UV off 1	32	42	44	1.00E-03	38.96	8	2.43E+04
UV off 2	40	37	39	1.00E-03	38.65	8	2.42E+04
UV off 3	32	28	27	1.00E-03	28.92	8	1.81E+04

Appendix 4. Data analysis of the bioassay data in appendix 3

Flow rate 11LPM

	Spores concentration in air CFU/L		
Sample	no baffle	head baffle	mid baffle
UV on 1	1.17E+03	6.51E+03	1.83E+03
UV on 2	1.97E+03	4.80E+03	1.40E+03
UV on 3	1.29E+03	3.71E+03	5.61E+02
UV off 1	4.07E+04	6.92E+04	9.53E+04
UV off 2	6.18E+04	1.23E+05	7.07E+04
UV off 3	5.27E+04	8.65E+04	5.92E+04
Possible log reduction rate -log(Non/Noff)			
1	1.54	1.03	1.72
2	1.72	1.28	1.59
3	1.65	1.12	1.51
4	1.31	1.16	1.83
5	1.50	1.41	1.70
6	1.43	1.26	1.63
7	1.50	1.27	2.23
8	1.68	1.52	2.10
9	1.61	1.37	2.02
Statistics			
Mean	1.55	1.27	1.81
stdev	0.13	0.15	0.25
SE	0.04	0.05	0.08
t 8, 0.025	2.31	2.31	2.31
t * SE	0.10	0.12	0.19

Notes:
Mean is the average of the nine possible log reduction rates.
stdev is the standard deviation of the nine possible log reduction rates.
SE means Standard Error
t 8,0.025 is the Student t-distribution value at 5% possibility and 8 degree of freedom
t*SE is the value of the confidence interval about the mean at 95% confidence level.

Flow rate 26.5LPM

	Spores concentration in air CFU/L		
Sample	no baffle	head baffle	mid baffle
UV on 1	2.81E+03	7.39E+03	1.05E+04
UV on 2	4.11E+03	8.35E+03	3.49E+03
UV on 3	3.10E+03	8.17E+03	5.49E+03
UV off 1	1.31E+04	1.67E+04	2.46E+04
UV off 2	6.54E+03	1.63E+04	1.55E+04
UV off 3	9.26E+03	1.66E+04	1.48E+04
possible log reduction rate -log(Non/Noff)			
1	0.67	0.35	0.37
2	0.37	0.34	0.17
3	0.52	0.35	0.15
4	0.50	0.30	0.85
5	0.20	0.29	0.65
6	0.35	0.30	0.63
7	0.63	0.31	0.65
8	0.32	0.30	0.45
9	0.47	0.31	0.43
Statistics			
Mean	0.45	0.32	0.48
stdev	0.15	0.03	0.23
SE	0.05	0.01	0.08
t 8, 0.025	2.31	2.31	2.31
t * SE	0.12	0.02	0.18

Flow rate 44LPM

	Spores concentration in air CFU/L		
Sample	no baffle	head baffle	mid baffle
UV on 1	6.55E+03	1.29E+04	1.38E+04
UV on 2	9.50E+03	1.88E+04	1.37E+04
UV on 3	4.89E+03	1.36E+04	1.34E+04
UV off 1	2.52E+04	4.06E+04	2.43E+04
UV off 2	2.27E+04	3.96E+04	2.42E+04
UV off 3	1.72E+04	3.85E+04	1.81E+04
Possible log reduction rate -log(Non/Noff)			
1	0.59	0.50	0.25
2	0.54	0.49	0.24
3	0.42	0.48	0.12
4	0.42	0.33	0.25
5	0.38	0.32	0.25
6	0.26	0.31	0.12
7	0.71	0.48	0.26
8	0.67	0.46	0.26
9	0.55	0.45	0.13
Statistics			
Mean	0.50	0.42	0.21
stdev	0.15	0.08	0.06
SE	0.05	0.03	0.02
t 8, 0.025	2.31	2.31	2.31
t * SE	0.11	0.06	0.05

Appendix 5 . Source code list of the UDFs used in Fluent modeling.

Code Name	Functions	Source
Centroid.c	Read the co-ordinates of the centroid points of the cells in the modeling domain and write the values to centroid.txt file.	(Munoz 2004)
VFfluence.cpp	Read the co-ordinates of the centroid points from the centroid.txt file. Apply View Factor theory to calculate the fluence rate for each point. Write the fluence rates to 'vffluence.txt'	This study
Addfluence.c	Read the fluence rate value from 'vffluence.txt' and write the values into Fluent solver.	(Munoz 2004)
Dose.c	Source term for the cumulative fluence scalar	This study
Disinfect.c	Source term for the concentration scalar	This study
Name_UDSM.c	Rename the UDS and UDM to appropriate names.	This study
P_dose.c	Initial the UDS in particle tracking modeling, calculate the fluence along a particle trajectory, output the fluence to a *.dpm file.	(Munoz 2004)
stepUDS.c	Calculate the volume average microorganism concentration inside the validation column. Output the value at the end of each time step to 'sporeleft.txt' file	This study

Source codes can be found in the attached disc.